# FUNDAMENTALS AND APPLICATIONS OF ELECTROSPRAY IONIZATION – QUADRUPOLE ION TRAP MASS SPECTROMETRY FOR THE ANALYSIS OF EXPLOSIVES

By

JOSEPH EDWARD M$^{c}$CLELLAN

A DISSERTATION PRESENTED TO THE GRADUATE SCHOOL
OF THE UNIVERSITY OF FLORIDA IN PARTIAL FULFILLMENT
OF THE REQUIREMENTS FOR THE DEGREE OF
DOCTOR OF PHILOSOPHY

UNIVERSITY OF FLORIDA

2000

The fruit of this work is dedicated to those individuals who kept me sane during my time at the University of Florida: the bartenders and wait-staff of both Buffalo's Café, which was closed for demolition in September of 1998 for the construction of an Eckerd's Drug Store, and the Gainesville Ale House, which is thankfully still standing. These individuals will never know how much their kind nature and support meant to me in my trying times. Buffalo's will always have a special place in my heart for a multitude of reasons: it was the first restaurant I ate at in Gainesville during my visit to UF and, therefore, was instrumental in my choice of this school, it had an a.u.c.e special on wings and beer that can never be replaced, and I was always provided a bucket to contain my ever-present mess. Both establishments always provided a safe, friendly, and familiar environment for me when I needed it the most. My dear appreciation also goes out to those who partook in many a fine adult beverage with me at these establishments, especially my past and present roommates.

In Memory of My Grandfather, Joseph Edward McClellan:

**An Irish Blessing**

*May the road rise*
*to meet you,*
*May the wind be*
*always at your back,*
*May the sun shine warm*
*upon your face,*
*The rains fall soft*
*upon your fields and,*
*Until we meet again,*
*May God hold you in*
*the palm of His hand.*

ACKNOWLEDGMENTS

Foremost, I would like to acknowledge the two people who have always been a constant in my life, my parents, Marilyn A. and Joseph R. McClellan, for their continual support. Throughout my entire life, they have been there for me, providing anything and everything I could ever need or want. Their undying support, whether emotional, financial, or motivational, has allowed me to explore every opportunity and given me every chance to succeed. I will be forever grateful to (and for) them.

I would like to thank Professor Richard A. Yost for accepting me in to the Yost Group, where I have been able to do a lot of "cool stuff" and "good science" (Rick's terms, not mine). As with my parents, Rick provided me an environment where I could only succeed. From him, I have learned a lot about research and integrity, as well as how to survive among the many different personalities in science.

During my years at the University of Florida, I have had the pleasure of interacting with diverse group of people who have made me a better person and scientist, including my tremendous roommates, interesting lab mates, and assorted friends. I would like to thank my two roommates from Erie, George Pfeiffer and Mark Stufft, for bringing a little bit of home to Gainesville and helping me at the start of this wonderful adventure. I would like to thank Tracie Williams, who has been both a roommate and lab mate, for teaching me about life (never run away from a challenge and never run from a confrontation with someone you care about), science, and cooking. I would like to thank A. Cameron Church, who has been a wonderful friend and (briefly) roommate, for our

enchanting dinner conversations and for being a true friend (even when I did not deserve her to be one). I will miss our "dinner dates". I would like to thank Pat O'Donnell for being a fabulous roommate during this last year. I am sorry that he had the misfortune of living with two Holy Cross graduates, who often unfairly ganged up on him, but I think he survived the experience intact.

My roommate of longest duration at UF has been Jim Murphy (Holy Cross '96), who has also been a wonderful lab mate. I have known Jim since 1994, while we were still at HC, but we did not truly become friends until he arrived here at UF. I will forever be thankful for his friendship. Jim has always been there as a confidant and as a friend, especially during the stressful times of the month prior to my dissertation defense. I can not tell him enough how much his support and friendship has meant to me over the last few years. My greatest hope is that he will complete his Ph.D. quickly and return to his beloved Boston to embark on a more fulfilling adventure with his friends and family.

I would like to extend my gratitude to the members of the Yost Group, both past and present, for an endless supply of support, conversation, interaction, and amusement. I would like to thank Drs. Scott Quarmby, Chris Reddick, Tracie Williams, and Brody Guckenberger for making me comfortable in the Yost Group and helping me in the early stages of my time here. I would especially like to thank Scott for introducing me to hotter than hot peppers and Burrito Brothers. I would like to thank my contemporaries, Dr. Rick Troendle, Jim Murphy, Joe Muhlholland, and Kevin McHale for providing insight, support, and great conversations. I would like to thank Andria Hobbs, who has been an undergraduate member of our research group, for her wonderful friendship and

refreshing outlook on life. I would like to thank the present second- and first-year group members, especially Todd Huml and Beth Pierz, for providing continual amusement.

I would also like to thank those friends who affected my life outside of science during my time at the University of Florida, including past students, drinking companions, and random individuals. As a teaching assistant and course instructor, I have met many diverse people, some of whom have become good friends of mine, especially Olivia Bautista and Suzanne Solivan. My experiences at UF would not have been as fulfilling without the friendships of these students. I would like to thank my friends from Buffalo's Café and The Gainesville Ale House, especially Julie Crabtree, who was a wonderful friend and is a great person. I would like to thank the Banisauki, T.J. and Heather, for being good friends, intramural teammates, and a constant source of laughs. Lastly, I would like to thank Kerri Ann Sass for being a special friend and a wonderful travelling companion. I will never forget the good times I have had with these individuals.

TABLE OF CONTENTS

LIST OF TABLES

LIST OF FIGURES

Abstract of Dissertation Presented to the Graduate School
of the University of Florida in Partial Fulfillment of the
Requirements for the Degree of Doctor of Philosophy

FUNDAMENTALS AND APPLICATIONS OF ELECTROSPRAY IONIZATION – QUADRUPOLE ION TRAP MASS SPECTROMETRY FOR THE ANALYSIS OF EXPLOSIVES

By

Joseph Edward M$^{c}$Clellan

August 2000

Chairman: Richard A. Yost
Major Department: Chemistry

This dissertation presents a detailed investigation into the fundamentals of negative electrospray ionization (ESI) – mass spectrometry (MS) and tandem mass spectrometry (MS/MS) of explosives for the development of a novel method for the analysis of explosives. ESI is a "soft", or gentle, ionization process, which produces molecular ions with minimal fragmentation, and has applications for both small and very large molecules. The ultimate goal of the research presented here is to develop analytical methods for the detection and quantitation of explosives by employing the sensitivity and selectivity of liquid chromatography (LC)/ESI-MS/MS using a quadrupole ion trap mass spectrometer (QITMS). Over the past decade, the QITMS has emerged as a remarkably sensitive and selective instrument that is small in size, low in cost, and capable of efficient MS/MS.

In this work, the fundamentals of negative ESI-MS for the analysis of explosives and the impact of additives on the negative-ESI of explosives are investigated. Negative-ESI produces characteristic ions of explosives, which may be employed for the analysis of nitroaromatic compounds, nitramines, and nitrate esters. The mass spectra for the negative-ESI of explosives are influenced by the presence of impurities or additives. The effects of fragile ions, including some of the ions produced by negative-ESI of explosives, on mass resolution and MS/MS are also investigated. Fragile ions exhibit a chemical mass shift because they fragment during the application of the resonance ejection amplitude during mass analysis. Fragile ions affect mass resolution by causing broader peaks than non-fragile ions, especially at slower scan speeds, as the result of the application of the resonance ejection frequency. Fragile ions may also be fragmented by the application of the isolation waveform during selection of the parent ion for MS/MS experiments, making it impossible to achieve unit isolation of a fragile ion.

The knowledge obtained from these fundamental investigations is incorporated into the development of LC/ESI-MS and LC/ESI-MS/MS methods for the analysis of trace levels of explosives for both forensic and environmental applications. The application of a novel method for parent and neutral loss monitoring on the QITMS is also described.

# CHAPTER 1
# INTRODUCTION

## Quadrupole Ion Trap Mass Spectrometry

Over the past decade, the quadrupole ion trap mass spectrometer (QITMS) has emerged as a remarkably sensitive and selective instrument that is small in size, low in cost, and capable of efficient tandem mass spectrometry (MS/MS) [Johnson et al., 1990; Todd, 1991; March, 1998]. The QITMS is a specific type of ion trap. Simply, an ion trap is any device capable of trapping and storing ions or other charged particles in a confined space for a period of time. The operation of the quadrupole ion trap was initially described by Paul and Steinwedel in a patent filed in 1953 in Germany and awarded as a U.S patent in 1960 [Paul and Steinwedel, 1960]. Incidentally, this patent also described the quadrupole mass filter, which has become the most common mass spectrometer in use today. The quadrupole ion trap is often described as a Paul trap to differentiate it from other ion trapping devices. Since its initial commercialization in 1984, the quadrupole ion trap has continued to evolve from an instrument that required an expert user to an instrument that can be effectively used by many scientists.

## Quadrupole Ion Trap Theory

The quadrupole ion trap has been previously described at length [March, 1998; March and Hughes, 1989; March and Todd, 1995] and will be briefly describe below. The quadrupole ion trap is a three-electrode device that consists of a ring electrode placed between two endcap electrodes (Figure 1-1). Typically, the endcap electrodes are held at

ground potential and radio frequency (RF) and direct current (DC) potentials are applied to the ring electrode. The applied, trapping RF potential is characterized by its amplitude (zero-to-peak) and its angular frequency, $\Omega$. The trapping RF signal applied is equal to $V_{rf}\cos(\Omega t)$, where $\Omega = 2\pi f_{rf}$ [Bier and Schwartz, 1997]. A potential difference, created by the application of a DC voltage, U, and an AC voltage, V, at a particular frequency, produces a dynamic electric field for the trapping of ions. The field can be imagined to have a saddle shape at any particular point in time (Figure 1-2A). The dynamic nature of the electric field can be envisioned as a "saddle" spinning to keep ions of specific mass-to-charge (m/z) trapped within the ion trap device. An ion, of specific m/z, will have either a "stable" or "unstable" trajectory in the trap depending upon its m/z, the amplitudes of the RF and DC potentials, the frequency of the RF drive potential, and the internal dimensions of the ion trap electrodes. An ion that is "stable" will posses a trajectory that allows the ion to be trapped, or contained, within the specific electric field of the ion trap. These stable ions will have a trajectory that has the general appearance of a Lissajous figure (Figure 1-2B). An "unstable" ion will have a trajectory that increases in magnitude towards the ring of the endcaps and, thus, are lost through collisions with the electrodes.

The dimensions and geometry of the ion trap are arranged to produce a quadrupolar trapping field. Theoretically, this requires an orientation among the ring electrode and the two hyperbolic endcaps to result in a mathematical relationship of $r_o^2=2z_o$, where $r_o$ is the radius of the ring electrode and the $z_o$ is the distance between the center of the device and each endcap (see **Figure 1-2A**) [March and Todd, 1995]. Therefore, if $r_o$ is equal to 10.0 mm, the theoretically defined $z_o$ distance is 7.07 mm.

However, during the commercialization of the QITMS, the scientists at Finnigan noticed that this theoretical geometry produced both positive and negative mass shifts. They initially suggested that these mass shifts were due to differences in ion radial distributions, the high pressure of the helium in the trap, and the effects of higher-order fields caused by the field imperfections due to the holes in the endcap electrodes [Syka, 1995]. Through experimentation, they determined that if the endcap electrodes were radially displaced, the mass shifts could be minimized. Therefore the endcaps were both displaced by 0.76 mm, to obtain a new $z_o$ value of 7.83 mm and create a "stretched" geometry in the quadrupole ion trap. The new trap geometry produced a better field for mass analysis, but also created a field that had higher-order fields and was not purely quadrupolar. Although commercial instruments were made with the displaced endcap spacings since 1984, Finnigan did not release this information until 1992 [Syka, 1992, 1995].

Ion motion

The motion of ions in the dynamic electric field created by the difference in both the DC and AC potentials can be calculated from the solutions of a second-order linear differential equation described by the mathematician Mathieu in 1868. The equations were originally used to characterize the vibrational motion of a stretched skin or membrane [Mathieu, 1868]. The solutions to the Mathieu equations have been studied extensively [March and Hughes, 1989; March and Todd, 1995]. The solutions to these equations are in terms of two reduced parameters, $a_u$ and $q_u$. These two parameters may used to calculate whether an ion will have a stable or unstable trajectory in the trap under the defined conditions of the electric field. The values of $a_u$ and $q_u$ can be calculated for

the motion of the ions in both the r and z direction by the following solutions in Eqs. 1-1 and 1-2:

$$a_z = -2a_r = \frac{-16eU}{m\Omega^2\left(r_o^2 + 2z_o^2\right)} \tag{1-1}$$

$$q_z = -2q_r = \frac{8eV}{m\Omega^2\left(r_o^2 + 2z_o^2\right)} \tag{1-2}$$

In Eqs 1-1 and 1-2, r symbolizes the radial direction, z symbolizes the axial direction, e is the charge of an ion, U is the DC amplitude applied to the ring electrode, V is the RF amplitude, m is the mass of an ion, $\Omega$ is the angular drive frequency, $r_o$ is the radius, and $z_o$ is the center-to-endcap distance. The angular drive frequency is equal to $2\pi f_{rf}$. It should be noted that $a_z$ is proportional to the negative DC voltage applied and $q_z$ is proportional to the RF amplitude applied to the ring electrode. The Mathieu solutions are valid for the $a_{z,r}$ and $q_{z,r}$ parameters in both a theoretical geometry and stretched geometry trap.

Because the ion trap is a quadrupolar device, the electric fields are uncoupled in the three coordinate directions, x, y, and z, where $x^2 + y^2 = r^2$. Therefore, a given ion may have a stable trajectory in one direction and not another. If the ion is unstable in either direction, the ion will be lost through collisions with one of the ion trap electrodes. A stable ion is thus defined as any ion that has a periodic motion within the ion trap, which continues indefinitely and is bounded by the maximum volume of the trapping device. This will only occur when ions are stable in both the r and z directions simultaneously.

Mathieu stability diagram

The operating parameters $a_{r,z}$ and $q_{r,z}$ that result in stable trajectories can be calculated and displayed graphically as the Mathieu stability diagram (Figure 1-3). Although an infinite number of regions of stable solutions to the Mathieu equation exist, due to voltage limitations and other practical limitations, only one region is of interest for use with commercial instruments. The region depicted in this Mathieu stability diagram is that which produces stable trajectories in both the r and z directions. Typically, the stability diagram is plotted in the $a_z$ and $q_z$ dimensions. This region of stability is defined by the boundaries at $\beta_z=0$, $\beta_z=1$, $\beta_r=0$, and $\beta_r=1$. Therefore, if an ion has an $a_z$ and $q_z$ value confined by these boundaries, the ion will be stable in both the r and z directions and be available for mass analysis. Different points in $a_z$, $q_z$ space correspond to different values of $\beta_r$ and $\beta_z$ values. These $\beta_u$ values determine the fundamental frequency of motion, $\omega_u$, of ions in both the r and z directions by the following equation.

$$\omega_u = \frac{1}{2}\beta_u\Omega \qquad (1\text{-}3)$$

Therefore, the frequency of an ion is given by its $\beta_u$ value and therefore its position in $a_z$, $q_z$ space. Because $a_z$ and $q_z$ are functions of the ion's m/z (see equation 1-2), the frequency of an ion at a given RF and DC voltage is a function of its m/z.

Ultimately, the stability of an ion in a quadrupole ion trap is dependent on a variety of instrumental parameters including the DC amplitude applied to the ring electrode, the RF amplitude and angular drive frequency, the radius of the ring electrode, and the distance from the center of the ion trap to the endcap electrodes. For any given set of conditions, including the RF and DC voltages applied, it is possible to store ions

with a range of m/z values and polarity simultaneously in the ion trap. At given RF amplitudes, ions of increasing m/z will be stored at decreasing $q_z$ values. Typically, the Mathieu stability diagram is depicted for positive ions, but it can be readily applied to negative ions by inverting the sign of the $a_z$ values. At certain $a_z$ values, including $a_z = 0$, both positive and negative ions will have a stable ion trajectory.

The Finnigan LCQ – A Commercial QITMS

All experiments reported in this dissertation were performed on the Finnigan LCQ (San Jose, CA), a commercial, bench-top QITMS instrument (Figure 1-4) [Bier and Schwartz, 1997]. This instrument is capable of external ionization and may be equipped with either of two atmospheric pressure ionization (API) sources. API sources are continuous ionization sources that create ions at atmospheric pressure. Atmospheric pressure chemical ionization (APCI) and electrospray ionization (ESI) sources are the two major API sources used today and both are available for use with the LCQ. The LCQ is capable of analyzing ions of both negative and positive polarity. The instrument allows for the production of ions at atmospheric pressure; these ions, after passing through a heated metal capillary and a series of lenses and ion guides are injected into the ion trap. The heated metal capillary helps desolvate the ions. The ions exiting the capillary are then focused by a tube lens to pass through a skimmer cone and into the first of two RF-only octapoles. The octapoles act only as ion guides and are not used in any mass-selective capability. After exiting the first octapole, the ion is then passed through an interoctapole lens, the second RF-only octapole, and, ultimately, into the ion trap.

The LCQ ion trap

As with all previous commercial Finnigan QITMS instruments, the LCQ ion trap has a stretched geometry caused by the non-theoretical electrode spacing. While all

previous instruments have had a $r_o$ of 10.0 mm and a $z_o$ of 7.83 mm, the LCQ has a $r_o$=7.07 mm and $z_o$=7.85 mm, instead of the theoretical $z_o$=5 mm [Quarmby, 1997]. Each endcap electrode has one hole in the center of the electrode for the transmission of ions into and out of the ion trap. The endcap electrodes are designated the entrance endcap electrode, which allows ions to enter the ion trap, and exit endcap electrode, which allows ions to exit the trap to the detector. The radius of the ring electrode was reduced to increase the upper mass limit, $m/z_{max}$, of the instrument. The $m/z_{max}$ of any quadrupole ion trap is defined by the following equation:

$$m/z_{max} = \frac{8eV_{max}}{q_{ej}\Omega^2\left(r_o^2 + 2z_o^2\right)} \tag{1-4}$$

For the above equation, $V_{max}$ is the upper limit of the RF amplitude that may be applied to the ring electrode, and $q_{ej}$ is the $q_z$ value for the ejection of ions from the ion trap. On the LCQ, the $V_{max}$ is 8500 $v_{p-p}$. Therefore, by reducing the $r_o$, the $m/z_{max}$ was increased. The drive frequency ($\Omega/2\pi$) was also decreased from 1.1MHz to 760 kHz to increase the mass range of the instrument. With these alterations, the LCQ has a $m/z_{max}$ of 2000. The $m/z_{max}$ may be further increased by lowering the $q_{ej}$, which can be used to increase the $m/z_{max}$ beyond 2000 on the LCQ.

The LCQ operates along the $a_z = 0$ line in the Mathieu stability diagram. This is accomplished by having a 0 V DC potential difference between the ring electrode and the endcap electrodes. On the LCQ, the ion trap electrodes are all maintained at the same potential, but not ground potential. The potentials are held at an offset of 10 V (–10 V for positive ions and + 10 V for negative ions) to assist in the injection of ions into the ion trap. While operating on the $a_z = 0$ line, all ions with a $q_z$ value between 0 and 0.908 will be stable in both the r and z direction. Any ion with a $q_z$ value larger than 0.908 will be

unstable in the z direction, but stable in the r direction. This instability will cause the ions to either have collisions with an endcap electrode or be ejected from the trap through the hole in the endcap electrodes. To determine what m/z ions will have stable trajectories, the low mass cut-off (LMCO) is used. The LMCO is defined as the m/z that is at the far point of stability on the $a_z = 0$ line for a given RF amplitude applied to the ring electrode, and, therefore, $q_z = q_{ej}$. All ions of a lower m/z than the LMCO will have a $q_z$ greater than the $q_{ej}$, and thus be unstable in the z direction.. The LMCO may be calculated by either of the two equations:

$$\mathrm{LMCO} = \frac{8eV}{q_{ej}\Omega^2\left(r_o^2 + 2z_o^2\right)} \tag{1-5}$$

$$\mathrm{LMCO} = \frac{q_z}{q_{ej}}(m/z) \tag{1-6}$$

Equation 1-6 is a more practical equation for the routine calculation of the LMCO because only the $q_z$ of an ion at a particular m/z and the $q_{ej}$ are necessary to complete the calculation.

Mass analysis

Since the LCQ operates on the $a_z = 0$ line, the mass analysis of trapped ions is relatively simple. Because $q_z$ is inversely proportional to m/z, all m/z ions line up on the $a_z = 0$ line in order of decreasing m/z from low $q_z$ to high $q_z$. Mass analysis on the LCQ is accomplished by moving the ions to the right in $q_z$ space until they reach the LMCO and are ejected and detected. The ions are moved to the right in $q_z$ space by increasing the amplitude of the RF potential applied to the ring electrode. The trapped ions are, thus, marched to the edge of stability by ramping the RF amplitude on the ring. This

originally lead to the first method of mass selectively ejecting ions out the ion trap over a large m/z range, called mass-selective instability scanning [Stafford et al., 1985]. On the first-generation Finnigan QITMS instruments, mass analysis was accomplished by ramping the RF voltage on the ring electrode, where ions of increasing m/z consecutively become unstable in the axial direction as they cross the $\beta_z$=1 edge of the stability diagram, at a $q_z$ of 0.908. These ions are then ejected from ion trap through the holes in the endcaps; those exiting through the exit endcap electrode will be detected by the electron multiplier. This method, while sensitive, did not provide adequate resolution due to the influence of space charge (ion-ion repulsions).

Later generations of Finnigan QITMS, such as the LCQ, employ the method of resonant ejection, or axial modulation, to selectively eject ions from the ion trap [Bier and Schwartz, 1997]. In this method, dipolar AC signals are applied to the endcap electrodes 180° out of phase. Each signal is equal to $V_{res}\cos(2\pi f_{res}t)$, where $V_{res}$ is the amplitude and $f_{res}$ is the frequency of the resonant ejection signal. On the LCQ, the resonant ejection signal has a frequency of 348 kHz, corresponding to a $\beta_z$ = 0.916 and amplitude is applied at a resonant ejection $q_z$ ($q_{ej}$) of 0.900. Mass analysis is accomplished by ramping the RF voltage on the ring electrode, such that ions of increasing m/z consecutively come into resonance with the resonance ejection amplitude. As the ion comes in resonance with the resonant ejection signal, the ions gain kinetic energy and are quickly ejected, in a tight packet, from the ion trap in the z direction; those that exit through the exit endcap are detected. The amplitude of the resonant ejection signal is mass calibrated, as ions of increasing m/z require an increasing resonant ejection amplitude to be efficiently ejected in a tight packet. The sensitivity and resolution are

vastly improved utilizing resonant ejection versus mass-selective instability ejection. The use of resonant ejection also enables the trapping of a larger number of ions in the ion trap without sacrificing resolution and peak shape, since resonant ejection is more tolerant of space charge.

The resolution, peak shape, and sensitivity on the LCQ are also improved by the use of a buffer gas and automatic gain control (AGC). The sensitivity and resolution of the QITMS is improved by the use of a light gas, such as helium (He), as a buffer gas in the ion trap [Stafford et al., 1984]. Effective pressures are generally a few mtorr. The LCQ ion trap operates with a He pressure of approximately 3.5 mtorr when a pressure of 5 psi of He is applied to the head of a capillary restricter [J.C. Schwartz, personal communication, 2000]. The helium is introduced into the trap through a nipple on the exit endcap electrode. The AGC scan is used to control the number of ions in the trap and, thus, limit the extent of space charging which may occur in the ion trap. Space charging results from ion-ion interactions and can lead to distortions of the electrodynamic fields. This distortion can lead to degradation in resolution, a reduction in mass heights, and a shift in mass assignments [Cleven et al., 1994; Cox et al., 1995]. The effects of space charging can be limited by reducing the number of ions in the trap, as space charging increases as the number of ions in the trap increase. The AGC scan, which is essentially a prescan preceding all analytical scans, has a fixed ionization time. From the total ion current in the AGC scan, a suitable ionization time is determined by the data system for the analytical scan that allows for the maximum ion population before the peak shape and resolution of the scan degrades due to space charging [Stafford et al., 1987; Yost et al., 1987]. On the LCQ, setting the AGC targets controls the number of

ions in the trap. These targets are based upon the optimum total ion current and are set individually for each of the different scan types.

LCQ scan functions

On the LCQ, there are three distinct scan functions in the MS mode. Each scan function has two steps in common, ion injection and mass analysis. The first type of scan function is full scan. The LCQ full scan has up to four distinct ion injection RF levels during the ion injection period, which are calculated by the data system. In each of the segments, a different RF amplitude is applied to the ring in order to obtain maximum ion intensity over the entire m/z range. As the m/z of an ion increases, the optimum injection RF amplitude, or LMCO, also increases [Quarmby and Yost, 1999]. The trapping of injected ions is highly dependent on the RF amplitude applied to the ring. Once injected and trapped, the ions are then mass analyzed by ramping the RF on the ring electrode at a rate of 0.18 ms / amu. The mass range in full scan mode may be set from m/z 15 to 200 (low mass range), m/z 50 to 2000 (normal mass range), or m/z 100 to 4000 (high mass range). To utilize the low and high mass range capabilities, the instrument must utilize the advanced scan features of the LCQ. During the ion injection process, the tube lens is on (voltage is applied), the octapole lens is on (set to a negative voltage for positive ions and to a positive voltage for negative ions), the octapole RF is on, and the electron multiplier is off. During mass analysis, the tube lens and octapole RF are off, the multiplier and resonant ejection amplitudes are on, and the octapole lens is switched in polarity [Bier and Schwartz, 1997].

The other two MS scan functions are the selected ion monitoring (SIM) scan mode and a high resolution scan mode, the LCQ ZoomScan. Both of these scan functions utilize an ion isolation step in conjunction with the ion injection and mass

analysis steps. For each scan function, a small m/z range is utilized for analysis and requires only one ion injection RF level. The m/z range may be set for any m/z in the SIM mode, but is confined to a range of 10 amu for ZoomScan. The ion isolation step is used to eject all unwanted ions from the trap and is accomplished by applying a sum-of-sines tailored waveform (TWF). The TWF applies a potential at all frequencies corresponding to the unwanted m/z. The TWF leaves a "frequency notch" around the frequencies corresponding to the m/z of the set mass range. This TWF is calibrated and applies a higher amplitude at lower frequencies (higher m/z) to facilitate the ejection of all unwanted ions. This isolation step allows for greater sensitivity in the SIM mode and for greater resolution in the ZoomScan mode. The mass analysis step in the SIM mode uses the same scan rate as in full scan, 0.18 ms/ amu. The LCQ ZoomScan utilizes a scan rate of 3.6 ms / amu for mass analysis, which is 20 times slower than the normal full scan rate, and, therefore, may be referred to as a slow scan.

## Tandem Mass Spectrometry

Tandem mass spectrometers have found widespread use in analytical chemistry because of the sensitivity and selectivity provided by two (or more) stages of mass spectrometry (MS/MS and $MS^n$) [Yost and Fetterolf, 1983; Busch et al., 1988]. Traditionally, tandem mass spectrometry (MS/MS) has been performed on tandem-in-space instruments such as triple quadrupole mass spectrometers (TQMS) and multiple sector mass spectrometers [Gross, 1990; Yost and Boyd, 1990]. More recently, tandem-in-time instruments, in which the stages of mass spectrometry are performed sequentially, as in the quadrupole ion trap mass spectrometer (QITMS) [March, 1989; Johnson, 1990; March, 1995] and the Fourier transform ion cyclotron resonance mass spectrometer

(FTMS) [Marshall, 1998], have become common. The QITMS instrument has inherently greater MS/MS efficiency due to its tandem-in-time, rather than tandem-in-space, configuration, which leads to greater sensitivity and selectivity.

MS/MS Fundamentals

Multiple stages of mass analysis in a QITMS require at least two steps besides ion injection and mass analysis. These two steps are isolation of the parent, or precursor, ion and the fragmentation of that ion. Methods for ion isolation include RF/DC isolation, forward and reverse resonant ejection isolation, and the application of a broadband, tailored waveform [Bier and Schwartz, 1997]. Presently, the most common method used to isolate the parent ion on a quadrupole ion trap is to apply a broadband waveform that ejects all of the unwanted ions from the trap. The application of this waveform will result in the isolation of the targeted parent ion. The next step is to fragment the parent ion and is conventionally accomplished by collision-induced dissociation (CID) [Louris, 1987], which is also referred to as collisionally-activated dissociation (CAD).

CID is an example of an ion activation method that results in the production of daughter, or product, ions via a unimolecular dissociation. For CID, the parent ion is first excited by the application of a dipolar signal, 180° out of phase, across the endcap electrodes. This method, called resonant excitation, is applied at a particular frequency, corresponding to a $q_z$ of resonant excitation ($q_{ex}$), and with a specific amplitude. The $q_{ex}$ is generally applied at a constant $q_z$ value (frequency), but may be applied at varying magnitudes and times. Once the parent ion is excited, and, thus, has gained kinetic, it will undergo a collision with a molecule of the buffer (target) gas. During this collision, some of the kinetic energy of the ion may be converted into internal energy. If this collision (or a series of collisions) imparts enough internal energy into the parent ion, the

parent ion will dissociate (fragment) to produce daughter, or fragment, ions. The amount of kinetic energy that is given to an ion can be increased by either increasing the resonant excitation amplitude or the time of resonant excitation [March and Todd, 1995]. Within compound classes, the amount of energy required to fragment an ion is generally proportional to the m/z of the ion. Ions of higher m/z generally require a greater resonant excitation amplitude or a longer period of time.

There are four possible, "classic" MS/MS experiments: daughter ion scan, parent ion scan, neutral loss scan, and selected reaction monitoring (SRM) [Busch et al., 1988]. The most common MS/MS experiment is the daughter ion scan, which acquires a mass spectrum of the daughter ions produced from the fragmentation of a selected parent, or precursor, ion. Inherently, daughter ion scans can be performed on both tandem-in-space and tandem-in-time instruments [Johnson et al., 1990]. Often, when the term MS/MS is used, it is referring to daughter ion scans. A parent ion scan detects all of the parent ions in a sample that fragment to produce a common daughter ion, whereas a neutral loss scan detects those ions that fragment to produce daughter ions with a common difference in m/z, therefore, losing a specific neutral fragment. Parent and neutral loss scans are important mass spectrometric techniques for mixture analysis and the screening of samples for the presence of specific compound classes. The SRM experiment selectively monitors the production of one (or more) targeted daughter ions from a specified parent ion. On a QITMS, the only MS/MS experiments that are commercially available are the daughter ion and SRM scans.

MS/MS on the LCQ

The LCQ uses a sum-of-sines TWF, as used in SIM and ZoomScan modes, to isolate parent ions for MS/MS experiments. For all MS/MS experiments, the parent ion

of interest is placed at an isolation $q_z$ ($q_{iso}$) of 0.83, by placing the appropriate RF amplitude on the ring electrode. At higher $q_z$ values, there is greater frequency spacing of ions. Therefore, it is easier (less precise waveforms are necessary) to isolate an ion with unit resolution at higher $q_z$ than lower $q_z$. The TWF is applied with a frequency notch around the $q_{iso}$ to isolate the ions placed at that $q_z$ [Bier and Schwartz, 1997]. The TWF is somewhat similar to the stored-waveform inverse Fourier transform (SWIFT) waveform [Marshall et al., 1985; Chen et al., 1987] as both create a defined, time-domain waveform. However, the sum-of-sines approach uses pre-calculated frequency combs and is not calculated by using an inverse Fourier transform. The applied TWF on the LCQ has both a width and time component. The width of the frequency notch may be changed by specifying a particular isolation width for the MS/MS experiment. Conventionally, the TWF is applied for a period of 16 ms in four bursts of 4 ms. This time is sufficient to eject all unwanted ions.

The LCQ uses resonant excitation and CID to fragment the selected parent ion during an MS/MS experiment. The resonant ejection signal is typically applied at a frequency equal to a $q_{ex}$ of 0.25. This value is the default for the LCQ software. However, using the Advanced Scan Features of the LCQ, it is possible to change this value. By changing the $q_{ex}$, it is possible to change the LMCO of the scan function, in accordance to the equation:

$$LMCO = \frac{q_{ex}}{q_{ej}}(m/z) \tag{1-7}$$

In this equation, the LMCO is equal to the lowest m/z daughter ion that may be trapped and mass analyzed. Therefore, if the $q_{ex}$ is decreased from 0.25 to 0.2, it is possible to

trap and mass analyze lower m/z daughter ions. It is important to keep in mind the limitations of the LMCO when designing an MS/MS experiment.

The resonant excitation amplitude is applied as a collision energy percentage. In the original software packaged with the LCQ, this percentage was a fixed percentage of 5 $V_{p-p}$. The implementation of the Advanced Scan Features in the LCQ software allowed for the direct application of the resonant excitation amplitude, without using the collision energy percentage. With both methods, the user had direct knowledge pertaining to the magnitude of the resonant excitation amplitude. In the newest revision of the software, packaged as LCQ Xcalibur, the user does not have direct knowledge regarding the magnitude of the resonant excitation amplitude. In this software version, the resonant excitation amplitude is applied as an activation amplitude percentage. The input activation percentage is then mass normalized to generate the appropriate resonant excitation amplitude to be applied to the endcaps [Schwartz et al., 1999]. For the work in this dissertation, different software versions were used, and, thus, has an impact on the discussion of the applied resonant ejection amplitude for MS/MS experiments. The latest version of the software was used for experiments in Chapters 2 and 5 and the reported activation percentages are using the mass normalized processing method. In Chapters 3 and 4, the original software was utilized and, thus, the reported collision energies are reported as percentages of 5 $V_{p-p}$. The typical time of resonant excitation is 30 ms, but can be readily increased or decreased.

## Electrospray Ionization

Electrospray ionization (ESI) [Yamishita and Fenn, 1984; Aleksandrov et al., 1984] is a "soft", or gentle, ionization process, which produces molecular ions with

minimal fragmentation, and has applications for both small and very large molecules [Fenn et al., 1989; Smith et al., 1990]. Many excellent reviews are available on ESI, including works by Kebarle [Ikonomou et al., 1991], Gaskell [1997], Bruins [1998], and a text edited by Cole [1997]. In its most classic function, ESI is a method for the transfer of ions present in solution into the gas phase. The ESI process consists of producing highly charged droplets at atmospheric pressure, followed by the evaporation of the droplets to liberate the gas-phase ions [Gaskell, 1997]. Applying a high voltage to a needle through which a liquid sample is passed produces the charged droplets. Both positively and negatively charged ions may be transferred to the gas phase, depending upon the polarity of the high voltage. Typically voltages of 3 to 4.5 V are applied for traditional, macro-ESI. ESI can also be viewed as a special kind of electrolytic cell [Kebarle and Tang, 1993; Van Berkel and Zhou, 1995], where the addition (negative ions) or removal (positive ions) of electrons plays a part in ion production [Bruins, 1998]. In this sense, ESI may be thought of as true ionization source. For the purposes of this dissertation, the ESI process will be described for the application of a negative bias to the needle (Figure 1-5) to produce negative ions. For positive ESI, the polarity of all potentials and ions would be reversed.

The first step in the process of negative-ESI, charged droplet formation, occurs with the application of the high negative potential to the electrospray needle. On the LCQ, this potential is applied to a 26 gauge stainless steel needle (460 μm o.d. and a 260 μm i.d). The solution passes through the needle within a 100 μm i.d. piece of fused silica (200 μm o.d.). The end of the fused silica capillary is slightly recessed from the end of the needle to allow for direct contact between the solution and the high potential ESI

needle. The application of this negative potential causes negative ions to be drawn to the surface. In negative-ESI, reduction will occur at the needle tip, while oxidation will occur at the counter electrode [Van Berkel, 1997]. On the LCQ, the counter electrode is the heated capillary and spray shield, which is held at a ground potential. The negative ions in solution are drawn outward direction from the needle to form a Taylor cone. When the imposed electric field is high enough that the surface tension is exceeded by the electrostatic force, negatively charged droplets are produced [Gaskell, 1997]. The use of a high velocity gas, such as $N_2$, assists in the formation of these droplets in pneumatically assisted ESI [Bruins, 1998]. On the LCQ two sources of $N_2$ gas, a sheath gas, which is parallel to the liquid flow, and an auxiliary gas, which flows off axis to the liquid flow, are used for this purpose. In negative-ESI, the charged droplets are formed with the negatively charged ions attracted to the outside of the droplets.

The next step of the ESI process is the liberation of the ions from the charged droplets via droplet shrinkage and gaseous ion formation. The droplet shrinkage occurs as the droplets travel from the high pressure region of the source to the low pressure regions of the mass spectrometer. The pressure gradient causes the solvent to evaporate from the droplets and results in the decrease of the diameter of the droplet [Gaskell, 1997]. The solvent evaporation is assisted by the use of a heated capillary. The decrease in the size of the droplet results in an increased coulombic repulsion as the charge-to-volume ratio increases as the solvent evaporates from the droplet. When the charge density at the surface increases to the point where the coulombic repulsion is greater than the surface tension, known as the Rayleigh limit, droplet fission, or coulombic explosion, occurs [Gaskell, 1997]. It has been demonstrated that droplet fission occurs for all

droplets with a radius greater than 1 μm [Gomez and Tang, 1994]. During this fission process, off-spring droplets are created with a diameter roughly one-tenth the size of the parent droplet. This process occurs until droplets with radii less than 10 nm are produced [Kebarle and Ho, 1997].

Upon sufficient droplet shrinkage, gas-phase ions may be liberated from the very small charged droplets. After over a decade of ESI use in MS, the method of ion formation from the charged droplet is still highly debated [Kebarle and Ho, 1997; Gaskell, 1997]. There are two proposed methods, assume that the ions are either produced by the direct ion evaporation, or emission, model as predicted by Iribarne and Thomson [1976] or by a continual coulombic fission model. The Iribarne and Thomson model suggests that gas-phase ions are directly emitted from small droplets, while the coulombic fission model suggests that coulombic fission continues to occur until droplets containing only one ion are formed. Though, there have been attempts to quantitatively investigate these two models, no conclusive data have been attained to fully support either method; the mass spectral observations can be explained by both [Kebarle and Ho, 1997]. The gas-phase ions may then be directed by a series of lenses and ion guides into the ion trap for mass analysis.

## Analysis of Explosives

Trace analysis of explosives is of major importance for both forensic and environmental applications. Forensic detection and identification of explosives is necessary for the analysis of post-explosion residues, establishing individual contact with illegal explosives, and determining the illicit manufacturing of explosives [Yinon and Zitrin, 1993]. The analysis of post-explosion residue is difficult because it is dependent

on finding unexploded residues from the original explosives, rather than detecting the products formed from the explosion. Preliminary field tests may be used for the screening of samples, but the trace analysis of post-explosion residue generally requires more in-depth laboratory investigation. The analysis of extracts from individuals, personal effects, and housing is vitally important for establishing contact between an individual and illegal explosives. The verification of this illicit contact must be highly reliable in order for the evidence to be used in courtroom proceedings.

The detection of explosives and related synthesis materials in manufacturing waste and in the environment surrounding manufacturing sites is valuable for regulating the production output of manufacturers, enforcing restrictions against illegal explosive production, and monitoring illegal waste disposal. Also, trace analysis of explosives and explosive residues could potentially be used for the determination of an explosive's manufacturing origin, either by country or by manufacturer. This could be highly beneficial for investigations conducted by military and law enforcement agencies. As there are only small differences in the production of military explosives from site to site, the only characteristic differences in the manufacturing process may be low levels of organic impurities [Urbanski, 1964] and detection agents with which manufacturers are required to mark explosives [Montreal, 1991]. An analytical method to identify the origin of an explosive, via the presence of organic impurities, degradation products, compound isomers, or detection agents would be an extremely valuable tool.

Explosives constitute an environmental contamination problem as the result of the disposal of ammunition and explosive manufacturing waste in buried sites, ground water, and rivers [Yinon, 1999]. In order to assess the extent of contamination by explosives in

an area, trace analysis for explosives and their degradation products in both ground and surface water must be accomplished. An analytical method that can detect and identify trace amounts of explosives in aqueous samples, with limited sample preparation, would be valuable for assessing the contamination of explosives in the environment.

The analysis of explosives samples is routinely accomplished using gas chromatography (GC) / electron capture detector (ECD) [Douse, 1981, Yinon and Zitrin, 1993; Kolla, 1994; Welsh et al., 1997; Walsh and Ranney, 1998], GC/MS [Yinon and Zitrin, 1993; Yinon, 1996], and LC [Jenkins et al., 1985; Kolla, 1994; Renner et al., 1997; Lang and Burns, 1999] for both forensic and environmental applications. The LC research has led to and are based upon the standardized US Environmental Protection Agency (EPA) Method 8330 [SW-846, 1994]. However, these methods are generally either susceptible to thermal degradation (GC/ECD and GC/MS) or are too insensitive (LC) for many applications. Recently, research has been published on the analysis of explosives using LC/MS [Berberich et al., 1988; Miller et al., 1997; Yinon et al., 1997, Cassada et al., 1999] and capillary electrophoresis (CE) [Oehrle, 1996; Bailey and Yan, 1998] to improve the limits of detection for the analysis of explosives.

ESI-MS has only been minimally employed for the analysis of explosives (Straub and Voyksner, 1993; Cassetta and Garofolo, 1994; Yinon et al., 1997], but appears to be a more sensitive method amenable to the analysis of both environmental and forensic applications. Most recently, methods have been developed for the analysis of explosives via LC/ESI-MS [Miller, 1997; Cassada et al., 1999]. These investigations have shown that the ionization of explosives via ESI, while sensitive is not highly reproducible. ESI-MS spectra of explosives vary greatly, in terms of fragment and adduct ion formation,

among the work of the different investigators. There are, currently, no published methods employing LC/ESI-MS/MS for the analysis of explosives.

## Overview of Dissertation

This dissertation presents a detailed investigation into the fundamentals of negative ESI-MS and MS/MS of explosives for the development of a novel method for the analysis of explosives. The ultimate goal of the research presented here is to develop analytical methods for the detection and quantification of explosives using minimal sample preparation and the sensitivity and selectivity of LC/ESI-MS/MS on a QITMS. In this work, the fundamentals of negative ESI-MS for the analysis of explosives (Chapter 2), the effects of fragile ions, including some of the ions produced by negative-ESI of explosives, on mass resolution and MS/MS (Chapter 3), and the impact of additives on the negative-ESI of explosives (Chapter 5) are investigated. The knowledge obtained from these fundamental investigations is incorporated into the development of LC/ESI-MS and LC/ESI-MS/MS methods for the analysis of trace levels of explosives for both forensic and environmental applications (Chapter 5). The application of a novel method for parent and neutral loss monitoring on the QITMS will also be described (Chapter 4).

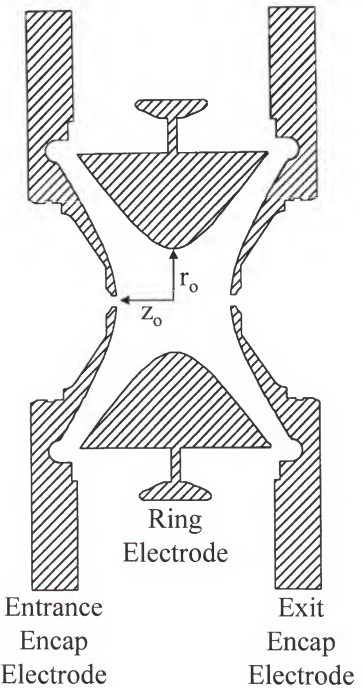


FIGURE 1-1: Cross Section of a Quadrupole Ion Trap

Cross section of a quadrupole ion trap showing the arrangement of the three electrodes. The holes in the two endcap electrodes allow for ions to enter and exit the ion trap. The spacings of the electrodes result in dimensions that can be displayed in both the radial direction ($r_o$) and the axial direction ($z_o$). Adapted from Quarmby, 1997.

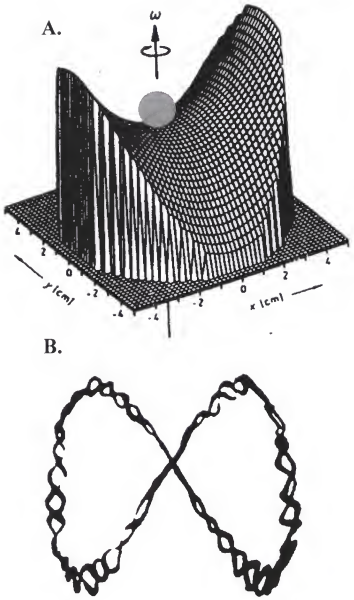


FIGURE 1-2: Ion Motion in a Quadrupole Ion Trap Mass Spectrometer

Ion motion in a quadrupole ion trap is depicted in terms of the dynamic electric field imposed on the ions and the trajectory that a stable ion will have in the ion trap. A: Application of the "saddle" shape dynamic electric field in a quadrupole ion trap. Adapted from Paul, 1990. B: Lissajous figure of stable charge aluminum microparticles suspended in quadrupole ion trap to demonstrate the trajectory of a stable ion in the trap. Reproduced from Wuerker, 1959.

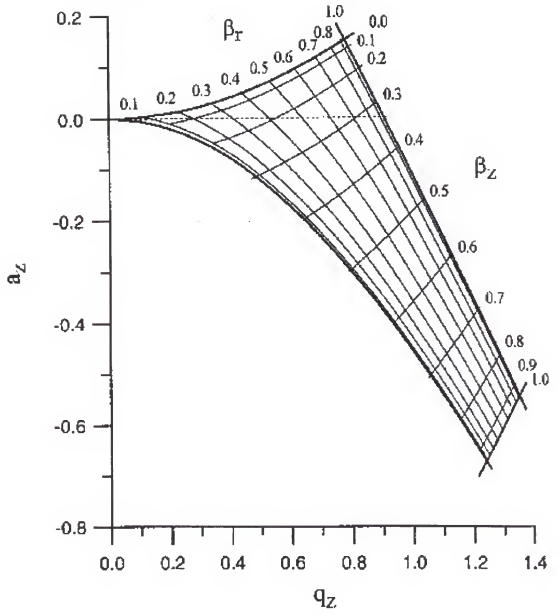


FIGURE 1-3: Mathieu Stability Diagram

Mathieu stability diagram plotted in $a_z$ and $q_z$ space for positive ions. For negative ions, the shape of the stable region is rotated about the $a_z = 0$ line. Region of stability utilized by commercial QITMS instruments, where ions are stable in both the r and z directions if held at $a_z$ and $q_z$ values within the boundaries of $\beta_z$=0, $\beta_z$=1, $\beta_r$=0, and $\beta_r$=1. The LCQ operates along the $a_z = 0$ line. Ions will have a stable trajectory between $q_z = 0$ and 0.908.

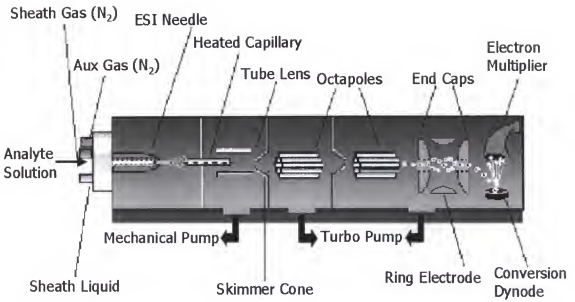


FIGURE 1-4: Diagram of Finnigan LCQ

A liquid sample is flowed through the ESI needle, where a high voltage is applied. The formation of droplets may be assisted by the use of a sheath gas, auxiliary (Aux) gas, or a sheath liquid. Charged droplets are passed through a heated capillary to assist in desolvation as the droplet transverses a pressure gradient. The tube lens focuses ions and the skimmer cone lens reduces the passage of neutral gas-phase molecules in the mass analyzer. Two octapoles guide ions into the ion trap. Ions are detected using a conversion dynode and electron multiplier. Adapted from www.thermoquest.com.

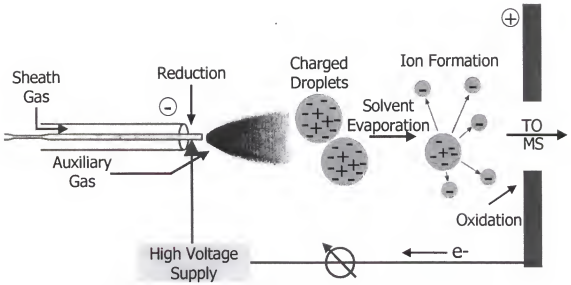


FIGURE 1-5: Mechanism of Negative Electrospray Ionization

Mechanism of for analysis by electrospray. The mechanism of negative ESI for the formation of negative ions includes charged droplet formation at a ESI needle with a high negative potential, droplet shrinkage via solvent evaporation, and the liberation of gas-phase ions. The ESI process may also be viewed as an electrolytic cell with reduction occurring at the ESI needle and oxidation occurring at the counter electrode.

# CHAPTER 2
# PRINCIPLES OF ELECTROSPRAY IONIZATION – MASS SPECTROMETRY AND TANDEM MASS SPECTROMETRY OF EXPLOSIVES

A method incorporating electrospray ionization (ESI)-mass spectrometry (MS) would be a valuable and powerful analytical method for the analysis of explosives for both forensic and environmental applications. Because of the thermal liability of explosives, hard ionization techniques that require high temperatures for the initial volatilization of the samples to produce gas-phase molecules, such as electron ionization (EI) and chemical ionization (CI), often result in excessive degradation and fragmentation of explosives. Therefore, soft ionization techniques, particularly those which can produce ions directly from solution or immediately following volatilization, such as ESI and atmospheric pressure chemical ionization (APCI), should produce less degradation and fragmentation during the ionization of explosive compounds. Various other groups have evaluated ESI-MS for the analysis of explosives [Straub, 1993, Casseta and Garofolo, 1994; Cole and Zhu, 1999], but there has been no definitive study for the ESI of explosives. The analysis of explosives by ESI-MS, has proven difficult because the ESI ionization mechanisms are highly dependent on the conditions of the mass spectrometer. From previous results [Yinon et al., 1997] and comparisons with other investigations, it has become apparent that impurities, additives, and solvent conditions all play an important role the ionization of nitro explosives. Therefore, the ESI-MS of explosives is often influenced by the condition of the analytical system and is not always directly dependent on the sample preparation and solvent system employed. We have

studied the ESI of a variety of nitro explosives, including nitroaromatic compounds, nitramines, and nitrate esters, on a commercial quadrupole ion trap mass spectrometer (QITMS), the Finnigan LCQ. Results from ESI-MS and tandem mass spectrometry (MS/MS and $MS^n$) are presented.

## Experimental

### Instrumentation

All experiments were performed on the Finnigan LCQ (San Jose, CA), a commercial, bench-top ESI-QITMS instrument. All samples were infused into the mass spectrometer at a flow rate of 5 μL/min using the LCQ syringe pump and analyzed in the negative ion mode of the LCQ. This mode uses negative-ESI for the ionization of all analyte molecules. Data were acquired utilizing the LCQ Tune window. Each spectrum presented is the average of 50 analytical scans, each consisting of 3 μscans. For data acquisition in negative ion mode, the AGC target values for full scan and $MS^n$ scans were lowered by a factor of three, compared to the values for positive ions, as there is an increased ion signal gain for the detection of negative ions [Schwartz et al., 1998], to values of $2 \times 10^7$ for full scan and $2 \times 10^6$ for $MS^n$.

The LCQ utilizes various Tune methods, created by the user, to control the instrumental parameter of the instrument. Two different LCQ Tune methods were used for the analysis of the explosives. One general Tune method, "TNT.LCQTune" (**Table 2-1**), was used for the analysis of nitroaromatic compounds while a different Tune method, "HMX.LCQTune" (**Table 2-2**), was used for the analysis of both the nitramines and nitrate esters. The main differences in the methods are the lower ESI source voltage

and heated capillary voltage, used to minimize fragmentation for the nitroaromatic compounds, and the precise values for the various lenses.

TABLE 2-1: Parameters for TNT.LCQTune Method

| Parameter | Value |
|---|---|
| Source Voltage (kV) | - 3.50 |
| Sheath Gas Flow Rate (arb.) | 80 |
| Auxiliary Gas Flow Rate (arb.) | 30 |
| Capillary Voltage (V) | - 4.00 |
| Capillary Temp (C) | 200 |
| Tube/Gate Lens (V) | - 83.0 |
| Tube Lens Offset (V) | 15.0 |
| Octapole 1 Offset (V) | 3.0 |
| Octapole 2 Offset (V) | 7.0 |
| Interoctapole Lens Voltage (V) | 14.0 |
| Trap DC Offset (V) | 10.0 |

Note: The values were obtained by running a "tune" on the different nitroaromatic compounds in the LCQ Tune Plus window and determining the average values which gave the greatest intensity for the $[M-H]^-$ or $M^-$ ion of the explosive.

TABLE 2-2: Parameters for HMX.LCQTune Method

| Parameter | Value |
|---|---|
| Source Voltage (kV) | - 3.75 |
| Sheath Gas Flow Rate (arb.) | 80.00 |
| Auxiliary Gas Flow Rate (arb.) | 30.00 |
| Capillary Voltage (V) | - 17.00 |
| Capillary Temp (C) | 200.0 |
| Tube/Gate Lens (V) | - 48.00 |
| Tube Lens Offset (V) | 50.00 |
| Octapole 1 Offset (V) | 1.00 |
| Octapole 2 Offset (V) | 5.50 |
| Interoctapole Lens Voltage (V) | 14.00 |
| Trap DC Offset (V) | 10.00 |

Note: The values were obtained by running a "tune" on RDX, HMX, and PETN in the LCQ Tune Plus window and determining the average values that gave the greatest intensity for the $[M-H]^-$ ion.

Samples

Three classes of nitro explosives were investigated for amenability to negative-ESI-MS. These compound classes were the nitroaromatic compounds, which contain a C-$NO_2$ group, nitramines, which contain a C-N-$NO_2$ group, and nitrate esters, which contain a C-O-$NO_2$ group. The nitroaromatic compounds investigated, as shown in **Figure 2-1**, include: 2,4,6-trinitrotoluene (TNT), MW 227; 2,6-dinitrotoluene (2,6-DNT), MW 182; 2-amino-4,6-dinitrotoluene (2A-4,6-DNT), MW 197; 4-amino-2,6-dinitrotoluene (4A-2,6-DNT), MW 197; 1,3,5-trinitrobenzene (TNB), MW 213; 2,4,6-trinito-*m*-cresol (TNC); tetryl, MW 287; 2,4,6-trinitroaniline (picramide), MW 228; and 1,3,5-trinitronaphthalene (TNN), MW 263. The nitramines investigated, as shown in **Figure 2-2**, included 1,3,5-trinitro-1,3,5,-triazacyclohexane (RDX), MW 222; and 1,3,5,7-tetranitro-1,3,5,7-tetrazacyclooctane (HMX), MW 296. One nitrate ester, pentaerythritol tetranitrate (PETN), MW 316 (**Figure 2-2C**), was investigated. All explosives, except for 2A-4,6-DNT and 4A-2,6-DNT, were provided by Dr. Jehuda Yinon of the Weizmann Institute of Science, and obtained from the Analytical Laboratory of the Israeli Police Headquarters. The 2A-4,6-DNT and 4A-2,6-DNT samples were provided by Dr. Fred Volk of the Fraunhofer Institute of Chemical Technology, Germany.

All samples were acquired in a crystalline form from one of our two collaborators. The samples were initially dissolved in acetone to a concentration of approximately 1000 to 2000 ppm (1-2 mg/mL). The samples were then diluted to a concentration of approximately 10 to 30 ppm in a 50% HPLC-grade isopropanol (IPA): 50% HPLC-grade water ($H_2O$) solution (v/v), with 0.1% ammonium hydroxide ($NH_4OH$) (**Table 2-3**).

Other solvent systems, including those using methanol (MeOH), acetonitrile (ACN), higher percentages of IPA, and higher percentages of $NH_4OH$, were examined. We have previously shown that negative-ESI of explosives from a solution of 50% MeOH: 50% $H_2O$ water produces mostly $M^-$ ions for TNT and results in a lot of fragmentation and adduct ion formation for TNT, RDX, and HMX [Yinon et al., 1997]. The solvent system used in this work was chosen because it allows for the greatest ionization efficiency and the production of the most intense $[M-H]^-$ ion, with limited fragmentation and adduct ion formation. Acetone was used to rinse all syringes between the analysis of different compounds.

TABLE 2-3: Concentration of Explosives Analyzed by ESI-MS

| Explosive | Concentration (ppm) |
|---|---|
| TNT | 18 |
| 2,6-DNT | 22 |
| 2A-4,6-DNT | 17 |
| 4A-2,6-DNT | 18 |
| TNB | 20 |
| TNC | 35 |
| Tetryl | 10 |
| Picramide | 23 |
| TNN | 13 |
| RDX | 19 |
| HMX | 16 |
| PETN | 17 |

Note: Each explosive was diluted in a 50% IPA: 50% $H_2O$ solution (v/v), with 0.1% $NH_4OH$ to be interrogated individually by negative-ESI-MS and MS/MS.

## Results and Discussion

### Nitroaromatic Compounds

#### TNT

TNT is one the most widely used military high explosives for a variety of reasons, including its relative stability, non-hygroscopic nature, and relative insensitivity to impact, friction, shock, and electrical energy [Yinon, 1999]. As a result, the analysis of TNT was a main focal point of this investigation. The ESI-MS spectrum of TNT (**Figure 2-3A**) shows the production of two molecular ions from the ESI of TNT including the $[M\text{-}H]^-$ ion at m/z 226 and the $M^-$ ion at m/z 227. The appearance of both the $[M\text{-}H]^-$ and $M^-$ ions for TNT in the ESI mass spectrum is of concern because negative-ESI generally produces only the $[M\text{-}H]^-$ ion (the deprotonated analyte molecule). The ratio of the $[M\text{-}H]^-$ ion to $M^-$ ion is influenced by the pH of the solution. A higher percentage of $NH_4OH$ in the analytical solution produces a greater abundance of the $[M\text{-}H]^-$ ion. Also, various instrumental conditions (e.g., capillary voltage and tube lens offset) can be altered to affect the ratio of the two ions. As a result, the mass spectrum varies based on both solution and instrumental conditions. Other intense ions appear at nominal m/z of 197, 210, 283 and 284. The ions at m/z 197 and 210 are fragment ions of TNT, which must form either during the ionization or desolvation processes in the heated capillary.

The ions at m/z 283 and 284 are suspected to be adduct ions of TNT related to the use of acetone to initially dissolve the sample and as a rinsing solvent for the syringe. To prove this hypothesis, a sample of TNT was dissolved at a concentration of 1800 ppm in acetonitrile. The sample was then diluted to a concentration of 18 ppm in the same solvent system used for all other ESI-MS experiments, a solution of 50% IPA: 50% $H_2O$ (v/v), with 0.1% $NH_4OH$. The negative-ESI mass spectrum for this sample (**Figure 2-**

**3B**) shows that the adduct ions at m/z 283 and 284 are absent in this spectrum. This would seem to support the belief that the adduct ions are related to the use of acetone. It is also noted that the ratio of the $[M-H]^-$ ion relative to the $M^-$ ion has been increased. The overall sensitivity is decreased for the analysis of TNT and other explosives using acetonitrile solvent as the initial solvent because the explosives do not dissolve as completely in acetonitrile as they do in acetone [Yinon and Zitrin, 1993].

Daughter ion MS/MS experiments were conducted for the ions at m/z 226 and 227. The daughter ion spectrum for the $[M-H]^-$ ion of TNT is presented in **Figure 2-4A**. The CID of the $[M-H]^-$ ion of TNT produces a variety of daughter ions. The three main daughter ions occur at m/z 196, a neutral loss of 30 that corresponds to a loss of NO, at m/z 183, a neutral loss of 43 that corresponds to the loss of both an NO and CH, and at m/z 166, a neutral loss of 60 corresponding to the loss of 2 NO. The daughter ions detected and their associated fragmentation pathways are consistent with those observed in the CID of the $M^-$ ion produced via negative-CI [Yinon and Zitrin, 1993]. The daughter ion mass spectrum of the $M^-$ ion of TNT produced by negative-ESI (**Figure 2-4B**) depicts a slightly different fragmentation pattern from that observed for the $[M-H]^-$ ion. The major fragment ion for the $M^-$ ion is a daughter ion at m/z 210, which corresponds to the neutral loss of 17 amu (OH). While there are no OH groups in the chemical structure of TNT, the $M^-$ ion loses the OH via a rearrangement reaction that involves the hydrogen on the methyl group and the adjacent oxygen on the nitro group [Yinon and Zitrin, 1993]. The CID of the $M^-$ also produces a daughter at m/z 197, corresponding to the neutral loss of 30 amu (NO), and other, less intense daughter ions that are complimentary to those produced from the CID of the $[M-H]^-$ ion of TNT.

To confirm the identity of the ions at m/z 283 and 284 ions, a daughter ion mass spectrum of each ion was acquired (**Figures 2-5A and 2-5B**). The ion at m/z 284 is suspected to be the $[M+Acetone-H]^-$ ion, or $[M+C_2H_5CO]^-$ ion, of TNT, while the identity of the other ion is not readily determined. The ion at m/z 284 was confirmed as an adduct ion of TNT through the daughter ion MS/MS experiment. The CID of the ion produced fragment ions at m/z 226, corresponding to the loss of the acetone adduct molecule. The CID of the ion at m/z 283 did not produce an ion that is readily identified as being from TNT. However, in the comparison of the two daughter ion mass spectra for m/z 283 and 284, the CID fragmentation of the two ions produce daughter ions with the same neutral losses, suggesting that the two ions are related. The two neutral losses are of 47 amu ($HNO_2$) and 65 amu ($HNO_2 + H_2O$).

TNT analogs

The first of the TNT analogs presented is picramide (**Figure 2-1H**). Picramide has a very similar structure to TNT, with the methyl group being replaced with an amine group. The negative-ESI of picramide produces a mass spectrum (**Figure 2-6**) very similar to that of TNT. The major ions are the $[M-H]^-$ ion at m/z 227, the $M^-$ ion at m/z 228, and the $[M+Acetone-H]^-$ adduct ion at m/z 285, as well as another related ion at m/z 284. The ESI mass spectrum shows an absence of fragmentation during the ionization and desolvation processes for picramide, as was evident in the TNT mass spectrum.

The CID of both the $[M-H]^-$ and $M^-$ ions produce complimentary MS/MS spectra. The daughter ion mass spectrum of the $[M-H]^-$ ion of picramide (**Figure 2-7A**) shows characteristic neutral losses, some of which are similar to those observed for the $[M-H]^-$ ion of TNT. The major daughter ion is at m/z 197, which corresponds to the neutral loss of 30 amu (NO). The second most intense daughter ion is at m/z 210 and corresponds to

the loss of an OH (17 amu), which occurs via a rearrangement reaction [Yinon and Zitrin, 1993]. Comparison of the two daughter ion spectra of the $[M-H]^-$ ions of TNT and picramide (**Figures 2-4A** and **2-7A**) shows that many of the fragment ions are the result of the same neutral losses. The subsequent daughter ions are shifted one amu higher in the picramide spectrum corresponding to the difference in mass between the amine group and methyl group on the two molecules. Some of the minor daughter ions include a daughter ion at m/z 184, which corresponds to the loss of a NO and CH, and at m/z 167, corresponding to the neutral loss of 60 amu (2 NO). The $[M-H]^-$ of picramide does undergo a loss of an OH, unlike the $[M-H]^-$ ion of TNT. The daughter ion spectrum of the $M^-$ ion of picramide (**Figure 2-7B**) shows the neutral loss of 17 amu (OH) and 30 amu (NO), which are the same neutral losses in the daughter ion spectrum of the $M^-$ ion of TNT.

The second TNT analog is trinitronaphthalene (TNN) (**Figure 2-1I**). TNN is a potential byproduct in the synthesis of TNT, but has minimal use as a high explosive. It was investigated to assist in the understanding of the ESI process for the TNT analogs. The negative ESI of TNN produces a complex mass spectrum (**Figure 2-8**) that has a variety of molecular, fragment, and adduct ions. Like the ESI of both TNT and picramide, the negative ESI of TNN produces both the $[M-H]^-$ ion, at m/z 262, and the $M^-$ ion at m/z 263. Fragmentation of the TNN molecular ion, during either the ionization or desolvation process, produces fragment ions at m/z 217, resulting from the loss of a $NO_2$, and at m/z 233, resulting from the loss of a NO. The ion at m/z 320 is suspected to be the $[M+Acetone-H]^-$ adduct ion.

The CID of both the $[M-H]^-$ and $M^-$ ions produce complimentary MS/MS spectra. The daughter ion mass spectrum of the $[M-H]^-$ ion of TNN (**Figure 2-9A**) shows characteristic neutral losses, some of which are similar to those observed for the $[M-H]^-$ ion of TNT and picramide. The major daughter ion is at m/z 232, which corresponds to the neutral loss of 30 amu (NO). The second most intense daughter ion is at m/z 204 and corresponds to the loss of 58 amu, which is presumably the step wise loss of both a $C_2H_4$ and NO. The daughter ion mass spectrum of the $M^-$ ion of TNN produces characteristic neutral losses of 30 amu (NO) and 46 amu ($NO_2$). There is not a neutral loss of 17 amu, as seen in the CID of the $M^-$ ion of both TNT and picramide, because there is not a methyl or amine adjacent to a nitro group to allow for the necessary rearrangement to occur.

The daughter ion mass spectrum of the adduct ion at m/z 320 (**Figure 2-10**) is a very complex mass spectrum. There appears to be a multitude of fragmentation pathways that occur during the CID process of this ion, although some of the fragment ions are similar to those produced from the CID of the $[M+Acetone-H]^-$ adduct ions of TNT and picramide. The major daughter ions of m/z 320 are at m/z 273, 243, 263, and 290. The ion produced at m/z 273 is the result of the loss of $HNO_2$ (47 amu) and the ion at m/z 263 is the result of the loss of the acetone adduct, both of which are seen for the CID of the $[M+Acetone-H]^-$ adduct ions of TNT and picramide. The ion at m/z 290 results from the neutral loss of 30 amu from the adduct ion. This neutral loss, while indicative of nitroaromatic compounds, was not observed for $[M+Acetone-H]^-$ adduct ions of TNT and picramide.

The negative-ESI of trinitrocresol, TNC, (**Figure 2-1F**) produced the simplest mass spectrum (**Figure 2-11A**) of all of the TNT analogs. TNC has an OH group on the aromatic ring of the molecule, which is readily deprotonated in solution. As a result, TNC preferentially produces the $[M-H]^-$ ion via negative-ESI at m/z 242. The CID of the $[M-H]^-$ ion of TNC produces a daughter ion mass spectrum (**Figure 2-11B**) with two major daughter ions at m/z 225 and 212. The most intense ion, at m/z 225, results from the neutral loss of 17 amu (OH). The next most intense daughter ion, at m/z 212, results from the neutral loss of 30 amu (NO). Other daughter ions are produced from the neutral losses of 18 amu, which corresponds to the loss of an $H_2O$, and a neutral loss of 29 amu, which corresponds to the loss of a CHO from the two constituents on the TNC molecule.

The last of the TNT analogs is tetryl (**Figure 2-1G**). The negative-ESI mass spectrum for this explosive, acquired in profile mode, (**Figure 2-12A**) is the most complex of all of the TNT analogs. The major ions in this spectrum are at m/z 344 and 241. The ion at m/z 344 is the $[M+Acetone-H]^-$ ion of tetryl and the ion at m/z 241 is the $[M-H]^-$ ion of N-methylpicramide, a hydrolysis product of tetryl in which the $NO_2$ on the amine nitrogen is replaced with an H. Two minor ions of interest are at m/z 286, which is the $[M-H]^-$ ion of tetryl, and at m/z 268, which is the $[M-H-H_2O]^-$ ion of tetryl. The daughter ion mass spectrum of the ion at m/z 344, acquired in profile mode, (**Figure 2-12B**) shows that the dissociation of the ion produces fragment ions indicative of tetryl, including the ions at m/z 268, corresponding to the neutral loss of 76, which is the successive loss of acetone and $H_2O$, and 286, corresponding to the neutral loss of 58, which is the loss of acetone. The daughter ion at m/z 250, a neutral loss of 94, corresponds to the successive losses of the acetone molecule and 2 $H_20$. The daughter

ion at m/z 241, corresponding to a neutral loss of 103, is suspected to be the loss of $C_3H_5O$ (from acetone) and a $NO_2$.

The daughter ion mass spectrum of the $[M-H]^-$ ion of tetryl, acquired in profile mode, (**Figure 2-13A**) shows a dominant CID fragment ion at m/z 240, a neutral loss of 46. This neutral loss is suspected to result from the loss of the $NO_2$ group on the amino nitrogen rather than the nitro group on the ring, which is suported by the $MS^3$ mass spectrum of the daughter ion at m/z 240 produces a (**Figure 2-13B**). This daughter ion mass spectrum shows a greater amount of structural information pertaining to the $[M-H]^-$ ion of tetryl. The mass spectrum shows the successive neutral losses of 17 amu, corresponding to the losses of OH, to produce the daughter ions at m/z 223 and 206. The ion at m/z 195, a neutral loss of 45, is suspected to be either the direct loss of $H_3CNO$ or successive losses of $H_2O$ and HCN. The ions produced at m/z 193, a neutral loss of 47, and at m/z 163, a neutral loss of 77, are the sequential losses of NO and 2 NO after the loss of an OH.

Tetryl is known to undergo a hydrolysis reaction and produce N-methylpicramide (**Figure 2-14A**) as the product. N-methylpicramide has a site that is readily deprotonated in solution (the H on the amine N). As a result, the negative-ESI of N-methylpicramide preferentially produces an $[M-H]^-$ ion at m/z 241. The daughter ion mass spectrum of the $[M-H]^-$ ion of N-methylpicramide, acquired in profile mode, (**Figure 2-14B**) shows that the major fragment ion is the ion at m/z 213. This ion results from the loss of a $CH_2N$, a neutral loss of 28 amu, from the deprotonated ion leaving the base trinitrobenzene ion. Other neutral losses of 60 amu, to produce the ion at m/z 181, and 47 amu, to produce the ion at m/z 194, correspond to the losses of 2 NO and $HNO_2$, respectively. Other, less

intense daughter ions result from the neutral losses of 18 amu, $H_2O$, to produce an ion at m/z 223, and 78 amu, corresponding to the loss of 2 NO and $H_2O$, to produce an ion at m/z 163.

TNT precursors and degradation products

In the synthesis of 2,4,6-TNT, the most common and energetic of the TNT isomers, the penultimate step in the production process is the synthesis of the 2,6-DNT isomer [Cooper and Kurowski, 1996]. As a result, the 2,6-DNT isomer is the most abundant impurity in TNT and is of concern in both forensic and analytical applications. The negative-ESI mass spectrum of 2,6-DNT (**Figure 2-15A**) shows the production of the $[M-H]^-$ ion at m/z 181. The mass spectrum is dominated by the production of the $[M-H]^-$ ion and there is neither an intense $M^-$ ion or adduct ion. The daughter ion mass spectrum of the $[M-H]^-$ ion (**Figure 2-15B**) shows two major daughter ions at m/z 151 and 89. The ion at m/z 151 results from a neutral loss of 30 amu, corresponding to the loss of NO. The daughter ion at m/z 89, corresponding to a neutral loss of 92, results from the loss of both $NO_2$ groups. Other, minor daughter ions are visible at m/z 135, which results from the loss of $NO_2$, at m/z 121, which results from the loss of 2 NO, and at m/z 116, which results from the loss of $H_2O$ and $HNO_2$. Each of these daughter ions correspond to those detected in CI-MS/MS experiments [Yinon and Zitrin, 1993].

The two main biodegradation products of 2,4,6-TNT are 2A-4,6-DNT and 4A-2,6-DNT (**Figure 2-1C and D**), which arise from the reduction of one nitro group to an amine. Both of these compounds were investigated for their amenability to negative-ESI and CID fragmentation patterns. The negative-ESI mass spectrum of both 2A-4,6-DNT (**Figure 2-16A**) and 4A-2,6-DNT (**Figure 2-17A**) indicate that both compounds preferentially from the $[M-H]^-$ ion at m/z 196, without any fragmentation or formation of

either an $M^-$ or adduct ion. The $[M-H]^-$ ion is readily formed because the deprotonation at the amine site can be stabilized and is favorable in solution. The CID fragmentation pattern of the two $[M-H]^-$ ions are slightly different. The daughter ion mass spectrum of both the 2A-4,6-DNT $[M-H]^-$ ion (**Figure 2-16B**) and the 4A-2,6-DNT $[M-H]^-$ ion (**Figure 2-17B**) show that the four major daughter ions for both parent ions are at m/z 166, 136, 149, and 179. The ion at m/z 166 results from the loss of a NO (30 amu) and the ion at m/z 136 results from the neutral loss of 2 NO (60 amu). The two ions at m/z 179 and 149 result from the loss of OH (17 amu) and $HNO_2$ (47 amu), respectively. The loss of the OH results from the same rearrangement that facilitates the loss of the OH from TNT and picramide. The main difference in the mass spectra is the relative abundance of the daughter ions at m/z 136 and 149. Because of the proximity of the $NO_2$ groups to the methyl group on 4A-2,6-DNT, the loss of 47 ($HNO_2$) is more favorable than the loss of 2 NO as compared to 2A-4,6-DNT.

The last of the TNT precursors is trinitrobenzene, TNB, which is a synthesis byproduct caused by the incomplete methylation of the aromatic ring during the synthesis of TNT [Urbanski, 1964]. The negative-ESI mass spectrum of TNB (**Figure 2-18A**) shows the production of three major ions. The base peak is at m/z 213, which is the $M^-$ ion of TNB. The other ions produced include the ion at m/z 183, which is a fragment ion resulting from the loss of NO, and the ion at m/z 270, which is the $[M+Acetone-H]^-$ adduct ion. The daughter ion mass spectrum of the $M^-$ ion of TNB (**Figure 2-18B**) shows only the neutral loss of 30 amu, due to the loss of a NO. The daughter ion mass spectrum of the $[M-NO]^-$ ion (**Figure 2-19A**) includes the fragments at m/z 153, a neutral loss of 30 amu (NO), at m/z 125, a neutral loss of 58 (NO + CO) and 95, a neutral loss of 88

(2NO + CO). These fragment ions are also produced from the $MS^3$ experiment for the CID of the daughter ion, at m/z 183, of the parent ion at m/z 213. The daughter ion mass spectrum for the $[M+Acetone-H]^-$ adduct ion (**Figure 2-19B**) shows major daughter ions at m/z 223, which is the neutral loss of $HNO_2$, and m/z 213, which is the neutral loss of a part of the acetone adduct ($C_3H_5O$). The $[M-H]^-$ ion of TNB, at m/z 212, from the neutral loss of the intact acetone is also produced from the CID of the adduct ion.

Nitramines

The first of the two nitramines to be discussed is HMX, which is used as a component in solid-fuel rocket propellants and as a burster charge in artillery shells. The negative-ESI mass spectrum of HMX (**Figure 2-20A**) shows three major ions at m/z 295, 357, and 399. The base peak, at m/z 295, is the $[M-H]^-$ ion, while the other two major ions are adduct ions of HMX. The ion at m/z 357 is the $[M+NO_3-H]^-$ adduct ion, while the ion at m/z 399 is the $[M+103]^-$ adduct ion. There is either an impurity or degradation product in the HMX, RDX, and PETN samples that produces an ion at m/z 103. The identity of this degradation product ion is suspected to be $NCH_2N(NO_2)CH_3^-$ and it probably arises from a degradation product of both RDX and HMX. No mass spectra have been obtained which conclusively prove this suspicion, but it has been also independently determined by scientists at the FBI analytical laboratory [D.D.Fetterolf, personal communication, 1999].

The daughter ion mass spectrum of the $[M-H]^-$ ion of HMX (**Figure 2-20B**) shows the production of four daughter ions. To acquire the daughter ion mass spectra, the isolation window for isolation was opened to a width of 5.5 amu in order to obtain sufficient intensity (see Chapter 3 for a discussion of fragile ions and their isolation). The two most intense daughter ions result from the loss of $N(NO_2)CH_2$, a neutral loss of 74

amu to produce the daughter ion at m/z 221, and the loss of 2 $N(NO_2)CH_2$ (148 amu) to produce the daughter ion at m/z 147. Daughter ions are also observed from the neutral loss of $NO_2$ (46 amu). The daughter ion mass spectra of the two adduct ions at m/z 357 (**Figure 2-21A**) and 399 (**Figure 2-21B**) illustrate that the two adduct ions readily lose the adduct molecule ($NO_3$ or 104) to form the $[M-H]^-$ of HMX, which then fragments by loss of one or two $N(NO_2)CH_2$ and, to a lesser extent, the loss of two $NO_2$.

The second of the two nitramines to be discussed is RDX. RDX is an important military explosive and is used as a booster in various military munition formulations. Because of potentially severe health effects, RDX is also of concern in environmental applications [Yinon, 1999]. The negative-ESI of RDX produces a low intensity $[M-H]^-$ ion, as well as a $[M+NO_3-H]^-$ ion and a $[M+103]^-$ ion (**Figure 2-22A**). It was challenging to obtain a daughter ion mass spectrum of either the $[M-H]^-$ ion or the $[M+NO_3-H]^-$ ion, as the isolation for each ion was very difficult. The $[M+103]^-$ ion at m/z 325 was readily isolated at a m/z of 3 amu. The daughter ion mass spectrum of the $[M+103]^-$ ion (**Figure 2-22B**) showed the loss of the adduct neutral (104) to form the $[M-H]^-$ ion of RDX, at m/z 221, and a commonly observed daughter ion, at m/z 93. The ion at m/z 93 has been observed in the ESI-MS/MS spectra for other ions of RDX, including the $[M-H]^-$ at m/z 221 and other RDX adduct ions.

Nitrate Ester

The only nitramine interrogated for this study was PETN. PETN is often used in blasting caps and detonators and as the core explosive in commercial detonating cord and plastic explosives [Yinon and Zitrin, 1993]. PETN is a possible environmental contaminant through the disposal of PETN-contaminated water into rivers and streams and the dumping of obsolete explosives into landfill sites [Yinon, 1999]. The negative-

ESI mass spectrum of PETN (**Figure 2-23A**) shows the production of a weak $[M-H]^-$ ion at m/z 315, a weaker $[M+Cl]^-$ ion at m/z 357 (the ion at m/z 359, also the $[M+Cl]^-$ ion, is lost in the noise) and two more intense ions at m/z 377 and 419. The ion at m/z 377 is the $[M+NO_3-H]^-$ ion and the ion at m/z 419 is the $[M+103]^-$ ion. Daughter ion mass spectra of these ions were difficult to obtain because it was necessary to extensively widen the isolation window in order to obtain adequate isolated ion intensity. The best daughter ion mass spectrum was obtained for the $[M+NO_3-H]^-$ ion at m/z 377 (**Figure 2-23B**), which required an isolation width of 7.0 amu. Because of the wide isolation window, all of the daughter ions in the spectrum can not be directly attributed to the parent ion of interest. However, the mass spectrum does show that CID of the $[M+NO3-H]^-$ ion did produce the $[M-H]^-$ ion of PETN.

Negative-ESI-MS Analysis and Conclusion

For the negative-ESI analysis of explosives, the production of analyte ions is of great concern. For most compounds analyzed by ESI, ions are preformed in solution by controlling the pH (i.e. by deprotonation to form $[M-H]^-$ ions or by protonation to form $[M+H]^+$ ions). Because of their chemical structure and their inability to be easily deprotonated or protonated in solution, explosives are not classically amenable to ESI; therefore electrochemical processes (redox) may play a part in ion production [Van Berkel, 1997]. As a result of the electrochemical processes involved in droplet and ion formation, ESI can be viewed as a special kind of electrolytic cell [Kebarle, 1993; Van Berkel and Zhou, 1995]. These electrochemical processes may play a keynote part in the ionization of many of the explosives investigated. During the negative-ESI process, reduction occurs at the ESI neddle tip and may potentially aid in the ionization of these

explosives. In previous work [Yinon et al., 1997], it was shown that negative-ESI of explosives produces a wide array of molecular ions (both $[M-H]^-$ and $M^-$ ions), adduct ions (e.g. $[M+NO_2-H]^-$ and $[M+CH_2ONO_2-H]$) and fragment ions (e.g. $[M-CH_2]^-$ and $[M-NO]^-$) in a slovent system of 50% MeOH : 50% $H_2O$ and 100% MeOH. Using a solvent system containing 50% IPA, 50% $H_2O$, and 0.1% $NH_4OH$, we have attempted to minimize both the adduct ion and fragment ion formation and drive the ionization towards the production of the $[M-H]^-$ ion. However, in even the most optimum of conditions, this is not always possible.

For the nitroaromatic compounds, there is a clear competition between the production of the $M^-$ and $[M-H]^-$ ion via negative-ESI. Among the nitroaromatic compounds, TNT and two of its analogs, picramide and trinitronaphthalene (TNN), produce both a $M^-$ and $[M-H]^-$ ion. From this, we can suppose that the $M^-$ ion is produced via a redox reaction and that the $[M-H]^-$ ion may be formed by the deprotonation of the analyte in solution. An alternate method of ionization may be a two-step mechanism where an adduct ion is first produced, followed by the loss of the neutral adduct molecule, leaving the charge on the nitroaromatic compound. The daughter ion spectra of the $[M-H]^-$ and $M^-$ ions depict some of the same fragment ions, but different dissociation pathways are favored for the two different molecular ions. The negative-ESI of these explosives also results in the formation of $[M+Acetone-H]^-$ adduct ions, which complicate the MS analysis of these explosives. The negative-ESI of trinitrocresol (TNC) preferentially produces the $[M-H]^-$ ion and no adduct ions. The only difference in structure between TNT and TNC is the addition of an OH group at 3-position on the aromatic ring for TNC. This difference, however, makes a big difference in the ESI

amenability of these compounds. The addition of the OH on the aromatic ring provides a site for deprotonation in negative-ESI and results in the production of a clean MS spectrum dominated by the [M-H]- ion and no adduct, fragment, or $M^-$ ions.

The negative-ESI-MS analysis of tetryl is complicated by the hydrolysis of the compound to produce N-methylpicramide. Therefore, the mass spectrum is populated by ions from both of the two compounds. While the hydrolysis reaction has been documented to occur in solution [Yinon and Zitrin, 1993], it is also suspected to occur at the ESI needle. LC/ESI-MS experiments have documented that even if N-methylpicramide and tetryl are be chromatographically resolved, the mass spectrum for the tetryl peak still shows the production of the $[M-H]^-$ ion of N-methylpicramide. Neither the production of the $M^-$ or the $[M-H]^-$ ion of tetryl is especially favored via negative-ESI. Therefore, the intense ions of tetryl are generally either adduct or fragment ions.

The negative-ESI mass spectra of the nitroaromatic compounds that have been classified as precursors and degradation products also produce varied mass spectra. The negative-ESI of the major impurity in TNT, the 2,6-DTNT isomer, produces a mass spectrum that is dominated by the $[M-H]^-$ ion of the compound at m/z 181. Presumably, DNT is not being deprotonated in solution, and another ionization method is dominating the ESI process. There appears to be little production of the $M^-$ ion or adduct ions. The negative-ESI mass spectra of the 2A-4,6-DNT and 4A-2,6-DNT show that the production of the $[M-H]^-$ ion also dominates the ionization mechanism of these compounds. The amine site, at either the 2- or 4-position on the aromatic ring, provides a deprotonation site that can allow the $[M-H]^-$ ion to be formed. No adduct ions were detected for these

analytes either. The negative-ESI of the synthesis precursor TNB produces ions at m/z 183, [M-NO]-, m/z 213, $M^-$, and m/z 270, $[M+Acetone-H]^-$. There is a very minor and low intensity ion formed at m/z 212, which would correspond to the $[M-H]^-$ ion. The lack of an intense $[M-H]^-$ ion and a dominant fragment and adduct ion arises from the lack of a deprotonation site on the molecule. Unlike the other nitroaromatic compounds such as the TNT, TNC, and A-DNT molecules, there are no hydrogens available for removal, except for those on the aromatic ring, which would be very difficult to remove.

The negative-ESI mass spectra of RDX, HMX, and PETN show that these analytes behave very similarly during the ionization process. They each produced a $[M-H]^-$ ion, a $[M+NO_3-H]^-$ adduct ion, and a $[M+103]^-$ adduct ion via negative-ESI. The ESI of the nitramines and nitrate esters is particularly susceptible to any impurities in the system. These compounds readily form adduct ions with a wide variety of impurities that may be in the system, including propionate, formate, chloride, nitrite, or nitrate (See Chapter 5). The spectra presented here were acquired under the cleanest of conditions, yet there is still the adduct ion at $[M+103]^-$ for each of the compounds. The impurity which produces the ion at m/z 103 can be viewed in the mass spectrum of each and is suspected to either be an additive in the sample or a degradation product that may occur either in solution or during the ESI process. When acquired in profile mode, some of the peaks in the full scan negative-ESI mass spectra of HMX, RDX, and PETN appear to be broader than those in the spectra of the nitroaromatic compounds, reflecting their fragile nature (See Chapter 3).

Daughter ion mass spectra were acquired for all of the ions detected in all of the negative-ESI mass spectra for the explosives interrogated. This enabled the identification

of adduct and fragment ions by comparing the fragmentation pattern of these ions with those of the molecular ions. For the nitroaromatic compounds, an isolation width of 1.0 amu was sufficient to isolate each of the ions, including the adduct ions. However, for the nitramines and nitrate esters, an isolation width of 1.0 amu was too narrow to isolate any of the ions for interrogation by MS/MS. To obtain adequate isolation of the nitramine and nitrate ester ions, the width of isolation had to be widened to a width of at least 3.0 amu and as wide as 7.0 amu, depending on the ion. The isolation of fragile ions such as these is discussed in detail in Chapter 3.

The CID fragmentation of the nitroaromatic compounds produced rich mass spectra that provided a number of characteristic daughter ions to enable their identification. To enable accurate identification of all ions in the mass spectra, data from the literature pertaining to EI-MS and CI-MS/MS experiments were consulted. For the compounds that produced both a $[M-H]^-$ and $M^-$ molecular ion, the daughter ion mass spectra of each ion was remarkably different. Generally, all nitroaromatic compounds undergo some of the same neutral losses, the most characteristic of which is the loss of 30 amu, corresponding to the loss of NO. The CID fragmentation of the HMX ions also provided rich daughter ion mass spectra. The acquisition of daughter ion mass spectra for RDX and PETN was complicated by the need to widen the isolation width to obtain adequate isolated intensity to perform the MS/MS experiments. Also, the daughter ions produced from the CID of these ions were at a low intensity. For HMX, RDX, and PETN, the daughter ion mass spectra were generally richer for the adduct ions than the $[M-H]^-$ ion.

In this chapter, negative-ESI has been shown to produce characteristic ions, which could be employed for the analysis of explosives, including nitroaromatic compounds, nitramines, and a nitrate ester. One question, however, lies in the reproducibility of these ESI mass spectra in real-world samples due to the influence of impurities. The formation of adduct ions is greatly influenced by cleanliness and conditions of the system. Therefore, if there are impurities in the samples or in the lines, inlets, or heated capillary of the LCQ, different adduct ions may be formed. This can lead to drastic changes in the appearance of the negative-ESI mass spectra. This is most important for the analysis of the nitramines and nitrate esters because they are more susceptible to the influences of the impurities in the system. The controlled use of additives may be important for sensitive analysis of nitramines and nitrate esters due to the preference to form adduct ions at high efficiency and the richer more intense daughter ion mass spectrum which can be obtained from these ions. Ultimately, the conditions for the most accurate detection of nitroaromatic compounds by ESI-MS may be those that limit the formation of adduct ions, while the conditions for the most accurate and sensitive detection of the nitramines and nitrate esters may be those which preferentially produce one adduct ion that can be used for both ESI-MS and MS/MS analysis.

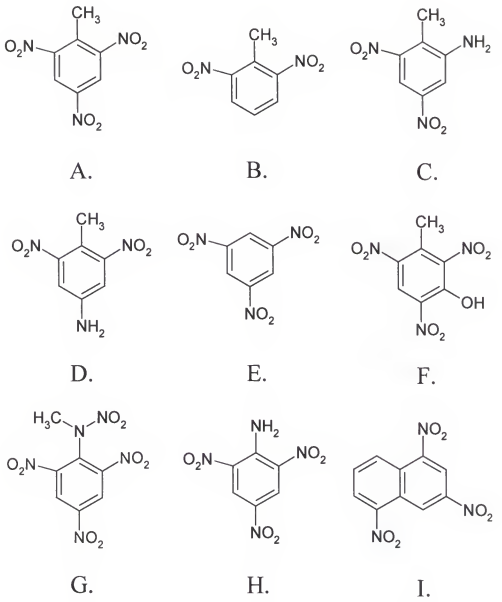


FIGURE 2-1: Chemical Structures for Nitroaromatic Compounds

A. 2,4,6-Trinitrotoluene (TNT); B. 2,6-Dinitrotoluene (2,6-DNT); C. 2-Amino-4,6-dinitrotoluene (2A-4,6-DNT); D. 4-Amino-2,6-dinitrotoluene (4A-2,6-DNT); E. 1,3,5-Trinitrobenzene (TNB); F. 2,4,6-Trinito-*m*-cresol (TNC); G. Tetryl; H. 2,4,6-trinitroaniline (picramide); I. 1,3,5-trinitronaphthalene (TNN).

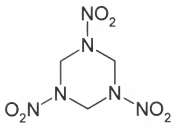


A.

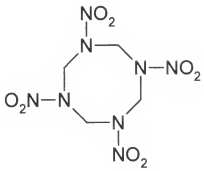


B.

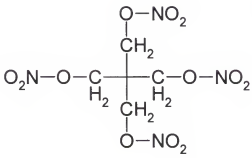


C.

FIGURE 2-2: Chemical Structures for Nitramines and Nitrate Esters

A. 1,3,5-Trinitro-1,3,5,-triazacyclohexane (RDX); B. 1,3,5,7-Tetranitro-1,3,5,7-tetrazacyclooctane (HMX); C. Pentaerythritol tetranitrate (PETN).

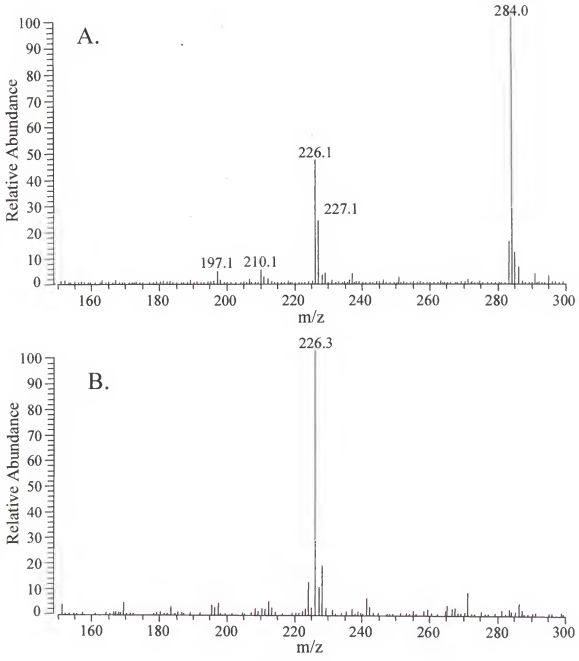


FIGURE 2-3: Negative-ESI Mass Spectra of TNT

A.. Negative-ESI mass spectrum of TNT sample initially dissolved in acetone and then diluted for MS analysis. B.. ESI mass spectrum of TNT sample initially dissolved in acetonitrile and then diluted for MS analysis. The molecular weight of TNT is 227 Da.

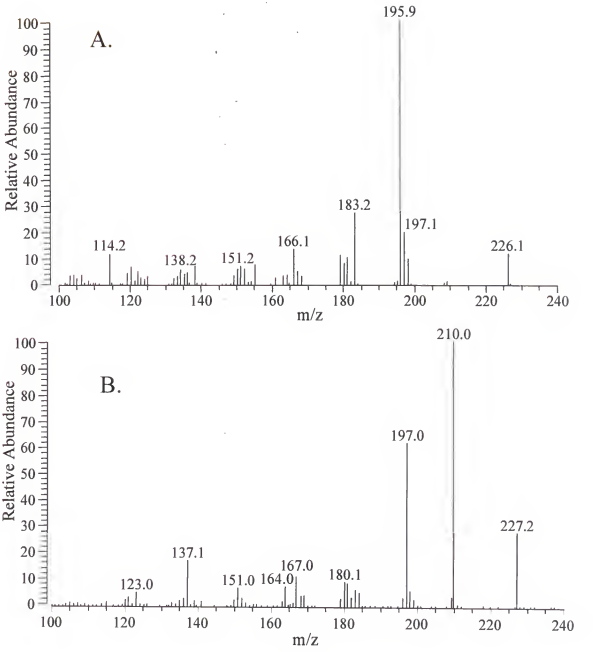


FIGURE 2-4: Daughter Ion Mass Spectra of $[M-H]^-$ and $M^-$ Ions of TNT

A.. Daughter ion mass spectrum of $[M-H]^-$ ion (m/z 226) of TNT. B.. Daughter ion mass spectrum of $M^-$ ion of TNT. Both spectra were acquired at a collision energy of 31% and a resonant excitation $q_z$ of 0.25.

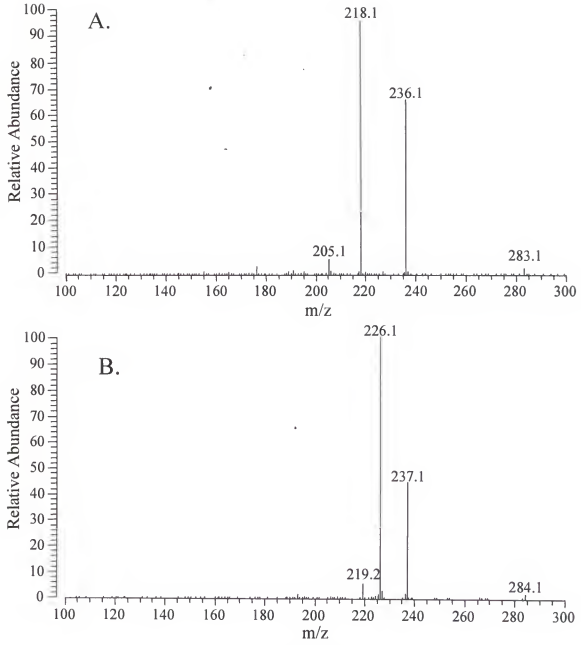


FIGURE 2-5: Daughter Ion Mass Spectra of TNT Adduct Ions

A.. Daughter ion mass spectrum of $[M+56]^-$ ion of TNT. B.. Daughter ion mass spectrum of $[M+Acetone-H]^-$ ion of TNT. Both spectra were acquired at a collision energy of 29% and a resonant excitation $q_z$ of 0.25.

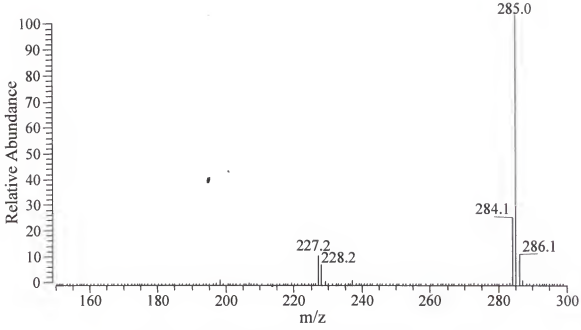


FIGURE 2-6: Negative-ESI Mass Spectrum of Picramide

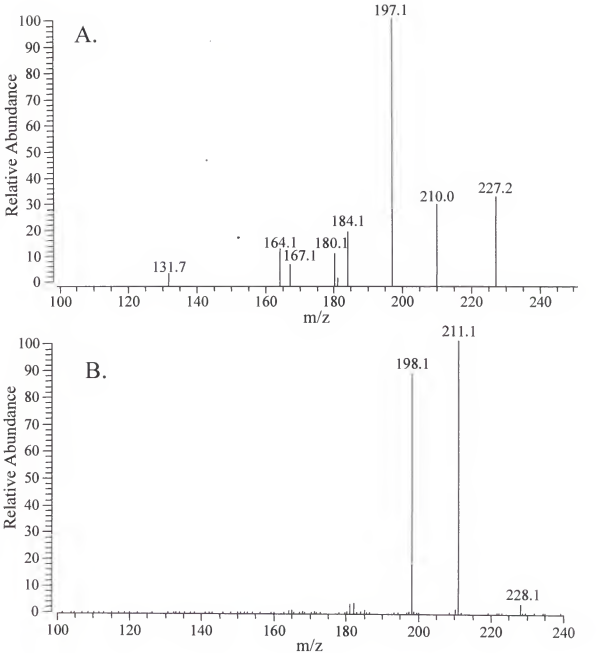


FIGURE 2-7: Daughter Ion Mass Spectra of $[M-H]^-$ and $M^-$ Ions of Picramide

A. Daughter ion mass spectrum of the $[M-H]^-$ ion (m/z 227) of picramide. B. Daughter ion mass spectrum of $M^-$ ion (m/z 228) of picramide. Both spectra were acquired at a collision energy of 33% and a resonant excitation $q_z$ of 0.25.

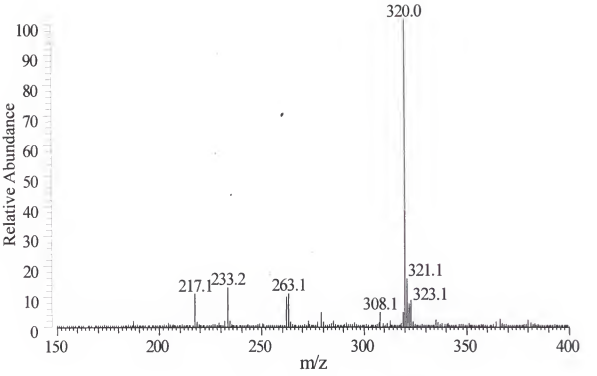


FIGURE 2-8: Negative-ESI Mass Spectrum of TNN

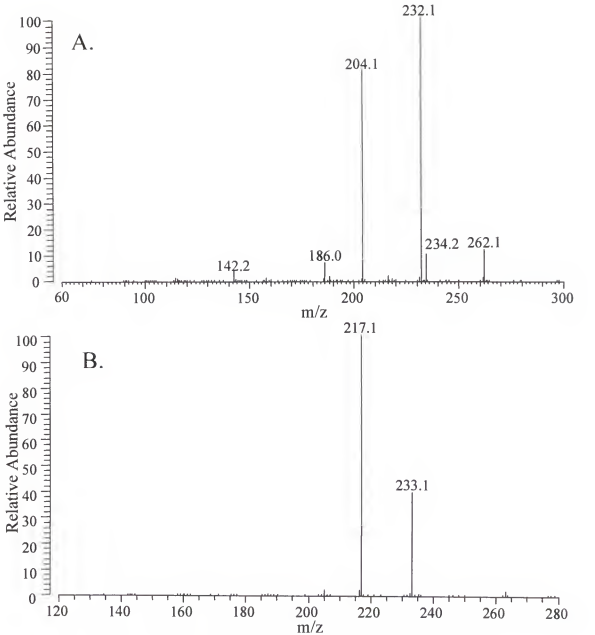


FIGURE 2-9: Daughter Ion Mass Spectra of $[M-H]^-$ and $M^-$ Ions of TNN

A. Daughter ion mass spectrum of $[M-H]^-$ ion (m/z 262) of TNN. B. Daughter ion mass spectrum of $M^-$ ion (m/z 263) of TNN. Both spectra were acquired at a collision energy of 29% and a resonant excitation $q_z$ of 0.25. The molecular weight of TNN is 263 Da.

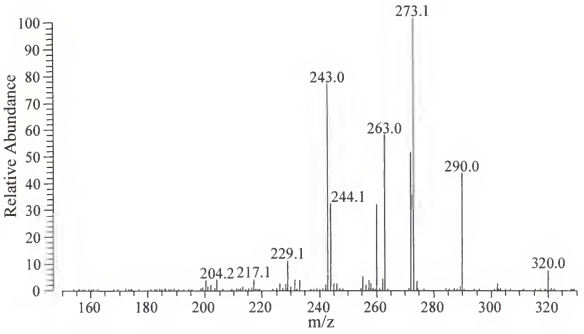


FIGURE 2-10: Daughter Ion Mass Spectrum of Adduct Ion of TNN

Daughter ion mass spectrum of $[M+ Acetone-H]^-$ ion (m/z 230) of TNN. The mass spectrum was acquired at a collision energy of 27% and a resonant excitation $q_z$ of 0.25.

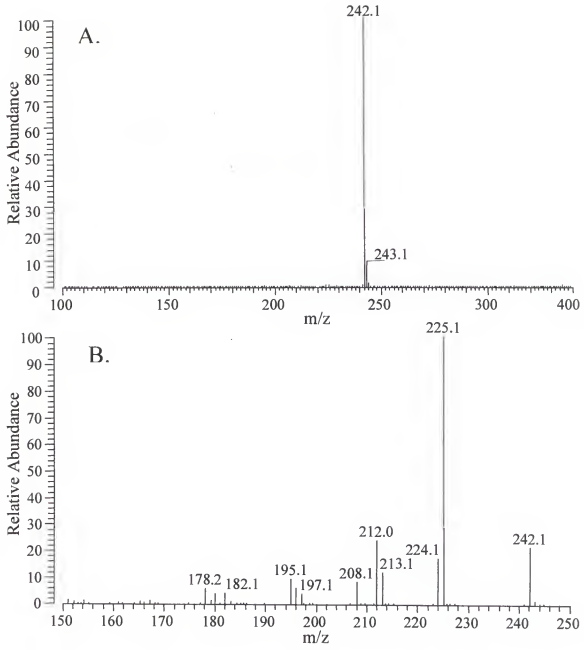


FIGURE 2-11: Negative-ESI Mass Spectrum and Tandem Mass Spectrum of TNC

A. Negative-ESI mass spectrum of TNC. The molecular weight of TNC is 243 Da. B. Daughter ion mass spectrum of $[M-H]^-$ ion (m/z 242) of TNC. The MS/MS spectrum was acquired at a collision energy of 31% and a resonant excitation $q_z$ of 0.25.

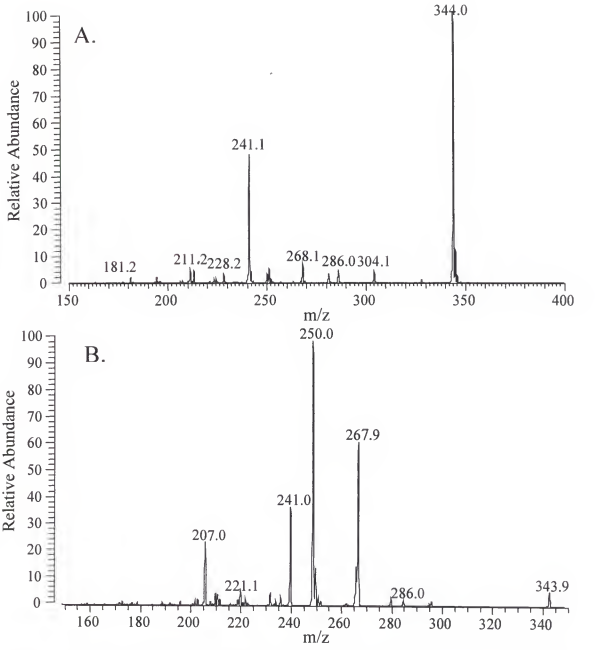


FIGURE 2-12: Negative-ESI Mass Spectrum and Daughter Ion Mass Spectrum of Tetryl

A. Negative-ESI mass spectrum of tetryl, acquired in profile mode. The molecular weight of tetryl is 287. B. Daughter ion mass spectrum of $[M+Acetone-H]^-$ ion (m/z 344) of tetryl, acquired in profile mode. The MS/MS spectrum was acquired at a collision energy of 23% and a resonant excitation $q_z$ of 0.25.

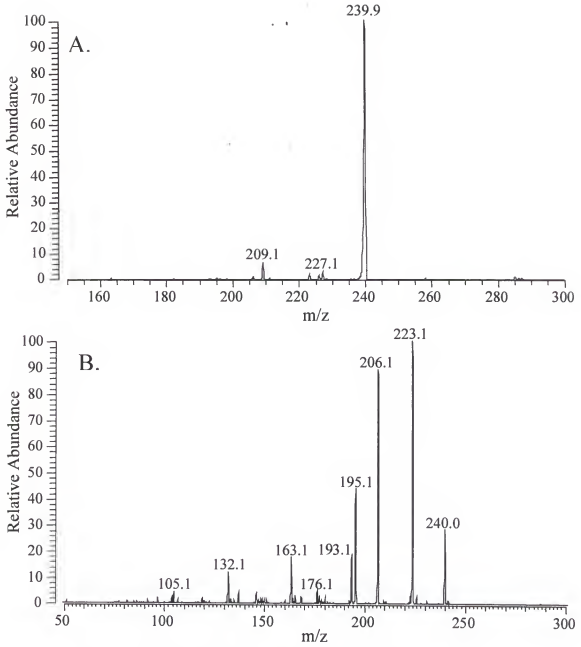


FIGURE 2-13: MS/MS and $MS^3$ Mass Spectra of $[M-H]^-$ Ion of Tetryl

A. Daughter ion mass spectrum of $[M-H]^-$ ion (m/z 286) of tetryl, acquired in profile mode. B. $MS^3$ mass spectrum of daughter ion at m/z 240 of the $[M-H]^-$ ion of tetryl, acquired in profile mode. Both spectra were acquired at a collision energy of 22% for the MS/MS experiment and 18% for the $MS^3$ experiment. The resonant excitation $q_z$ was 0.25.

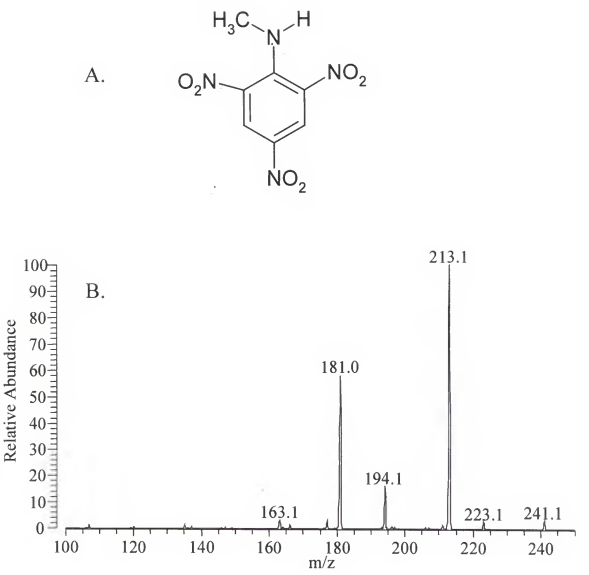


FIGURE 2-14: Daughter Ion Mass Spectrum of $[M-H]^-$ Ion of Methylpicramide

A. Chemical structure of N-methylpicramide. The molecular weight of N-methylpicramide is 242 Da. B. Daughter ion mass spectrum of $[M-H]^-$ ion (m/z 241) of N-methylpicramide. MS/MS spectrum was acquired at a collision energy of 23% and a resonant excitation $q_z$ of 0.25.

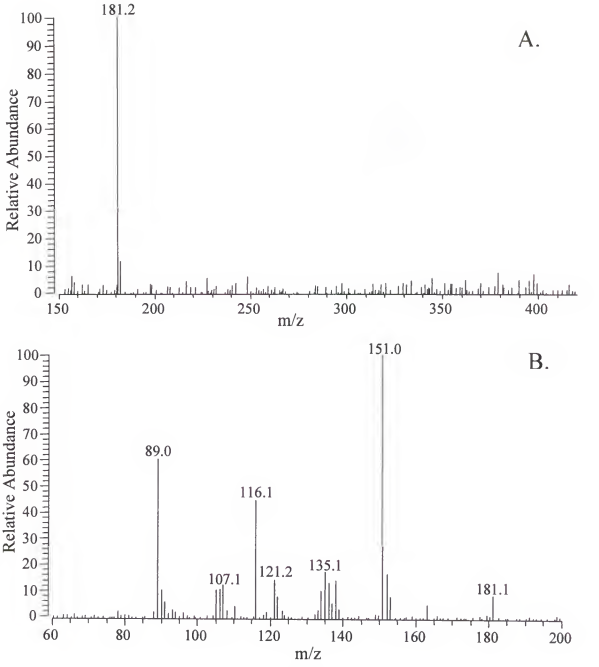


FIGURE 2-15: Negative-ESI Mass Spectrum and Daughter Ion Mass Spectrum of 2,6-DNT

A. Negative-ESI mass spectrum of 2,6-DNT. The molecular weight of DNT is 182 Da. B. Daughter ion mass spectrum of $[M-H]^-$ ion (m/z 181) of DNT. The MS/MS spectrum was acquired at a collision energy of 27% and a resonant excitation $q_z$ of 0.25.

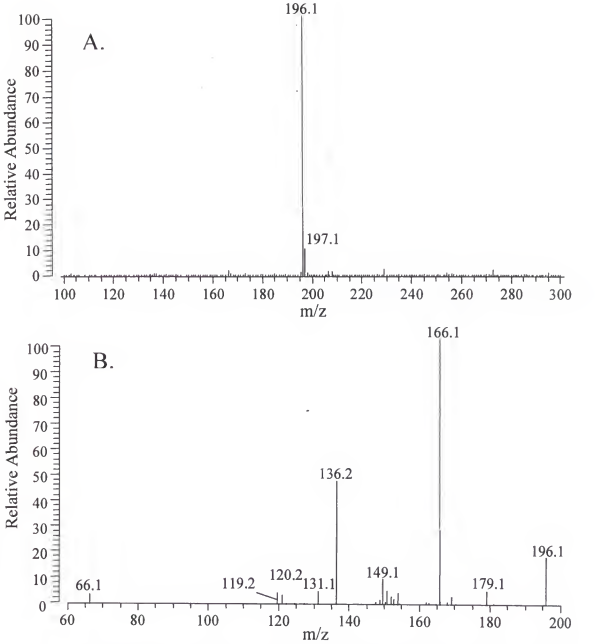


FIGURE 2-16: Negative-ESI Mass Spectrum and Daughter Ion Mass Spectrum of 2A-4,6-DNT

A. Negative-ESI mass spectrum of 2A-4,6-DNT. The molecular weight is 197 Da. B. Daughter ion mass spectrum of $[M-H]^-$ ion (m/z 196) of 2A-4,6-DNT. The MS/MS spectrum was acquired at a collision energy of 32% and a resonant excitation $q_z$ of 0.25.

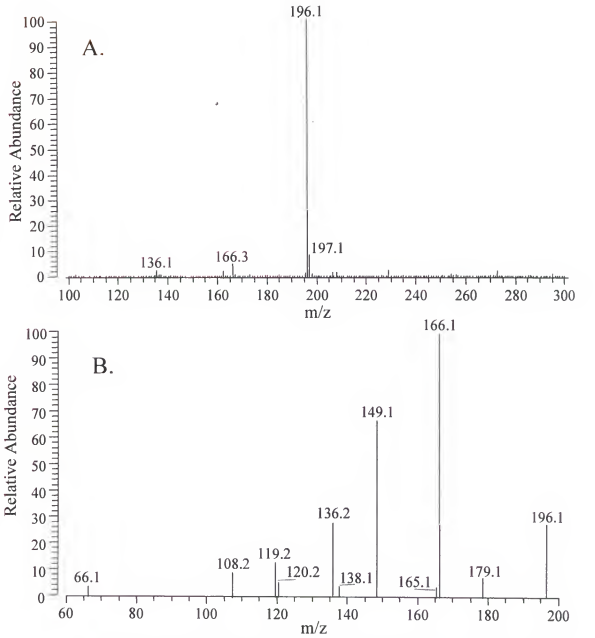


FIGURE 2-17: Negative-ESI Mass Spectrum and Daughter Ion Mass Spectrum of 2A-4,6-DNT

A. Negative-ESI mass spectrum of 4A-2,6-DNT. The molecular weight is 197 Da. B. Daughter ion mass spectrum of $[M-H]^-$ ion (m/z 196) of 4A-2,6-DNT. The MS/MS spectrum was acquired at a collision energy of 32% and a resonant excitation $q_z$ of 0.25.

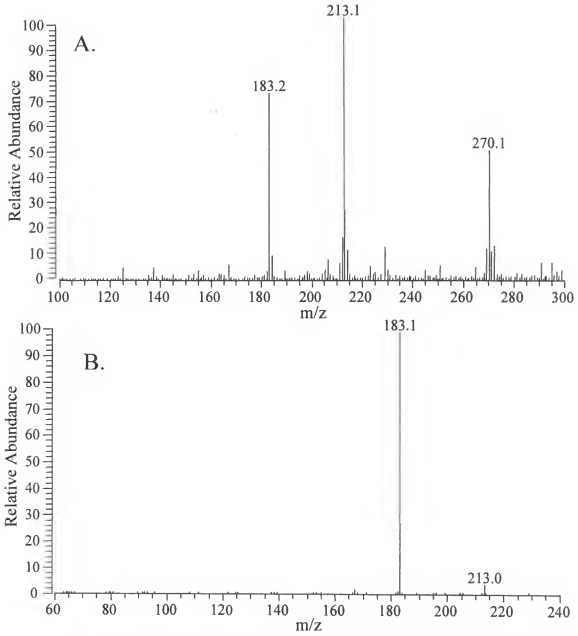


FIGURE 2-18: Negative-ESI Mass Spectrum and Daughter Ion Mass Spectrum of $M^-$ Ion of TNB

A. Negative-ESI mass spectrum of TNB. The molecular weight of TNB is 213 Da. B. Daughter ion mass spectrum of $M^-$ ion (m/z 213) of TNB. The MS/MS spectrum was acquired at a collision energy of 29% and a resonant excitation $q_z$ of 0.25.

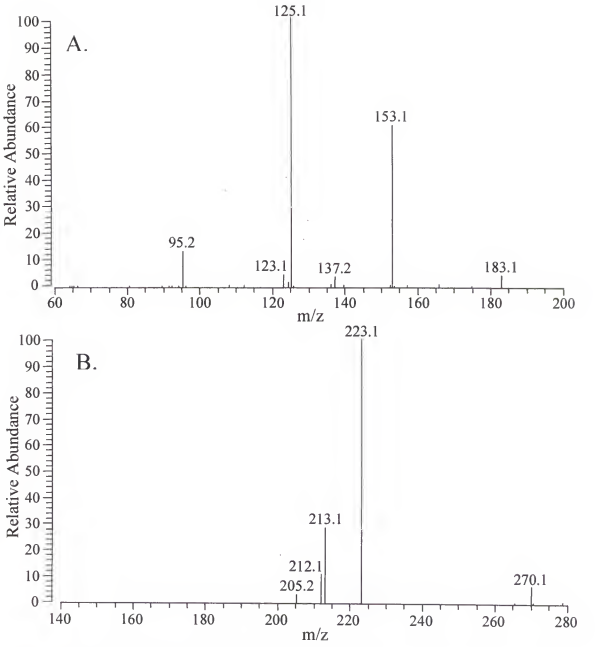


FIGURE 2-19: Daughter Ion Mass Spectra of the $[M\text{-}NO]^-$ Ion and the $[M+Acetone\text{-}H]^-$ Ion of TNB

A. Daughter ion mass spectrum of $[M\text{-}NO]^-$ ion (m/z 183) of TNB at a collision energy of 34%. B. Daughter ion mass spectrum of $[M+Acetone\text{-}H]^-$ ion (m/z 270) of TNB at a collision energy of 28%. Both spectra were acquired at a resonant excitation $q_z$ of 0.25.

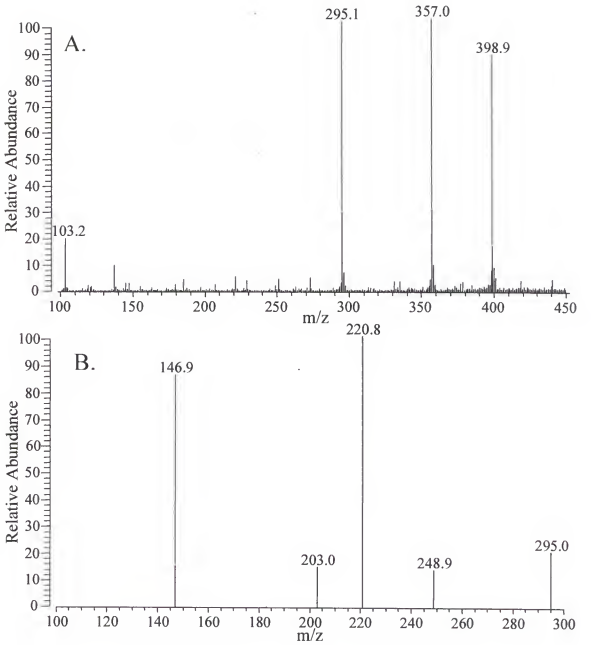


FIGURE 2-20: Negative-ESI Mass Spectrum and Daughter Ion Mass Spectrum of $[M-H]^-$ Ion of HMX

A. Negative-ESI mass spectrum of HMX. The molecular weight of HMX is 296 Da. B. Daughter ion mass spectrum of $[M-H]^-$ ion (m/z 295) of HMX. The MS/MS spectrum was acquired with a collision energy of 15%, an isolation width of 5.5 amu, and a resonant excitation $q_z$ of 0.25.

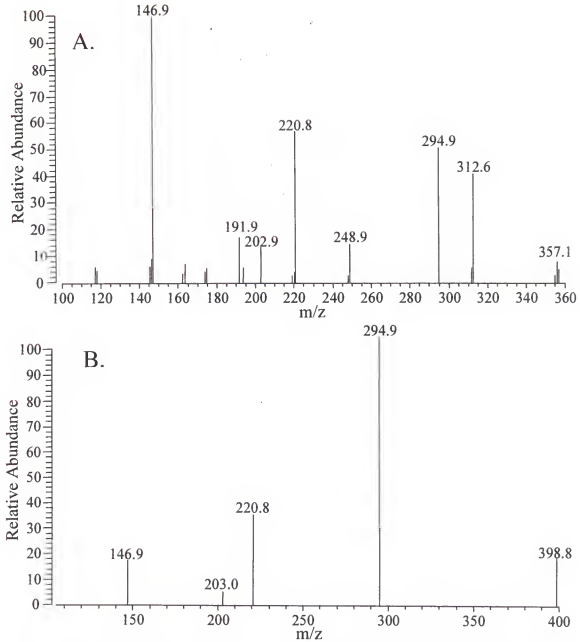


FIGURE 2-21: Daughter Ion Mass Spectra of $[M+NO3-H]^-$ and $[M+103]^-$ Ions of HMX

A. Daughter ion mass spectrum of $[M+NO_3-H]^-$ ion (m/z 357) of HMX at a collision energy of 16% and an isolation width of 6.0 amu. B. Daughter ion mass spectrum of $[M+103]^-$ ion (m/z 399) of HMX at a collision energy of 13% an isolation width of 6.5 amu. Both spectra were acquired at a resonant excitation $q_z$ of 0.25.

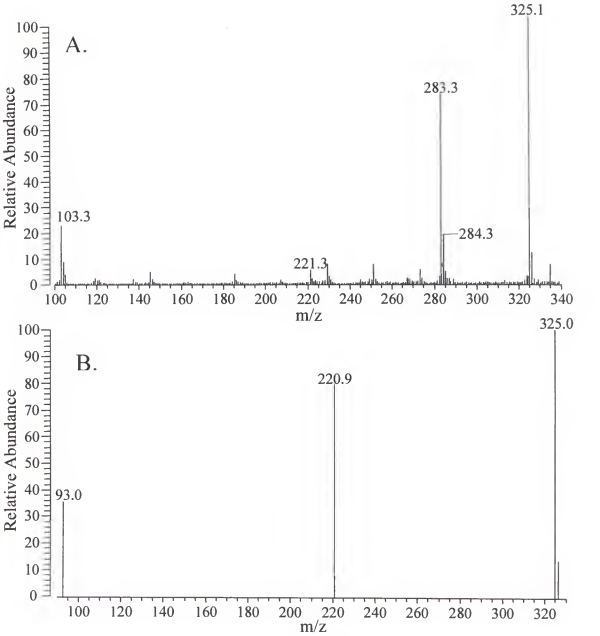


FIGURE 2-22: Negative-ESI Mass Spectrum and Daughter Ion Mass Spectrum of $[M+103]^-$ Ion of RDX

A. Negative-ESI mass spectrum of RDX. The molecular weight of RDX is 222 Da. B. Daughter ion mass spectrum of the $[M+103]^-$ ion (m/z 325) of RDX. The MS/MS spectrum was acquired with a collision energy of 16%, an isolation width of 3.0 amu, and a resonant excitation $q_z$ of 0.25.

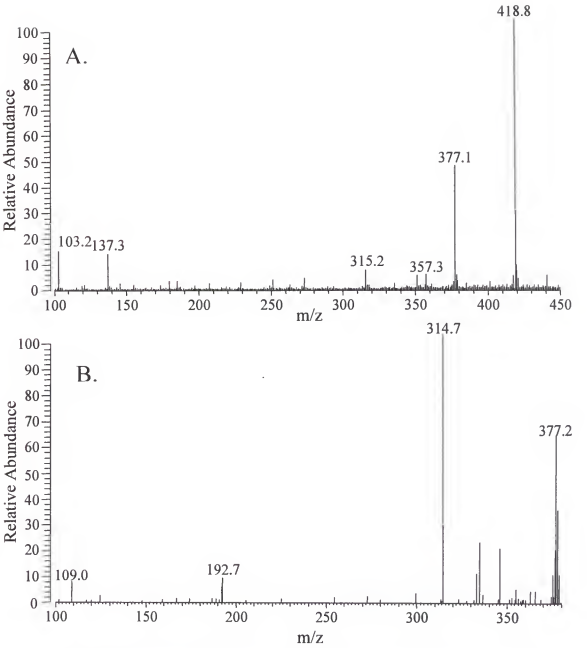


FIGURE 2-20: Negative-ESI Mass Spectrum and Daughter Ion Mass Spectrum of $[M+NO_3\text{-}H]^-$ Ion of PETN

A. Negative-ESI mass spectrum of PETN. The molecular weight of PETN is 316 Da. B. Daughter ion mass spectrum of $[M+NO3\text{-}H]^-$ ion of PETN. The MS/MS spectrum was acquired with a collision energy of 16%, an isolation width 7.0 amu, and a resonant excitation $q_z$ of 0.25.

# CHAPTER 3
# EFFECTS OF FRAGILE IONS ON MASS RESOLUTION AND TANDEM MASS SPECTROMETRY IN A QUADRUPOLE ION TRAP MASS SPECTROMETER

## Introduction

An inherent assumption in mass spectrometry is that the only factors that affect the measured mass-to-charge ratio (m/z) of an ion are its mass and its charge. Nevertheless, violations of this assumption are not uncommon in mass spectrometric measurements. Mass spectra obtained on sector instruments, for instance, often include broad, diffuse peaks that occur at non-integral m/z values [Cooks et al., 1973]. It has long been recognized that these peaks arise from ions (often termed "metastable ions") which dissociate in the field-free regions of the mass spectrometer. The resulting fragment ions appear in the mass spectrum at a point determined by their momentum and kinetic energy, which are functions of both the m/z of the precursor ion and the m/z of the fragment ion. Furthermore, these peaks are typically broad due to kinetic energy released during the fragmentation.

In the quadrupole ion trap mass spectrometer (QITMS), it has also been noted that factors other than an ion's mass and charge may affect its measured m/z. Space charging in the ion trap, for instance, can shift the apparent m/z of an ion [Stafford et al., 1987], as well as affecting its peak width. It has also been observed that the measured m/z of an ion may be shifted due to its chemical structure [Syka, 1995]. Various explanations for compound-dependent, or "chemical", mass shifts have been proposed, including interaction of ions of high-polarizability with the higher-order quadrupolar fields [Traldi

et al., 1992; Traldi et al., 1993; Bortolini et al., 1994] and the radial distribution of ions in the ion trap [Cox et al., 1995]. Chemical mass shifts are the most intriguing and most debated type of mass shift and are the objective of ongoing research [Degnore, 1997; Gill et al., 1998; McClellan et al., 1999B; Wells et al., 1999].

An alternative hypothesis can be proposed, that ions can exhibit a chemical mass shift because they are "fragile" and may fragment during the application of the resonance ejection amplitude during mass analysis. The mass spectral peaks of such fragile ions are characterized by peak-fronting and an overall broader peak in profile data acquisitions. Generally, the peak top will remain at the correct m/z in profile mode, but the centroid of the peak will shift to lower m/z and display an apparent mass shift. Both the peak-fronting and mass shift are directly due to the application of a resonance ejection amplitude, which is used to facilitate ion ejection during scan-out of the ions from the ion trap for mass analysis. As an ion comes into resonance with the resonant ejection amplitude, it will gain kinetic energy and undergo collisions with the helium buffer gas present in the trap. These collisions may lead to fragmentation due to collision-induced dissociation (CID). Under normal operating conditions for MS or tandem mass spectrometry (MS/MS), the resonance ejection frequency is applied at a $q_z$ value close to the edge of axial stability. Thus, the fragment ions produced by CID, with their lower m/z, will fall below the low-mass cutoff, have unstable trajectories in the axial direction, and be quickly ejected. The ejection of the fragment ions, which appears as premature ejection of the fragile ion, leads to the appearance of peak-fronting and a mass shift. The role of ion fragmentation has been also suggested by Londry [Londry et al., 1995] and Brittain [Brittain et al., 1993].

A quadrupole ion trap / quadrupole mass filter hybrid instrument was recently constructed in this laboratory to test this hypothesis [Murphy et al., 1999; Murphy and Yost, 2000]. The quadrupole mass filter was utilized to mass analyze the ions as they were ejected from the quadrupole ion trap. These experiments clearly demonstrated that the peak-fronting observed for the $M^+$ ion of n-butylbenzene at m/z 134, which has been demonstrated to undergo a mass shift [Londry et al., 1995], corresponds to fragment ions produced at m/z 91 and 92 and not m/z 134. When the $M^+$ ion was ejected without resonance ejection, no peak-fronting was observed and no fragment ions were detected. Furthermore, when the $M^+$ ion was ejected at a low enough $q_z$ that the fragment ions had stable trajectories, there was no peak-fronting observed or fragment ions detected.

In this chapter, the effects of fragile ions on MS and MS/MS in an electrospray ionization (ESI)/QITMS instrument are explored. Specifically, the effects of ion fragility on peak widths observed at slow scan speeds and on the efficiencies of ion isolation and fragmentation in MS/MS are investigated. The vast majority of the ions produced by ESI do not exhibit fragile ion characteristics on a QITMS. In the development of liquid chromatography-MS/MS methods for nitro-explosives [McClellan et al., 1999A], however, we observed that ESI of some explosives produces some ions that have large peak widths and are difficult to isolate for MS/MS experiments. For this study, we have focused on ions that display these fragile ion characteristics. These ions include protonated, deprotonated, and adduct ions of explosives, acylcarnitines, and macrolide antibiotics. Based on these data, a method is suggested for quantifying the fragility of an ion.

## Experimental

All experiments were performed on the Finnigan LCQ (San Jose, CA), a commercial, bench-top ESI-QITMS instrument. The LCQ uses a resonant ejection amplitude for ion ejection applied at a $q_z$ of 0.90 for full scan MS and MS/MS and at a $q_z$ of 0.83 in LCQ ZoomScan. The applied resonant ejection amplitude increases with increasing m/z and is calibrated to achieve optimum resolution and peak shape for the calibrant ions (protonated caffeine, MRFA, and Ultramark 1621).

Isolation of a specific m/z or m/z range for MS/MS is accomplished by applying a notched broadband waveform. The m/z range to be isolated and its corresponding notch are centered at a $q_z$ of 0.83. The width of the waveform at the base of the notch is termed the width of isolation. During the application of the waveform, all ions above or below the m/z range of the notch width are ejected from the trap. For MS/MS experiments, the defaults for the isolation waveform are a width of 1 amu, or unit isolation, (which can be altered by the user) and a time of 16 ms (which may not be altered by the user). Fragmentation for MS/MS on the QITMS is accomplished by applying a resonant excitation amplitude to excite the isolated m/z ion, or range of ions, resulting in CID with the helium buffer gas. The amplitude of the resonant excitation waveform, termed the collision energy, is specified by the user as a percentage of the 5 $V_{p-p}$ maximum. For a standard MS/MS experiment, resonant excitation occurs at a $q_z$ of 0.25 for 30 ms.

The LCQ uses the $[M+H]^+$ ion of caffeine, m/z 195.1, the $[M+H]^+$ ion of the tetrapeptide MRFA, m/z 524.2, and the $[M+H]^+$ ions of Ultramark 1621 at m/z 1122.0, 1622.0, and 1822.0 for calibration. All data were acquired under "calibrated conditions". Before each day's data acquisition, the calibration was checked via the calibration software. If the calibration was not within tolerances, the instrument was recalibrated.

The data reported in this study were acquired using programs written in the ITCL language for the LCQ. The use of ITCL computer control allows us to design a series of scan events without requiring continual direct personal interface. Great care was taken to assure that all data were acquired free of space charging, thus eliminating any physical causes of mass shifts. The preset, default AGC target values were used for the acquisition of all data in positive ion mode. For acquisition of data in negative ion mode, the AGC target values were lowered by a factor of three, as there is an increased ion signal gain for negative ions versus positive ions [Schwartz et al., 1998]. Data for MS scans were acquired in full scan at a scan rate of 0.18 ms/amu and at a slower scan speed, using the LCQ ZoomScan, at a scan rate of 3.6 ms/amu. For the purposes of distinction between the two scan speeds in this study, the scans utilizing a scan rate of 0.18 ms/amu will be referred to as normal scan and scans utilizing a scan rate of 3.6 ms/amu will be to as slow scan (or ZoomScan).

For this work, a select series of compounds, which produce some fragile ions by ESI (nitro-explosives, macrolides, and acylcarnitines), plus the LCQ calibrant compounds were investigated. The nitro-explosives investigated include: 2,4,6 trinitrotoluene (TNT); 1,3,5-trinitro-1,3,5,-triazacyclohexane (RDX); 1,3,5,7-tetranitro-1,3,5,7-tetrazacyclooctane (HMX); and pentaerythritol tetranitrate (PETN). All explosives were provided by Dr. Jehuda Yinon, of the Weizmann Institute of Science, and obtained from the Analytical Laboratory of the Israeli Police Headquarters. We have previously shown that these explosives are amenable to negative ion ESI. All explosives were initially dissolved in acetone at a concentration of approximately 1 mg/ mL. For ESI/MS, each was diluted to approximately 20 ppm in a 50% HPLC-grade isopropanol (IPA): 50%

HPLC-grade water ($H_2O$) solution (v/v), with 0.1% ammonium hydroxide ($NH_4OH$) added to improve ionization efficiency.

Three macrolide compounds, oleandomycin, erythromycin, and troleandomycin, all purchased from Sigma (St. Louis, MO), were investigated. For analysis, the macrolide samples were prepared at a concentration of 1 μM in a 50% HPLC-grade methanol (MeOH): 50% HPLC-grade $H_2O$ (v/v) solution, with 8 mM sodium acetate (NAOAc). This mixture yields approximately a 1:1 ratio of $[M+H]^+$ to $[M+Na]^+$ ions during ESI-MS on the QITMS. In the case of troleandomycin, which is the triacetate ester of Oleadomycin, the ions observed were $[M+H]^+$ at m/z 814, $[M-42+H]^+$ at m/z 772, and $[M-42+Na]^+$ at m/z 794. The $[M-42+H]^+$ and $[M-42+Na]^+$ ions are produced as a result of the hydrolysis of one of the acetate esters, presumably in solution, accounting for the loss of the $C_2H_2O$ group (m/z 42). For the purpose of this study, the $[M-42+H]^+$ and $[M-42+Na]^+$ ions of troleandomycin will be used for comparisons with other macrolide ions.

A mixture of nine acylcarnitines (CMIX) was analyzed, including acetylcarnitine, propionylcarnitine, isobutrylcarnitine, isovalerylcarnitine, hexanoylcarnitine, octanoylcarnitine, lauroylcarnitine, myristoylcarnitine, and palmitoylcarnitine. All acylcarnitine samples were purchased from Sigma Tau (St. Louis, MO). The CMIX was initially prepared at a concentration of 3 mM for each acylcarnitine in a 50% HPLC-grade MeOH: 50% HPLC-grade chloroform (v/v) solution. For ESI-MS analysis, the CMIX was diluted to 3 μM in 50% HPLC-grade MeOH: 50% HPLC-grade $H_2O$ (v/v) solution, with 10 mM NAOAc. The mixture yielded an approximate 2:1 ratio of $[M+H]^+$ to $[M+Na]^+$ ions under ESI on the QITMS.

The LCQ ESI tuning solution compounds were used as reference compounds. The ESI tuning solution mixture is composed of 0.1 mM caffeine, 0.015 mM MRFA, and 0.3 mM Ultramark 1621 in a 50% HPLC-grade acetonitrile: 25% HPLC-grade MeOH: 25% HPLC-grade $H_2O$ solution (v/v), with 0.01% glacial acetic acid.

To study the effects of fragile ions on MS peak shape, experiments were designed to acquire a series of data values, including peak-top m/z, peak widths, and intensity, for each selected ion in normal scan mode and ZoomScan mode. For each scan mode of a selected ion, 25 analytical scans, each consisting of 10 μscans, were acquired and averaged. For each selected ion, three to five experiments were performed and averaged.

To study the effects of fragile ions on MS/MS, experiments were conducted on the sample population of ions. A program was written in ITCL to isolate each ion in a non-consecutive order over a range of isolation widths from 0.5 amu to 10.0 amu, with increments of 0.5 amu. The time of the isolation waveform was kept constant at the standard 16 ms. Each data point represents 25 analytical scans (250 μscans). The data for each ion included the peak-top m/z, isolation width, and intensity. The effects of fragile ions on optimum collision energy were investigated using the $[M+H]^+$ and $[M+Na]^+$ ions of the acylcarnitines. Both the $[M+H]^+$ and $[M+Na]^+$ for each acylcarnitne were isolated, at an isolation width of 3 amu, and fragmented via CID at successive collision energies from 0% to 50% of 5 $V_{p-p}$, with increments of 0.25%. For each ion, five analytical scans (10 μscans each) were acquired at each collision energy. The intensity values were averaged to create a breakdown curve for each ion.

## Results and Discussion

A wide variety of ions were studied for the assessment of ion fragility, including multiple types of ions produced by the ESI of explosives, macrolides, acylcarnitines, caffeine, MRFA, and Ultramark 1621. We have previously shown [Yinon et al., 1997] that negative ESI of explosives produces a wide array of ions including molecular ions ($[M-H]^-$ and $M^-$), adduct ions (e.g. $[M+NO_2]^-$ and $[M+CH_2ONO_2-H]^-$) and fragment ions (e.g. $[M-NO_2-H]^-$). For the four explosives, the most intense ion or ions were chosen to study for ion fragility, including the $[M-H]^-$ of RDX, TNT, HMX, and PETN, the $[M+Cl]^-$ ion of RDX, HMX, and PETN, and $[M+NO_2]^-$ and $[M+103]^-$ ions of HMX. Both $[M+H]^+$ and $[M+Na]^+$ ions were studied from the macrolide and acylcarnitine compounds. Finally, the $[M+H]^+$ ions of caffeine, MRFA, and Ultramark 1621 were analyzed as non-fragile, reference ions.

### Peak Width

The width of a peak acquired in profile and the degree of peak-broadening are related to the degree of fragility of the ion, as well as the scan rate utilized for data acquisition. The LCQ ZoomScan is a higher resolution scan, over a range of 10 amu, and is commonly used for charge-state determination of multiply charged ions. This slow scan mode results in narrower peaks, typically less than 0.3 amu wide at 10% peak height. The difference in peak width between fragile ions and non-fragile ions becomes greater as the scan rate decreases, due to the longer time that the ion is in resonance with the resonance ejection amplitude. This allows the ion to undergo more collisions and thus gain enough internal energy to cause greater fragmentation if the ion is fragile.

The peak width, at the slower scan speed, is the most obvious indicator of ion fragility for ions analyzed by the QITMS. Peak widths (W) were measured at three

points (50%, 25%, and 10% peak height) on a profile peak, at both the normal scan speed and slower scan speed, to obtain a trend for fragile and non-fragile ions. Initially, the ions produced by the explosives, macrolides, and tuning solution compounds were investigated for peak-top m/z in profile, peak widths, and intensity. The resulting data are displayed in **Table 3-1** and **Table 3-2**, grouped by compound class and listed in order of increasing m/z.

The value for the $W_{10\%}$ was chosen as an indicator of ion fragility because peak-fronting and peak-broadening are most evident at 10% peak height. From **Table 3-1**, it is apparent that the widths of the $[M-H]^-$ ions for HMX and PETN, the $[M+Cl]^-$ ion of PETN and the $[M+103]^-$ of HMX are significantly larger than those of the other ions. These ions are characterized by a substantial degree of peak-fronting, which results in the larger peak widths. The existence of peak-fronting in the slower scan speed spectrum of a fragile ion and the difference in peak shape between a fragile ion and non fragile ion is depicted in **Figure 3-1**. Note that the peak width of the $[M-H]^-$ ion of HMX is much larger than that of the $[M+Cl]^-$ ion of HMX due to the excessive peak-fronting in the fragile ion. We have determined that the calibrant ions, as well as the other ions that do not exhibit peak-fronting, have $W_{10\%}$ values less than or equal to 0.30 amu. Therefore, a threshold of 0.31 amu for $W_{10\%}$ in ZoomScan may be employed to differentiate between fragile and non-fragile ions.

Some general observations can be made concerning ion fragility. First, ionization of a compound may produce some ions that are fragile, while other ions are quite stable. For example, HMX forms fragile $[M-H]^-$ and $[M+103]^-$ ions, but a stable $[M+Cl]^-$ ion. The $[M+H]^+$ ions of the macrolides are fragile, while the $[M+Na]^+$ ions are not. In

contrast, the $[M+Na]^+$ ions of the acylcarnitines are more fragile than the $[M+H]^+$ ions. Therefore, the adduction of the Na can provide either a more or less stable ion than does protonation, depending on the ion's structure. The calibrant ions consistently have narrower peak-widths, with the $[M+H]^+$ of caffeine producing the narrowest peak. Note, however, that the $[M+Cl]^-$ ions of RDX and HMX produce even narrower peaks.

Width of Waveform Isolation

For MS/MS, the parent ion of interest must be successfully isolated, ideally at unit (1 amu) isolation. For a QITMS, this requires having a notch in the isolation waveform of 1 amu. As noted in our experiments and in the literature [Weieboldt et al., 1998], some ions can not be isolated with a 1 amu isolation width; therefore, the notch width, or the window of isolation, must be increased to successfully isolate the ion and keep it trapped. Failure to recognize this need can make it impossible to acquire an MS/MS spectrum of the ion. This poses particular problems when standard conditions, which may not obtain adequate isolation intensity for the selected parent ion, are utilized during the acquisition of automated MS/MS scans, such as when employing data-dependent scan functions. Conversely, increasing the width of the isolation notch can be detrimental to MS/MS analyses due to the possible production of daughter ions from multiple parent ions within the isolation window, as noted in Chapter 2. This can lead to confusion in the analysis of data for structure elucidation or compound identification.

Our hypothesis for the need to increase the isolation waveform notch width is that the parent ions are fragile and will fragment during isolation. When the isolation waveform is applied, energy is applied at specific frequencies to eject all ions of all m/z values other than the selected parent ion. Unfortunately, the waveform will also impart some kinetic energy to the parent ion which is to be isolated. As the ion gains kinetic

energy, it will undergo collisions with the buffer gas; if the ion is fragile, the collisions may impart enough energy into the ion to cause fragmentation via CID. This will result in a decrease (or even a complete loss) in the intensity of the parent ion during the isolation process. Increasing the width of the notch in the isolation waveform, or applying the waveform for a shorter period, will reduce the kinetic energy imparted to the ion and, thus, decrease the likelihood that a fragile parent ion will be dissociated and lost.

To test this hypothesis, the minimum isolation width, defined as the narrowest width that provides an isolation intensity of 90% of the maximum isolated ion intensity, was determined for each ion (**Table 3-3**). The ions with a minimum isolation width greater than 2.0 amu are the same ions which yielded broad peaks ($W_{10\%} > 0.31$) in the ZoomScan speed spectra and were determined to be fragile. The effects of the width of isolation on the intensity of the isolated parent ion are illustrated by two examples. To visualize the general trend, three non-fragile ions ($[M+H]^+$ ions of caffeine and MRFA, and $[M-H]^-$ ion of TNT) and two fragile ions ($[M-H]^-$ ions of HMX and PETN) were selected (**Figure 3-2**). The minimum isolation width for each non-fragile ion is 1 amu. Therefore, these ions can be readily isolated with unit isolation. In contrast, the fragile ions require a much larger isolation width to achieve 90% of the maximum isolated ion intensity. The $[M-H]^-$ ions of HMX and PETN require a minimum isolation width of 5.5 amu and 7.5 amu, respectively. For the fragile ions there is nearly zero ion intensity as the isolation window is increased until a breakpoint width is reached where the intensity begins to rise; the breakpoint for the $[M-H]^-$ ions of HMX and PETN are at 2.5 amu and 5.5 amu, respectively. The intensity variations may simply reflect the inherent instability of the ESI source.

The second example compares the intensity of the isolated $[M+H]^+$ and $[M+Na]^+$ ions of oleadomycin and the $[M-42+H]^+$ and $[M-42+Na]^+$ ions of troleandomycin (**Figure 3-3**). As previously determined by ZoomScan peak width, the $[M+H]^+$ ions of these compounds are fragile while the $[M+Na]^+$ ions are not. It is observed that the minimum isolation width for the $[M+Na]^+$ and $[M-42+Na]^+$ ions is 1.5 amu, which will allow for isolation with near-unit resolution. The $[M+H]^+$ ion of oleandomycin requires a minimum isolation width of 3.5 amu and the $[M-42+H]^+$ ion of troleandomycin requires 3.0 amu (**Table 3-3**), which precludes parent ion selection for MS/MS with anywhere close to unit resolution. **Figure 3-3** also shows a peculiar trend, a plateau in the isolated parent ion intensity between the breakpoint isolation width and the minimum isolation width. This plateau was consistently observed for the $[M+H]^+$ ion of all three macrolides and is an artifact of the way the isolation waveform is calculated and applied. The isolation waveform is a sum-of-sines tailored waveform (TWF) consisting of many discrete frequencies applied at spacings of 500 Hz [Bier and Schwartz, 1997]. For certain m/z and notch width combinations, the calculated spacings are not at least 500 Hz apart and the requested waveform can not be applied as requested. Therefore, for some m/z values, the same waveform is applied over a range of requested notch widths. In the case of the $[M+H]^+$ ion of oleadomycin, for example, the same isolation waveform is applied at isolation widths of 2.5, 3.0, and 3.5 amu and results in the observed plateau in **Figure 3-3**. For smaller m/z ions, where the frequency distribution is greater per unit m/z, the calculated frequency spacings are larger for a particular isolation width than for larger m/z ions; thus, 0.5 amu increments produce different isolation waveforms.

Time of Waveform Isolation

A key parameter of the isolation waveform is the length of time the waveform is applied. The waveform must be applied for long enough to eject all of the undesired ions from the ion trap. On the QITMS, under standard conditions, the waveform is applied in four cycles of 4 ms each for a total of 16 ms. For stable ions, this is long enough to eject the unwanted ions without affecting the selected parent ion. For fragile ions, however, enough energy may be deposited into the ion over the 16 ms to cause fragmentation by CID. Thus, the likelihood of fragmentation and loss of ion intensity of the isolated ion should be a function of both the isolation waveform width and the period for which the waveform is applied.

Indeed, it was observed that as the isolation waveform was applied for a greater length of time, the isolated intensity of the fragile ions decreased, whereas the intensity of the non-fragile ions remained constant. For each ion, the intensity of the selected ion was acquired after the application of the isolation waveform for a specific period of time. The waveform was applied over a time range of 2 to 24 ms, at intervals of 2 ms, for isolation widths of 1, 2, 3, 4, and 5 amu. **Figure 3-4** shows the results for two ions, the $[M+H]^+$ ion of caffeine, a non-fragile ion, and the $[M-H]^-$ ion of HMX, a fragile ion. The intensity of the caffeine ion remains constant over the entire time range for each isolation width. Conversely, the intensity of the $[M-H]^-$ ion of HMX decreases as the time of the waveform increases for each of the five isolation widths studied. Generally, it was observed that an isolation waveform application time of 6 to 8 ms was sufficient to achieve isolation of the desired m/z ions from other ions in the ion trap.

It was also observed that, if the waveform was applied at the minimum isolation width (as determined at the normal period of 16ms), the intensity of the isolated ion

remained constant over the entire time period from 2 to 24 ms. This is depicted in the trends for the $[M+H]^+$ and $[M+Na]^+$ ions of oleandomycin (**Figure 3-5**). The $[M+H]^+$ ion for oleandomycin has a minimum isolation width of 4.0 amu. When the waveform is applied at a width less than the minimum width, the intensity significantly decreases as the application time is increased. This is evident when the width is 1, 2, or 3 amu wide. When the width is increased to either 4 or 5 amu, the intensity remains constant. This same trend is observed for the $[M+Na]^+$ ion, which has a minimum isolation width of 1.5 amu. When the isolation width is 1 amu, the intensity decreases as the time of the isolation waveform is increased. When the isolation width is greater than the minimum isolation width (in this case, greater than the determined 1.5 amu), the intensity remains constant over the time range.

Optimum Collision Energy

In order to fragment a selected parent ion efficiently, an appropriate resonance ejection amplitude must be applied to resonantly excite the ion for CID. If too low a resonant excitation amplitude is applied, the ion will not fragment efficiently; if the resonant ejection amplitude is too great, the ion will be ejected from the trap. On the LCQ, the resonant amplitude is controlled by the collision energy parameter, entered by the user as a percentage of the 5 $V_{p-p}$ maximum. Research is presently being conducted to devise methods for automatically setting the applied collision energy [Mulholland and Yost, 1999; Schwartz et al., 1999]. One method, devised by Schwartz et al., increases the collision energy with increasing ion m/z. While m/z is a major factor in the determination of an appropriate collision energy, the ion's type and structure, including whether it is fragile or not, also has an effect on the optimum collision energy (defined as the energy that reduces the intensity of the parent ion by 95%). Mulholland et al. have

recently demonstrated multi-level CID, in which a series of increasing collision energies are employed to automatically fragment a parent ion regardless of whether an ion is fragile or non-fragile.

One example of the effect of ion stability or fragility is the difference in optimum collision energy required for the $[M+H]^+$ and $[M+Na]^+$ ions of acylcarnitines. The ZoomScan peak widths are 10% - 30% wider for the $[M+Na]^+$ ions than for the $[M+H]^+$ ions (**Table 3-2**), indicating that they are more fragile. Each ion fragments through the same pathway; the main fragment for each ion is the loss of neutral $N(CH_3)_3$, a loss of 59 amu. To determine the optimum collision energy for both the $[M+H]^+$ and the $[M+Na]^+$ ions for each of the nine acylcarnitines, breakdown curves were constructed. The optimum collision energy, defined as the energy required to reduce the parent ion intensity by 95%, is plotted versus m/z in **Figure 3-6**. The optimum collision energy is significantly less for the $[M+Na]^+$ ions compared to the $[M+H]^+$ ions, as we would expect given their greater fragility (as reflected in ZoomScan peak width).

Predicting Fragile Ions

In this chapter, ions have been classified as either fragile or non-fragile. However, ions can have varying degrees of fragility. To assess the degree of ion fragility, a relationship between the ZoomScan $W_{10\%}$ and the minimum isolation width, the two main forecasters of ion fragility on the QITMS, has been developed (**Figure 3-7**). For ions which have been classified as fragile through experimentation there appears to be a linear trend between the $W_{10\%}$ and the minimum isolation width. As a result of this trend, we suggest criteria for classifying an ion as fragile. If the ZoomScan $W_{10\%}$ is greater than 0.31 amu and the minimum isolation width is 2.5 amu or greater, the ion is classified as fragile. An increase in the ZoomScan $W_{10\%}$ and/or the minimum isolation

width above these thresholds signifies greater ion fragility. It should also be noted that there is a variation in the minimum isolation width for non-fragile ions. While all non-fragile ions have a $W_{10\%}$ in ZoomScan of 0.30 amu or less, the range of minimum isolation widths range from 0.5 amu for the Ultramark 1621 ions to 2.0 amu for the $[M+Cl]^-$ ion of RDX. This range of minimum isolation widths may indicate that (1) the Ultramark 1621 ions are more stable than the $[M+Cl]^-$ ion when the isolation waveform is applied, or (2) there is a slight mass dependency in the application of the isolation waveform that favors the isolation of the high m/z ions.

## Conclusion

In this chapter, it has been shown that the fragility of ions has an affect on both mass resolution and the intensity of the ion isolated for MS/MS. The effects of a fragile ion on mass resolution are most evident at the slower scan speeds, as the difference in peak widths between fragile ions and non-fragile ions become more significant and more readily detected. In ZoomScan, the peak widths of fragile ions, at 10% peak height, are greater than 0.31 amu and may approach values as great as 1.09 amu. Conversely, the $W_{10\%}$ for non-fragile ions is consistently 0.30 amu or less. It has also been shown that different ions formed from the same compound, including protonated, deprotonated, or adduct ions, may result in peaks with different peak widths. Examples include the macrolide compounds, where the $[M+H]^+$ ions are fragile and, thus, have a larger peak width than the $[M+Na]^+$ ions, and the acylcarnitine compounds, where the $[M+H]^+$ ions have smaller peak widths than the fragile $[M+Na]^+$ ions.

The ability to obtain an adequate isolation intensity for a selected parent ion at unit resolution during MS/MS is dependent on the ion's fragility. Fragile ions are more

greatly affected by the application of the isolation waveform during the selection of the parent ion for MS/MS experiments. As a result, if a fragile ion is isolated at unit resolution, the intensity of the ion will diminish substantially (often completely). For the isolation of fragile ions, the isolation waveform notch width must be increased and/or the time period of isolation must be decreased to obtain adequate isolation. Fragile ions also require lower collision energies to achieve efficient CID. Taking into account these data, we have developed a criterion, based on the minimum isolation width and the ZoomScan $W_{10\%}$ of each ion, for assessing the degree of ion fragility. As either or both of the minimum isolation width and the ZoomScan $W_{10\%}$ increase, so does an ion's fragility.

Ultimately, the goal of this research is to develop methods for the analysis of fragile compounds, such as explosives, to minimize the effects of ion fragility both on mass resolution and on MS/MS isolation and fragmentation. To minimize the effects of fragile ions on the acquisition of good MS/MS spectra, the user may need both to increase the isolation width and to decrease the CID collision energy. For all but the most fragile ions, an isolation width of 4 amu is adequate to obtain maximum isolated intensity for ESI-MS/MS experiments.

TABLE 3-1: ZoomScan Peak Widths for Low m/z Ions

| Compound / Ion | m/z | $W_{10\%}$* (amu) | $W_{25\%}$* (amu) | $W_{50\%}$* (amu) |
|---|---|---|---|---|
| Nitrophenol $[M-H]^-$ | 138.1 | 0.21 ± 0.02 | 0.16 ± 0.02 | 0.11 ± 0.03 |
| DNT $[M-H]^-$ | 181.1 | 0.26 ± 0.04 | 0.16 ± 0.03 | 0.09 ± 0.03 |
| Caffeine $[M+H]^+$ | 195.0 | 0.26 ± 0.01 | 0.20 ± 0.01 | 0.14 ± 0.01 |
| 4-Amino-2,6-DNT $[M-H]^-$ | 196.1 | 0.24 ± 0.02 | 0.18 ± 0.01 | 0.13 ± 0.01 |
| RDX $[M-H]^-$ | 220.9 | 0.32 ± 0.03 | 0.22 ± 0.02 | 0.13 ± 0.02 |
| TNT $[M-H]^-$ | 226.1 | 0.29 ± 0.03 | 0.23 ± 0.02 | 0.16 ± 0.02 |
| Picramide $[M-H]^-$ | 227.1 | 0.25 ± 0.02 | 0.19 ± 0.01 | 0.13 ± 0.01 |
| Methylpicramide $[M-H]^-$ | 241.0 | 0.29 ± 0.03 | 0.22 ± 0.02 | 0.14 ± 0.02 |
| RDX $[M+Cl]^-$ | 257.1 | 0.25 ± 0.04 | 0.18 ± 0.03 | 0.12 ± 0.03 |
| Tetryl $[M-H]^-$ | 285.9 | 0.33 ± 0.04 | 0.26 ± 0.03 | 0.15 ± 0.03 |
| HMX $[M-H]^-$ | 294.9 | 0.63 ± 0.03 | 0.45 ± 0.03 | 0.28 ± 0.03 |
| PETN $[M-H]^-$ | 314.6 | 1.09 ± 0.01 | 0.73 ± 0.01 | 0.36 ± 0.01 |
| HMX $[M+Cl]^-$ | 331.1 | 0.24 ± 0.02 | 0.18 ± 0.02 | 0.12 ± 0.02 |
| HMX $[M+NO_2]^-$ | 341.6 | 0.34 ± 0.02 | 0.25 ± 0.02 | 0.16 ± 0.02 |
| Tetryl $[M+Acetone-H]^-$ | 344.0 | 0.29 ± 0.02 | 0.23 ± 0.02 | 0.16 ± 0.02 |
| HMX $[M+NO_3]^-$ | 358.0 | 0.26 ± 0.02 | 0.18 ± 0.02 | 0.12 ± 0.02 |
| PETN $[M+Cl]^-$ | 350.9 | 0.70 ± 0.01 | 0.51 ± 0.01 | 0.33 ± 0.01 |
| PETN $[M+NO_2]^-$ | 361.7 | 0.69 ± 0.03 | 0.49 ± 0.03 | 0.29 ± 0.03 |
| HMX $[M+103]^-$ | 398.7 | 0.95 ± 0.01 | 0.64 ± 0.01 | 0.33 ± 0.01 |

Note: The mean peak widths for each ion in ZoomScan mode at 10% peak height ($W_{10\%}$), 25% peak height ($W_{25\%}$), and 50% peak height ($W_{50\%}$) are presented. The listed relative error for each measurement is one standard deviation, as calculated from the average of a minimum of three experiments, consisting of 25 analytical scans (10 μscans each), for each ion.

TABLE 3-2: ZoomScan Peak Widths for High m/z Ions

| Compound / Ion | m/z | $W_{10\%}$* (amu) | $W_{25\%}$* (amu) | $W_{50\%}$* (amu) |
|---|---|---|---|---|
| Octanoylcarnitine $[M+H]^+$ | 288.0 | 0.26 ± 0.02 | 0.20 ± 0.01 | 0.14 ± 0.01 |
| Octanoylcarnitine $[M+Na]^+$ | 309.9 | 0.29 ± 0.02 | 0.21 ± 0.02 | 0.14 ± 0.01 |
| Lauroylcarnitine $[M+H]^+$ | 344.0 | 0.27 ± 0.01 | 0.20 ± 0.01 | 0.14 ± 0.01 |
| Lauroylcarnitine $[M+Na]^+$ | 365.9 | 0.33 ± 0.01 | 0.23 ± 0.01 | 0.16 ± 0.01 |
| Myristolcarnitine$[M+H]^+$ | 372.3 | 0.31 ± 0.01 | 0.23 ± 0.01 | 0.16 ± 0.01 |
| Myristolcarnitine $[M+Na]^+$ | 394.1 | 0.41 ± 0.01 | 0.30 ± 0.01 | 0.20 ± 0.01 |
| Palmitoylcarnitine $[M+H]^+$ | 400.3 | 0.34 ± 0.01 | 0.24 ± 0.01 | 0.17 ± 0.01 |
| Palmitoylcarnitine$[M+Na]^+$ | 422.2 | 0.43 ± 0.01 | 0.31 ± 0.01 | 0.21 ± 0.01 |
| MRFA $[M+H]^+$ | 524.1 | 0.30 ± 0.02 | 0.23 ± 0.01 | 0.16 ± 0.01 |
| Oleandomycin $[M+H]^+$ | 687.9 | 0.51 ± 0.02 | 0.38 ± 0.01 | 0.24 ± 0.01 |
| Oleandomycin $[M+Na]^+$ | 710.1 | 0.30 ± 0.05 | 0.23 ± 0.05 | 0.16 ± 0.05 |
| Erythromycin $[M+H]^+$ | 733.9 | 0.39 ± 0.06 | 0.29 ± 0.04 | 0.20 ± 0.07 |
| Erythromycin $[M+Na]^+$ | 756.5 | 0.29 ± 0.02 | 0.22 ± 0.01 | 0.15 ± 0.01 |
| Troleandomycin $[M-42+H]^+$ | 772.0 | 0.41 ± 0.02 | 0.29 ± 0.01 | 0.19 ± 0.01 |
| Troleandomycin $[M-42+Na]^+$ | 794.1 | 0.29 ± 0.01 | 0.22 ± 0.01 | 0.15 ± 0.01 |
| Troleandomycin $[M+H]^+$ | 814.0 | 0.34 ± 0.04 | 0.26 ± 0.03 | 0.17 ± 0.04 |
| Ultramark 1121 $[M+H]^+$ | 1121.9 | 0.29 ± 0.01 | 0.23 ± 0.01 | 0.16 ± 0.01 |
| Ultramark 1421 $[M+H]^+$ | 1422.1 | 0.30 ± 0.01 | 0.23 ± 0.02 | 0.16 ± 0.02 |
| Ultramark 1621 $[M+H]^+$ | 1622.1 | 0.30 ± 0.02 | 0.23 ± 0.02 | 0.15 ± 0.02 |
| Ultramark 1821 $[M+H]^+$ | 1822.0 | 0.30 ± 0.02 | 0.24 ± 0.02 | 0.15 ± 0.03 |

Note: The mean peak widths for each ion in ZoomScan mode at 10% peak height ($W_{10\%}$), 25% peak height ($W_{25\%}$), and 50% peak height ($W_{50\%}$) are presented. The listed relative error for each measurement is one standard deviation, as calculated from the average of a minimum of three experiments, consisting of 25 analytical scans (10 μscans each), for each ion.

TABLE 3-3: Minimum Isolation Width

| Compound / Ion | m/z | Isolation Width (amu) | $W_{10\%}$ ZoomScan (amu) |
|---|---|---|---|
| Nitrophenol $[M-H]^-$ | 138.1 | 1.0 | 0.21 ± 0.02 |
| DNT $[M-H]^-$ | 181.1 | 1.5 | 0.26 ± 0.04 |
| Caffeine $[M+H]^+$ | 195.0 | 1.0 | 0.26 ± 0.01 |
| 4-Amino-2,6-DNT $[M-H]^-$ | 196.1 | 1.0 | 0.24 ± 0.02 |
| RDX $[M-H]^-$ | 220.9 | 3.0 | 0.32 ± 0.03 |
| TNT $[M-H]^-$ | 226.1 | 1.0 | 0.29 ± 0.03 |
| Picramide $[M-H]^-$ | 227.1 | 1.0 | 0.25 ± 0.02 |
| Tetryl $[M^*-H]^-$ | 241.0 | 1.5 | 0.29 ± 0.03 |
| RDX $[M+Cl]^-$ | 257.1 | 2.0 | 0.25 ± 0.04 |
| Tetryl $[M-H]^-$ | 285.9 | 2.5 | 0.33 ± 0.04 |
| HMX $[M-H]^-$ | 294.9 | 5.5 | 0.63 ± 0.03 |
| PETN $[M-H]^-$ | 314.6 | 7.5 | 1.09 ± 0.01 |
| HMX $[M+Cl]^-$ | 331.1 | 1.5 | 0.24 ± 0.02 |
| HMX $[M+NO2-H]^-$ | 341.6 | 2.5 | 0.34 ± 0.02 |
| Tetryl $[M+Acetone-H]^-$ | 344.0 | 2.0 | 0.29 ± 0.02 |
| PETN $[M+Cl]^-$ | 350.9 | 5.5 | 0.70 ± 0.01 |
| PETN $[M+NO_2]^-$ | 361.7 | 6.0 | 0.69 ± 0.03 |
| HMX $[M+NO_3]^-$ | 358.0 | 2.0 | 0.26 ± 0.02 |
| HMX $[M+103]^-$ | 398.7 | 6.5 | 0.95 ± 0.01 |
| MRFA $[M+H]^+$ | 524.1 | 1.0 | 0.30 ± 0.02 |
| Oleandomycin $[M+H]^+$ | 687.9 | 4.0 | 0.51 ± 0.02 |
| Oleandomycin $[M+Na]^+$ | 710.1 | 1.5 | 0.30 ± 0.05 |
| Erythromycin $[M+H]^+$ | 733.9 | 4.0 | 0.39 ± 0.06 |
| Erythromycin $[M+Na]^+$ | 756.5 | 1.5 | 0.29 ± 0.02 |
| Troleandomycin $[M-42+H]^+$ | 772.0 | 3.0 | 0.41 ± 0.02 |
| Troleandomycin $[M-42+Na]^+$ | 794.1 | 1.5 | 0.29 ± 0.01 |
| Troleandomycin $[M+H]^+$ | 814.0 | 3.5 | 0.34 ± 0.04 |
| Ultramark 1121 $[M+H]^+$ | 1121.9 | 0.5 | 0.29 ± 0.01 |
| Ultramark 1421 $[M+H]^+$ | 1422.1 | 0.5 | 0.30 ± 0.01 |
| Ultramark 1621 $[M+H]^+$ | 1622.1 | 0.5 | 0.30 ± 0.02 |
| Ultramark 1821 $[M+H]^+$ | 1822.0 | 0.5 | 0.30 ± 0.02 |

Note: The minimum isolation width, defined as the isolation waveform notch width that preserves 90% of the maximum isolated ion intensity, is presented for each ion. For comparison with peak width data, the $W_{10\%}$ data for each ion is presented.

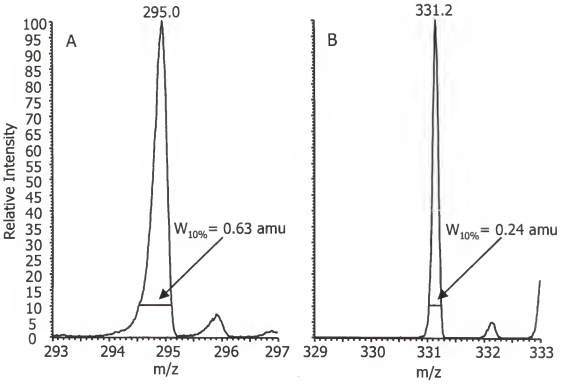


FIGURE 3-1: Comparison of ZoomScan Peak Width of a Fragile and a Non-Fragile Ion

A. ZoomScan spectrum of $[M-H]^-$ ion of HMX, a fragile ion. The peak width of the ion at 10% peak height ($W_{10\%}$) is 0.63 amu. B. Zoom scan spectrum of $[M+Cl]^-$ ion of HMX, a non-fragile ion. The $W_{10\%}$ is 0.24 amu.

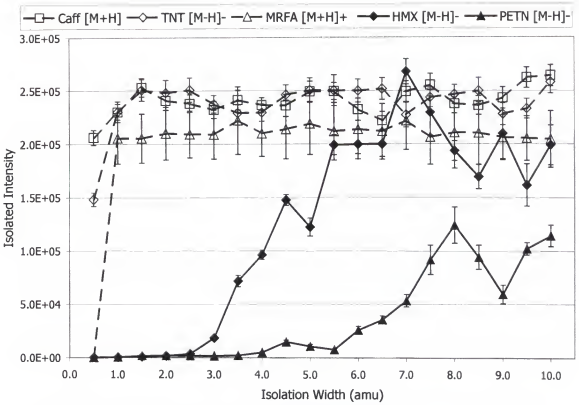


FIGURE 3-2: Effects of Isolation Waveform Notch Width on Isolated Intensity

Plots of the isolated intensity versus the isolation waveform notch width for the representative non-fragile ions (TNT $[M-H]^-$, MRFA $[M+H]^+$, and caffeine $[M+H]^+$) and the fragile explosives ions (HMX $[M-H]^-$ and PETN $[M-H]^-$). The non-fragile ions are represented with open symbols and the fragile ions are symbolized by closed symbols. The plot shows that the fragile ions cannot be isolated with reasonable intensity at unit resolution, as can the non-fragile ions. The minimum isolation width is 1.0 amu for TNT $[M-H]^-$, MRFA $[M+H]^+$, and caffeine $[M+H]^+$, 5.5 amu for HMX $[M-H]^-$ and 7.5 amu for PETN $[M-H]^-$. All points are the average of 25 analytical scans (10 μscans each). The error bars represent ± one standard deviation for each averaged point.

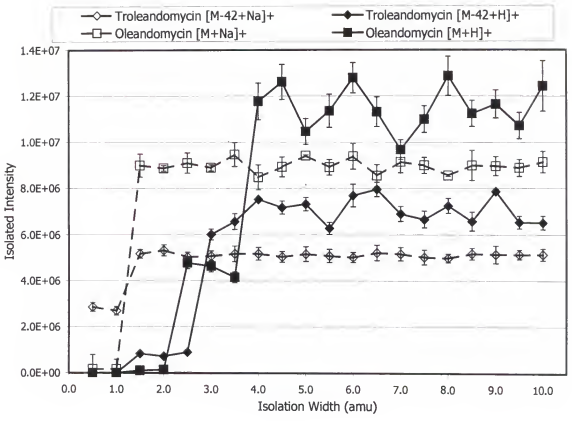


FIGURE 3-3: Effects of Isolation Waveform Notch Width on Isolated Intensity for $[M+H]^+$ and $[M+Na]^+$ of Selected Macrolide Ions

Plots of the isolated intensity versus the isolation waveform notch width for the $[M+H]^+$ ions (closed symbols) and $[M+Na]^+$ ions (open symbols) for the representative macrolides, troleandomycin and oleandomycin. The plot shows that the $[M-42+H]^+$ ion of troleandomycin and the $[M+H]^+$ ion of oleandomycin have minimum isolation widths of 1.5 amu. The minimum isolation width for the $[M-42+Na]^+$ ion of troleandomycin is 3.0 amu and the minimum isolation width for the $[M+Na]^+$ ion of oleandomycin is 4.0 amu. All points are the average of 25 analytical scans (10 μscans each). The error bars represent ± one standard deviation for each averaged point.

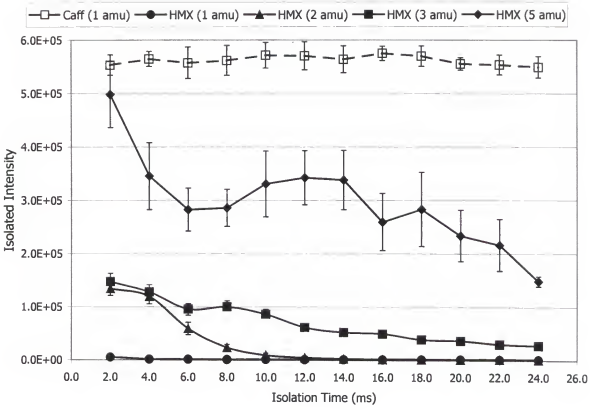


FIGURE 3-4: Effects of Isolation Waveform Time on Isolated Intensity

Plots of the isolated intensity versus the period of time the isolation waveform was applied at different isolation widths are presented for a non-fragile ion (caffeine $[M+H]^+$, open symbol) and a fragile ion (HMX $[M-H]^-$, closed symbols). For the $[M+H]^+$ ion of caffeine, the isolation intensity is plotted for each waveform application time at an isolation width of 1 amu. For the $[M-H]^-$ ion of HMX, the isolated intensity is plotted for each waveform application time at isolation widths of 1, 2, 3, and 5 amu. The intensity of the $[M+H]^+$ ion of caffeine remains constant, while the isolated intensity for the $[M-H]^-$ ion of HMX decreases for all isolation widths investigated (1-5 amu) as the time of the isolation waveform is increased.

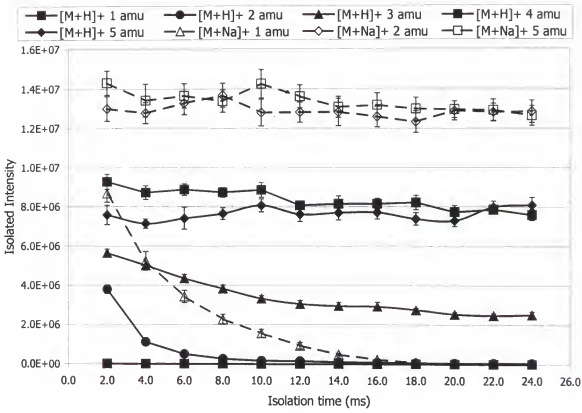


FIGURE 3-5: Effects of Isolation Waveform Time on Isolated Intensity for the $[M+H]^+$ and $[M+Na]^+$ Ions of Oleandomycin

Plots of the isolated intensity versus the period of time the isolation waveform was applied at different isolation waveform notch widths for a fragile ion ($[M+H]^+$ of oleandomycin, closed symbols) and a non-fragile ion ($[M+Na]^+$ of oleandomycin, open symbols). As the period of time for the isolation waveform is increased, the isolated intensity decreases if the isolation waveform notch widths is less than the minimum isolation width for the ion (1.5 amu for the $[M+Na]^+$ ion and 4.0 amu for the $[M+H]^+$ ion).

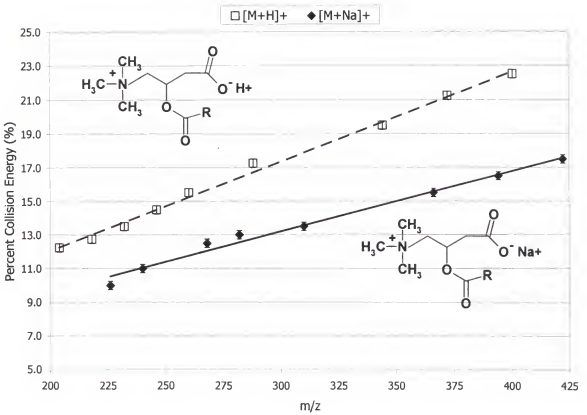


FIGURE 3-6: Comparison of the Optimum Collision Energies for the $[M+H]^+$ and $[M+Na]^+$ Ions of Acylcarnitines

The plot depicts the optimum collision energy for each of nine acylcarnitines versus their parent ion m/z. The optimum collision energy is defined as the energy required to reduce the parent ion intensity by 95%. The $[M+H]^+$ ions of each acylcarnitine requires an optimum collision energy that is 25-30% higher than the $[M+Na]^+$ ion. Collision energy is reported as a percent of the maximum, 5 $V_{p-p}$. Structures are provided for the $[M+H]^+$ and $[M+Na]^+$ ions of the acylcarnitines. All points are the average of the optimum collision energy determined from five breakdown curves. The error bars represent ± one standard deviation for each averaged point.

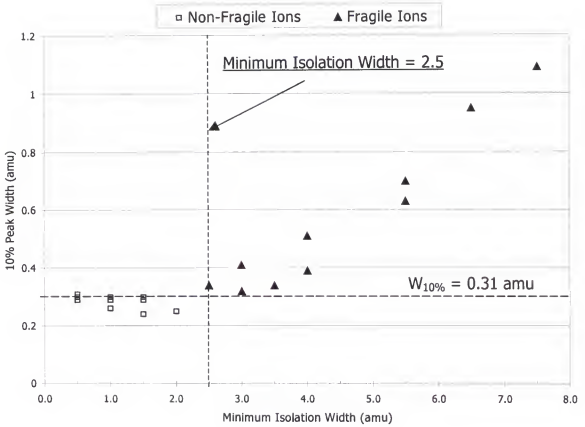


FIGURE 3-7: Predicting the Degree of Ion Fragility

For each ion investigated, the peak width, at 10% peak height, in ZoomScan mode is plotted versus the minimum isolation width. All ions with a $W_{10\%}$ greater than 0.31 amu and a minimum isolation width equal to or greater than 2.5 amu are fragile ions. As the minimum isolation width increases, the ion is more fragile.

# CHAPTER 4
# PARENT AND NEUTRAL LOSS MONITORING

## Introduction

Tandem mass spectrometers have found widespread use in analytical chemistry because of the sensitivity and selectivity provided by two (or more) stages of mass spectrometry (MS/MS and $MS^n$) [Yost and Fetterolf, 1983; Busch et al., 1988]. Traditionally, MS/MS has been performed on tandem-in-space instruments such as triple quadrupole mass spectrometer (TQMS) and multiple sector mass spectrometers [Gross, 1990; Yost and Boyd, 1990]. More recently, tandem-in-time instruments, in which the stages of mass spectrometry are performed sequentially, as in the quadrupole ion trap mass spectrometer (QITMS) [March and Hughes, 1989; March and Todd, 1995; Johnson et al., 1990] and the Fourier transform ion cyclotron resonance mass spectrometer (FTMS) [Marshall et al., 1998], have become more common.

There are four possible MS/MS experiments: product ion scan, parent ion scan, neutral loss scan, and selective reaction monitoring (SRM). The most common MS/MS experiment is the daughter ion scan, which acquires a mass spectrum of the daughter, or product, ions produced from the fragmentation of a selected parent, or precursor, ion. Inherently, daughter ion scans can be performed on both tandem-in-space and tandem-in-time instruments. A parent ion scan detects all of the parent ions in a sample that fragment to produce a common daughter ion, whereas a neutral loss scan detects those ions that fragment to produce daughter ions with a common difference in m/z, therefore,

losing a specific neutral fragment. Parent and neutral loss scans are important mass spectrometric techniques for mixture analysis and the screening of samples for the presence of specific compound classes. These scans are readily implemented on tandem-in-space instruments, but are not readily implemented on tandem-in-time instruments [Johnson et al., 1990]. The only direct approach to obtain this type of data on a tandem-in-time instrument is to acquire a series of separate daughter ion spectra for each parent ion. Each daughter ion spectrum requires a separate set of ionization, isolation, fragmentation, and mass analysis steps. While software has been developed to "mine" out parent and neutral loss data from a series of daughter ion spectra on a commercial instrument [Lopez et al., 1999], it is highly time-intensive and can not be accomplished on a chromatographic time scale. Two different approaches to obtaining parent and neutral loss scans on a QITMS have been previously developed in our lab [Johnson et al., 1991; Johnson et al., 1992A; Johnson et al., 1992B], but these approaches did not yield a practical method for implementation.

The challenge in implementing parent and neutral loss scans on tandem-in-time instruments can be understood by considering how MS/MS (daughter ion scans) are implemented on the QITMS. First, a pulse of ions is injected into (or formed within) the ion trap. For MS/MS ions of a single m/z are next isolated. These ions are then resonantly excited and undergo CID; finally the resulting daughter ions are scanned out of the ion trap in order of increasing m/z and detected. Since parent ions of all other m/z are ejected first, the only simple way to obtain MS/MS data from all of the other parent ions (as is required for parent and neutral loss scans) is to repeat the process (ionize, isolate, excite, and detect) for each parent ion. Performing parent and neutral loss scans

on a QITMS is challenging for a variety of reasons. First, tandem-in-time instruments, unlike tandem-in-space instruments, are not capable of continuous sample injection and generally require discrete ionization events for each mass analysis event. This is problematic because there is not a continuous source of ions to perform either a parent or neutral loss scan. Second, on a QITMS each analysis step, or process, in a MS/MS experiment occurs in the same physical space, unlike in tandem-in-space instruments. Therefore, any manipulation made to one ion, caused by altering the conditions in this physical space, will affect all ions in the ion trap. This is problematic for the implementation of a parent or neutral loss scan on a QITMS during the steps of parent ion fragmentation and trapping of the daughter ions. Lastly, the manner in which ions are mass analyzed in a QITMS, by ramping the RF amplitude and sequentially resonantly ejecting ions of increasing m/z, results in problems associated with the selective detection of the targeted daughter ion.

In this chapter, a novel and practical technique for performing both parent and neutral loss (P&NL) monitoring experiments on a QITMS [Quarmby and Yost, 1997] is presented. This technique is capable of performing scans analogous to the parent and neutral loss scans routinely applied on tandem-in-space instruments, and allows for the screening of a sample to detect analytes of a specific compound class on a chromatographic time-scale. Herein, both the functional capability and the analytical utility of P&NL monitoring will be demonstrated and discussed. The $[M+H]^+$ ions formed from Ultramark 1621, a mixture of fluorinated phosphazines, were chosen to demonstrate the function of P&NL monitoring because of their well-characterized ESI properties and unique CID fragmentation patterns.

Acylcarnitines were chosen as the model compound class to demonstrate the analytical utility of these techniques because of their amenability to ESI, their unique and informative MS/MS fragmentation pattern, and their importance in biological functions. Carnitine and acylcarnitines participate in a wide spectrum of biological functions including the metabolism of fatty acids [Borum, 1985]. The presence of abnormally high levels of acylcarnitines in a patient's urine and plasma is indicative of a wide variety of inborn errors of metabolism [Biebler, 1988; Feller and Rudman, 1988; Sewell, 1995]. The typical concentration of total short-chain and medium chain acylcarnitines is 6 – 10 nmol/mL of plasma in healthy patients and can be 2-3 times higher in patients with metabolic disorders [Millington et al., 1989]. Over the past decade, a large amount of effort has been invested to develop methods utilizing MS/MS to screen patients, specifically newborns, for inborn errors of metabolism related to abnormal acylcarnitine concentrations in blood (both red blood cells and plasma), urine, and tissue [Millington et al., 1989; Chace et al., 1997; Naylor and Chace, 1999; Heinig and Henion, 1999]. Because of the reliance on both parent and neutral loss scans for these screening methods, the triple quadrupole mass spectrometer has been the instrument of choice for these methods. In this chapter, the applicability of P&NL monitoring on a QITMS is demonstrated for screening physiological samples to detect the presence of acylcarnitines.

In this chapter, the potential use of neutral loss monitoring for the analysis explosives is explored. Neutral loss monitoring has the potential for the screening both environmental and forensic samples for the presence of explosives. In Chapter 2, it was demonstrated the CID of nitroaromatic compounds produce characteristic neutral losses

of 30 amu. In this chapter, experiments will be described that utilize this characteristic neutral loss as a method for the identification of nitroaromatic compound ions in a complex negative-ESI-MS spectrum.

## Experimental

### Instrumentation

All experiments were performed on the Finnigan LCQ (San Jose, CA), a commercial, bench-top ESI-QITMS instrument. The LCQ applies a resonant ejection frequency at a $q_z$ of 0.90 to facilitate mass analysis. For all MS/MS experiments, the parent ion of interest is moved to a $q_z$ of 0.25, where a resonant excitation waveform is applied to fragment the parent ion through CID with the He atoms in the ion trap. The energy applied to invoke CID is specified as a collision energy percentage of the total 5 $V_{p-p}$. The programs for P&NL monitoring were written in the ITCL language specifically for the LCQ. All experiments were performed in positive ion mode. The normal scan speed of 0.18 ms/amu was employed for all experiments. All samples were infused into the mass spectrometer at a flow rate of 3 μL/min using the LCQ syringe pump. Each spectrum presented in this paper is the average of either 10 or 25 scans (3 μscans each).

### Samples

#### Ultramark 1621

To prove the functional capability of P&NL monitoring, the ions of Ultramark 1621 (PCR, Gainesville FL) were investigated. Ultramark 1621 is present in the LCQ tuning solution, a mixture of 0.1 mM caffeine, 0.015 mM MRFA, and 0.3 mM Ultramark 1621 in a 50% HPLC-grade acetonitrile (ACN): 25% HPLC-grade methanol (MeOH):

25% HPLC-grade $H_2O$ solution (v/v), with 0.01% glacial acetic acid. Ultramark 1621 is a mixture of fluorinated phosphazines having molecular weights of 921 to 2221 amu at intervals of 100 amu. The possible chemical structure for each of the fluorinated phosphazines is presented in **Figure 4-1A**. For this study, the ions of interest are the $[M+H]^+$ ions of Ultramark 1621, at m/z 922 to 1922 in 100 amu intervals.

Acylcarnitines

To demonstrate the analytical utility of P&NL monitoring, a series of samples containing acylcarnitines was employed. For initial studies, a synthetic mixture of nine saturated acylcarnitines (CMIX) was analyzed. The components of CMIX are acetyl($C_2$)-L-carnitine chloride (MW 239.7), propionyl($C_3$)-L-carnitine chloride (MW 253.7), isobutryl($C_4$)-L-carnitine chloride (MW 267.7), isovaleryl($C_5$)-L-carnitine chloride (MW 281.8), hexanoyl($C_6$)-L-carnitine chloride (MW 295.8), octanoyl($C_8$)-L-carnitine chloride (MW 323.9), lauroyl($C_{12}$)-DL-carnitine chloride (MW 380.0), myristoyl($C_{14}$)-DL-carnitine chloride (MW 408.0), and palmitoyl($C_{16}$)-L-carnitine chloride (MW 436.1). Each acylcarnitine was purchased from Sigma Tau (St. Louis, MO). The CMIX was initially prepared at a concentration of 3 mM for each acylcarnitine in a 50% HPLC-grade MeOH: 50% HPLC-grade chloroform (v/v) solution. For ESI-MS analysis, the CMIX was diluted to 3 μM in 50% HPLC-grade MeOH: 50% HPLC-grade $H_2O$ (v/v) solution. The base chemical structure for each acylcarnitine is presented in **Figure 4-1B**. The identity and specifics of each acylcarnitine $[M+H]^+$ ion and its fragmentation data are displayed in **Table 4-1**.

Two physiological samples were investigated for the presence of acylcarnitines using P&NL monitoring. The first is a commercially available sample of pig plasma

(Sigma-Aldrich) that was spiked with 15 nmol/mL of each acylcarnitine (total concentration of 15 μM CMIX in the plasma) and then diluted by a factor of 10 in 50% HPLC-grade MeOH: 50% HPLC-grade $H_2O$ (v/v). The other sample was pig plasma obtained from a freshly slaughtered pig. Each was diluted by a factor of 5 in 50% HPLC-grade MeOH: 50% HPLC-grade $H_2O$ (v/v) for analysis.

TABLE 4-1: Daughter Ion Data for Acylcarnitine $[M+H]^+$ Ions

| Acyl ($C_n$) Carnitine | $[M+H]^+$ (m/z) | $[M-59+H]^+$ (m/z) | $[M-161+H]^+$ (m/z) | Common Ions Detected (m/z) | Optimum Collision Energy (%) |
|---|---|---|---|---|---|
| Acetyl ($C_2$) | 204 | 145 | ND | 60, 85 | 14.9 % |
| Propionyl ($C_3$) | 218 | 159 | ND | 85 | 15.3 % |
| Isobutryl ($C_4$) | 232 | 173 | ND | 85, 144 | 15.9 % |
| Isovaleryl ($C_5$) | 246 | 187 | 85 | 85, 144 | 17.0 % |
| Hexanoyl ($C_6$) | 260 | 201 | 99 | 85, 144 | 18.0 % |
| Octanoyl ($C_8$) | 288 | 229 | 127 | 85, 144 | 19.6 % |
| Lauroyl ($C_{12}$) | 344 | 285 | 183 | 144 | 23.1 % |
| Myristoyl ($C_{14}$) | 372 | 313 | 211 | 144 | 24.7 % |
| Palmitoyl ($C_{16}$) | 440 | 341 | 239 | 144 | 26.6 % |

ND = Not Detected

Note: The detected product ions from each MS/MS experiment for the $[M+H]^+$ ions of each acylcarnitine present in the synthetic CMIX sample at the specified m/z. Both the product ions from characteristic neutral losses and common product ions are presented. The optimum collision energy, defined as the energy required to dissociate 95% of the parent ion, was determined for the dissociation of each $[M+H]^+$ ion. All daughter ion experiments were conducted at a resonant excitation $q_z$ of 0.25.

Explosives - nitroaromatic compounds

To demonstrate the analytical utility of P&NL monitoring for the analysis of explosives, the nitroaromatic compound class of explosives was analyzed. A mixture of eight nitroaromatic compound explosives (ExpMix), was used for this investigation. The

mixture contained 18 ppm 2,4,6-trinitrotoluene (TNT); 34 ppm 2-amino-4,6-dinitrotoluene (2A-4,6-DNT); 20 ppm 1,3,5-trinitrobenzene (TNB); 35 ppm 2,4,6-trinito-*m*-cresol (TNC); 10 ppm tetryl; 25 ppm 2,4,6-trinitroaniline (picramide); 2,3-dinitronaphthalene; and 1,3,5-trinitronaphthalene (TNN) in a 50% HPLC-grade isopropanol (IPA): 50% HPLC-grade water ($H_2O$) solution (v/v), with 0.1% ammonium hydroxide ($NH_4OH$). All explosives, except for 2A-4,6-DNT, were provided by Dr. Jehuda Yinon, of the Weizmann Institute of Science, and obtained from the Analytical Laboratory of the Israeli Police Headquarters. The 2A-4,6-DNT sample was provided by Dr. Fred Volk, of the Fraunhofer Institute of Chemical Technology, Germany.

Daughter ion mass spectra

Daughter ion mass spectra were acquired for the $[M+H]^+$ ions of the fluorinated phosphazines and acylcarnitines to determine the characteristic fragmentation pattern of each compound class, and breakdown curves were constructed to determine the optimum and range of collision energies for each ion. Daughter ion mass spectra were also acquired for each of the fragment, molecular, and adduct ions of the nitroaromatic compound ions at a collision energy of 30%. The CID fragmentation pattern for the nitroaromatic compounds of interest has been discussed at length in Chapter 2. The fragmentation patterns were utilized to determine characteristic neutral losses and common daughter ions for each ion in the compound class. The breakdown curves were utilized to determine an appropriate collision energy to use during P&NL monitoring experiments for the Ultramark and acylcarnitine ions. For the $[M+H]^+$ ions of Ultramark, a collision energy of 60% was used for all P&NL monitoring experiments. For the acylcarnitine ions, a collision energy percentage of 25% was used for all P&NL

monitoring experiments. A collision energy percentage of 30% was used for all P&NL experiments for the analysis of the nitroaromatic compound ions.

Parent and Neutral Loss Monitoring

Programs, consisting of a series of computer-controlled events composed in the ITCL language for the LCQ, have been written for implementing P&NL monitoring on a QITMS. The series of computer-controlled events are the same for both parent ion monitoring and neutral loss monitoring, as shown in the flowchart in **Figure 4-2**; the only difference is the manner in which calculations, pertaining to the target daughter ions, are performed. In the case of the parent ion monitoring experiment, the detected daughter ion will remain constant for each parent ion interrogated and will be defined by the user. In the case of the neutral loss monitoring experiment, the detected daughter ion will be different for each parent ion interrogated and will be calculated from the neutral loss entered by the user. In this section, the computer-controlled events for P&NL monitoring will be described for both a prescan and an analytical scan. A pictorial representation of the process is presented in **Figure 4-3**.

First, ions may be either formed in the ion trap, via internal ionization, or injected into the quadrupole ion trap from an external ionization source. In the work presented here, an external electrospray ionization (ESI) source, was utilized to form analyte ions for analysis. The injected ions are then mass analyzed and an initial mass spectrum, or prescan, is acquired. The computer can then select ions to be interrogated for either the parent ion or neutral loss monitoring experiment, based a set of predetermined criteria. For the experiments described within, a m/z is selected for interrogation if it is one of the 18 most intense m/z ions in the acquired prescan. In **Figure 4-3**, the selected m/z ions are represented by the black closed-circles. The number of parent ions that may be

interrogated is restricted to 18 by the computer memory required for the method and not the P&NL monitoring method. In order to interrogate more than 18 parent ions and obtain a more "complete" P&NL spectrum, a series of P&NL monitoring experiments may be performed in sequence utilizing multiple ionization events. For example, the first P&NL monitoring experiment may interrogate the most 18 intense ions and then the second experiment could interrogate the next most intense 18 ions. The general strategy for determining the criteria is to allow the computer to choose m/z values of the ions with enough intensity to produce good MS/MS spectra for analysis. Other possible criteria that may be utilized for selecting m/z ions to be interrogated include selecting ions from a predetermined list of ions or selecting the most intense ions that are not on an exclusion list. The selected m/z values are then stored in an array for interrogation.

Next, a second ionization event takes place and all of the ions are trapped in the ion trap for analysis. The computer then selects the first (lowest) parent m/z that is to be interrogated. The RF amplitude is then ramped up until all of the ions of a m/z less than the selected m/z have a $q_z$ value greater than 0.9 and are resonantly ejected from the ion trap. The resonant ejection waveform is applied during this event to facilitate ion ejection, but the electron multiplier is off, and no ion signal is acquired. This action is represented pictorially as *Step 1* in **Figure 4-3**.

After all of the ions of a m/z lower than the selected m/z have been ejected from the ion trap, the RF amplitude is then ramped down to place the first selected parent m/z at a $q_z$ value of 0.25. A resonant excitation waveform is then applied at a frequency corresponding to a $q_z$ of 0.25 and the parent ion is fragmented via CID. All of the

daughter ions with a $q_z$ value between 0.25 and 0.90 are then trapped. These actions are represented in *Step 2* in **Figure 4-3**.

After a sufficient time for parent ion fragmentation, typically 30 ms, and the daughter ions have been effectively trapped, the RF amplitude is then ramped up to place the targeted product m/z at a $q_z$ slightly less than 0.90. The electron multiplier is off during this event. This action allows for all of the unwanted daughter ions to be ejected from the trap and not be detected. The targeted product m/z is then selectively ejected by ramping the RF amplitude with the electron multiplier on. If CID of the parent ion formed the targeted daughter ion, the ion will be detected. These actions are depicted in *Step 3* in **Figure 4-3**. The next step is to ramp the RF amplitude up until all of the ions of a m/z less than the second selected m/z are ejected from the ion trap. This action is represented in *Step 4* in **Figure 4-3**. The processes depicted in *Steps 1* through *3* are then repeated for each selected parent m/z until all of the selected m/z in the stored array are interrogated. An analytical scan is then assembled from the series of Steps 1 – 4 (**Figure 4-3**) and displayed to the user which depicts all of the selected m/z ions which fragment to produce the specified daughter ion (parent ion monitoring) or neutral loss (neutral loss monitoring).

For each P&NL ion experiment, a series of decisions must be made by the experimenter and specified as a set of parameters. The first decision is whether a parent ion monitoring or neutral loss monitoring experiment will be conducted. For a parent ion monitoring experiment, the target daughter ion m/z to be monitored must be specified. For a neutral loss monitoring experiment, the target neutral loss fragment must be specified so that the computer can calculate which daughter ion m/z should be monitored

for each parent ion m/z. Parameters which must be entered include the parent ion m/z range to be interrogated, the number of m/z to be interrogated, the collision energy percentage for the CID experiments, and the width of isolation for the parent ions. Both the prescan and analytical scans can be individually averaged over the specified m/z range. Other considerations for each P&NL monitoring experiment are the desired time scale and the number of μscans that will be averaged for one P&NL monitoring scan. For a P&NL ion experiment that implements the 18 most intense ion criterion and has both a prescan and analytical scan over a 1500 m/z range, the time required for each μscan is approximately 1.0 s. This includes approximately 300 ms for the prescan and approximately 700 ms for the analytical scan. The time for each scan will differ depending upon the selection criterion used, the number of ions interrogated, and the m/z range analyzed.

## Results and Discussion

### Ultramark 1621

To illustrate the functional capability of P&NL monitoring methods, the $[M+H]^+$ ions of Ultramark 1621 are used as a model system. To design an effective P&NL monitoring experiment for the detection of an Ultramark 1621 ion in a sample, the fragmentation pattern of the ions must be predetermined. To this end, CID experiments were performed on each Ultramark 1621 ion. It was determined that, while there are some differences in the fragmentation patterns, all $[M+H]^+$ ions of Ultramark 1621 produces daughter ions corresponding to neutral losses of 32, 132, 232, 244, 332, 344, and 444 amu. An example of the product spectrum for a representative $[M+H]^+$ ion of Ultramark 1621 at m/z 1422, corresponding to 11 $C_2F_4$ groups in its chemical structure, is

presented in **Figure 4-4**. It was determined that a collision energy of 60% is sufficient to fragment all of the Ultramark $[M+H]^+$ ions without ejecting any ions before fragmentation occurs.

The first step in either a neutral loss monitoring experiment or parent ion monitoring experiment is to acquire a prescan of the sample. In this case, the prescan is a full-scan mass spectrum of the LCQ tuning solution from m/z 500 to m/z 2000 (**Figure 4-5A**). The ion at m/z 524 is the $[M+H]^+$ ion of the tetrapeptide MRFA, a component of the tuning solution. The positive ESI of the various fluorinated phosphazines in Ultramark 1621 produces intense $[M+H]^+$ ions and minor $[M-CH_2+H]^+$ ions. The ions at 100 amu intervals from m/z 922 to 1922 are the $[M+H]^+$ ions and are of interest in this application. The m/z values that fit the predetermined criteria are then selected and stored in an array for interrogation in the analytical scan. In this experiment, the criterion is that the ion is one of the 18 most intense in the prescan. Next, the second ionization event occurs and ions corresponding to the stored m/z values are interrogated, in order of increasing m/z, to obtain the analytical scan for either a neutral loss or parent ion monitoring experiment.

In the product spectra of the $[M+H]^+$ ions of Ultramark 1621, the daughter ions resulting from the neutral loss of 132 amu were consistently intense. Therefore, a neutral loss of 132 amu was chosen as a characteristic neutral loss to screen for the $[M+H]^+$ ions of the fluorinated phosphazines. The neutral loss monitoring spectrum (**Figure 4-5B**) includes only the ions which are among the 18 most intense in the prescan (**Figure 4-5B**) and undergo a neutral loss of 132 amu. Using the 18 most intense ion criteria, all of the $[M+H]^+$ ions from m/z 1022 through 1922, plus five of the $^{13}C$-peaks of these $[M+H]^+$

ions at one amu higher, were selected. All of these ions undergo a neutral loss of 132. The other ions which were selected, including the $[M+H]^+$ ion of MRFA and some of the $[M-CH_2+H]^+$ ions of Ultramark, do not fragment with a neutral loss of 132 and, therefore, do not show up in the neutral loss spectrum. The relative intensity of the ions in **Figure 4-5B** is a function of the parent ion intensity plus the efficiency of the CID process to form the particular daughter ion at the selected collision energy. However, since the relative intensity is proportional to the intensity of a characteristic daughter ion from a specific parent ion, P&NL monitoring can potentially be used as a means for quantitation.

To design a parent ion monitoring experiment, which will identify all of the Ultramark ions, a common daughter ion should be chosen. However, the $[M+H]^+$ ions do not all produce a, common daughter ion under the CID conditions utilized for this experiment. At a collision energy of 60%, the $[M+H]^+$ ions at m/z 1122, 1222, 1322, and 1422 all produce a daughter ion at m/z 1090. However, the lower and higher m/z Ultramark $[M+H]^+$ ions, at m/z 922, 1022, 1522, 1622, 1722, 1822, and 1922, do not produce a daughter ion at m/z 1090. For our sample parent ion monitoring experiment, the daughter ion at m/z 1090 was chosen as the ion for which to screen the sample. The parent ion monitoring spectrum (**Figure 4-5C**) detects only the four Ultramark $[M+H]^+$ ions in the prescan (**Figure 4-5A**) that fragment to produce a daughter ion a m/z 1090. If a parent ion monitoring experiment was needed that would detect all of the Ultramark 1621 $[M+H]^+$ ions, then more than one daughter ion would have to be selected.

Acylcarnitines

To demonstrate the analytical capability of P&NL monitoring for compound class screening, experiments were conducted utilizing acylcarnitines. CMIX, a synthetic mixture of nine acylcarnitines, was first analyzed to determine characteristic daughter

ions and neutral losses. To evaluate P&NL monitoring on the ion trap, spiked and unspiked pig plasma samples were then analyzed.

Synthetic mixture - CMIX

To determine the fragmentation pattern of the $[M+H]^+$ ion for each acylcarnitine in the CMIX, product spectra were obtained for each ion. The characteristic daughter ions for the $[M+H]^+$ ions of each acylcarnitine at an excitation $q_z$ of 0.25 are presented in **Table 4-1**. The acylcarnitine $[M+H]^+$ ions fragment to produce common daughter ions at m/z 60 ($[N(CH_3)_3+H]^+$), m/z 85 ($[CH_2CHCHCO_2+H]^+$), and m/z 144 ($[N(CH_3)_3CH_2CHCHCO_2+H]^+$). During an MS/MS experiment on a QITMS, the lowest m/z daughter ion that may detected, or low mass cut-off (LMCO), is determined by the parent m/z, the $q_z$ of excitation and the $q_z$ for ion ejection at either the right-hand edge of the stability diagram ($q_z$ = 0.908), or the resonant ejection $q_z$ ($q_{ej}$), as determined by the following equation:

$$LMCO = \frac{q_z}{q_{ej}}\left(m/z_{Parent}\right) \qquad (4\text{-}1)$$

Since MS/MS excitation occurs at a default $q_z$ of 0.25 and the $q_{ej}$ is 0.90 on the LCQ, the daughter ion at m/z 60 can only be detected for acylcarnitines with a MW below 217 amu (i.e. only acetylcarnitine) and the daughter ion at m/z 85 can only be detected for acylcarnitines with a MW below 305 amu. By lowering the $q_z$ of excitation to 0.16, the daughter ion at m/z 85 was detected from the dissociation of each acylcarnitine $[M+H]^+$ ion in the mixture. Also, the daughter ion at m/z 60 was detected for all $[M+H]^+$ ions of the acylcarnitines m/z 288 and less. The common daughter ion at m/z 144, although observed for all of the acylcarnitines, is not a very intense daughter ion. Each acylcarnitine $[M+H]^+$ ion also produces a daughter ion that corresponds to a neutral loss

of 59 amu, $N(CH_3)_3$, and 161 amu, $N(CH_3)_3CH_2CH(OH)CHCO_2H$. The neutral loss of 59 was detected for all acylcarnitine $[M+H]^+$ ions at an excitation $q_z$ of 0.25. The daughter ion associated with the neutral loss of 161 could not be detected for the lowest MW acylcarnitines (acetylcarnitine, propionylcarnitine, and isobutrylcarnitine) at an excitation $q_z$ of 0.25 because of the LMCO. To detect the neutral loss of 161 amu for the low MW acylcarnitines, the $q_z$ of excitation was decreased. The daughter ion corresponding to the neutral loss of 59 is consistently the most intense daughter ion. Breakdown curves were constructed for the $[M+H]^+$ ion of each acylcarnitine and the optimum collision energy percentage was ascertained (**Table 4-1**). A collision energy percentage of 25% was found to be nearly optimum for the CID of each acylcarnitine ion.

Both neutral loss monitoring and parent ion monitoring experiments were conducted on the CMIX sample. In these experiments, the 18 most intense ion criterion was used for selection of the m/z to interrogate from a prescan (**Figure 4-6A**), over a m/z range of 100 to 600. The prescan is the average of the prescans from 20 successive P&NL monitoring experiments, and is representative for both the neutral loss monitoring and parent ion monitoring experiments.

The spectrum obtained by neutral loss monitoring of 59 amu of CMIX is shown in **Figure 4-6B**. All of the acylcarnitine $[M+H]^+$ ions selected as one of the most 18 intense from the prescan were detected, including the $^{13}C$ $[M+H]^+$ ion of some acylcarnitines. Comparison of the prescan (**Figure 4-6A**) and the analytical scan (**Figure 4-6B**) shows that ions which were selected as among the 18 most intense, but are not acylcarnitine $[M+H]^+$ ions, such as the ion at m/z 156, are not observed in the neutral loss monitoring

spectrum. Each neutral loss monitoring spectrum, consisting of 3 μscans for both the prescan and analytical scan, required an average of 3.3 s. to acquire.

**Figure 4-6C** shows the spectrum obtained by parent ion monitoring of m/z 85 for CMIX at an excitation $q_z$ of 0.25. Each of the $C_2$ through $C_8$ acylcarnitine $[M+H]^+$ ions were detected. The $C_{12}$ to $C_{16}$ acylcarnitine ions were not detected because their m/z 85 daughter ions fell below the LMCO during resonant excitation at a $q_z$ of 0.25. When designing a parent ion monitoring or neutral loss monitoring experiment on the ion trap, it is important that a common daughter ion for parent ion monitoring or a characteristic neutral loss for neutral loss monitoring, which produces daughter ions above the LMCO for all members of the compound class of interest.

Monitoring the neutral loss of 59 was selected as the best method for screening a sample for acylcarnitines because these daughter ions are intense and they can be monitored without any limitations associated with the LMCO. Note that parent monitoring of m/z 85 and neutral loss monitoring of 161 could be used as confirmation techniques for low and high MW acylcarnitines, respectively.

Spiked pig plasma

The spiked pig plasma was utilized to determine whether the P&NL monitoring methods would be capable of detecting acylcarnitines at physiologically relevant levels. Both neutral loss monitoring of 59 amu and a parent ion monitoring of m/z 85 experiments were conducted on the sample, which was introduced via infusion. A prescan (**Figure 4-7A**) was acquired over a m/z range of 100 to 600. The prescan shows that the $[M+H]^+$ ions of all the spiked acylcarnitines are detectable in the spiked sample along with a variety of other ions, including the $[M+Na]^+$ ions for some of the spiked

acylcarnitines. $[M+Na]^+$ ions were also detected in synthetic mixtures of acylcarnitines containing 10 mM sodium acetate. The fragmentation pattern for the $[M+Na]^+$ ions shows the neutral loss of 59, like the $[M+H]^+$ ions, but not the neutral loss of 161 amu nor the common ions at m/z 85 and 144.

Neutral loss monitoring of 59 amu for the spiked pig plasma sample (**Figure 4-7B**) shows the detection of many of the $[M+H]^+$ ions and $[M+Na]^+$ ions of the present acylcarnitines. The reason some acylcarnitine ions were not detected is that these ions were not selected as among the 18 most intense m/z and thus were not interrogated. If it were of concern to detect these ions, a different criterion for selection of the m/z for interrogation could be used, or the second most intense set of 18 m/z could be selected for interrogation. This experiment detected only one ion in the spiked pig plasma sample that could not be attributable to the spiked acylcarnitines, at m/z 340. A daughter ion spectrum of this ion confirmed that a daughter ion at m/z 281 was produced by CID, which corresponds to a neutral loss of 59, but the total daughter ion spectrum was not indicative of an acylcarnitine $[M+H]^+$ ion.

The parent ion monitoring of m/z 85 (**Figure 4-7C**) shows the detection of the $[M+H]^+$ ions for only isovalerylcarnitine, hexanoylcarnitine, and octanoylcarnitine in the sample. The higher MW acylcarnitines are not observed because the daughter ion at m/z 85 is not detectable for parent ions above m/z 306 at an excitation $q_z$ of 0.25. The lower MW acylcarnitines, acetylcarnitine, propionylcarnitine, and isobutrylcarnitine, are not detected since their $[M+H]^+$ ions are not among the 18 most intense m/z and therefore were not selected for interrogation. There were no $[M+Na]^+$ ions detected in the sample because those acylcarnitine ions do not produce a daughter ion at m/z 85.

Unspiked pig plasma

To demonstrate that this method is capable of detecting acylcarnitines in direct physiological samples, samples of fresh pig plasma were obtained and analyzed. The analysis of this sample was performed with no prior knowledge about the presence of acylcarnitines in the sample. Neutral loss monitoring of 59 amu was used as the screening technique to determine the presence of acylcarnitines.

Acylcarnitines could be detected by neutral loss monitoring in the plasma sample. The mass spectrum in **Figure 4-8A** displays the average prescan from 15 consecutive neutral loss monitoring experiments of the plasma sample from m/z 250 to 500. For each prescan, the 18 most intense m/z were selected for interrogation. The selected m/z varied from scan to scan, depending on the intensity of each m/z for each prescan. Over the 15 prescans, a total of over 50 different ions were selected and interrogated for the neutral loss of 59 amu. The mass spectrum of the average of the 15 neutral loss monitoring experiments is displayed in **Figure 4-8B**. The mass spectrum shows all of the ions that have a neutral loss of 59. Through inspection of the product spectra for each of the detected ions, it appears that only a few of these ions arise from acylcarnitines.

In the plasma sample, we were able to detect the $[M+H]^+$ and $[M+Na]^+$ ions of palmitoylcarnitine, one of the acylcarnitines in the synthetic mixture for which we were looking in this sample. We were also able to identify acylcarnitine ions we had not previously observed, including m/z 310, 316, and 330. The daughter ion spectrum for m/z 310 is presented in **Figure 4-8C**. The mass spectrum shows the common daughter ion at 144 and the characteristic neutral losses of 59 and 161 amu. Also, the daughter ion at m/z 103 is common to some of the acylcarnitines. The assumed identity of the three ions is as follows: (1) the ion at m/z 310 is the $[M+H]^+$ ion of the $C_9$ acylcarnitine

containing 3 double bonds in its acyl chain, (2) the ion at m/z 316 is the saturated $C_9$ acylcarnitine, and (3) the ion at m/z 330 is the saturated $C_{10}$ acylcarnitine; none of these compounds was available as standards for confirmation.

Explosives – Nitroaromatic Compounds

To demonstrate the analytical capability of P&NL monitoring for the analysis of explosives, experiments were conducted utilizing the nitroaromatic compound class of explosives. Nitroaromatic compounds were chosen because they produce non-fragile ions via negative-ESI and can be monitored by a specific neutral loss of 30 amu.

To determine the fragmentation pattern of the fragment, molecular, and adduct ions of each ion produced from the negative-ESI of the nitroaromatic compound mixture, daughter ion spectra were obtained. During CID, the molecular ions (both the $[M-H]^-$ and $M^-$ ions) of all the nitroaromatic compounds undergo a neutral loss of 30 amu. The fragment ions also undergo the same neutral loss upon fragmentation. The adduct ions observed, which are generally the $[M+Acetone-H]^-$ ions of the explosives, do not undergo the neutral loss of 30 amu. These adduct ions typically undergo the neutral loss of 58, 57 or 47 amu. A more detailed description of the MS/MS spectra and fragmentation pattern for the explosive ions is presented in Chapter 2.

Two different experiments were used to show the capabilities of monitoring the neutral loss of 30 amu as a method for screening for nitroaromatic compounds. The mixture of explosives contains eight different nitroaromatic compounds, which produce ions that can be identified, by inspection, in a full scan mass spectrum of the mixture. These ions range from m/z 196 to 320. To fully demonstrate the ability of the neutral loss method, experiments were conducted over two different m/z ranges. In both experiments, the 18 ions of highest intensity were chosen for interrogation. All

experiments were conducted at a resonant excitation $q_z$ of 0.25 and a collision energy of 30%. For all experiments, the mass spectra presented are the average of 15 prescans and/or analytical scans.

The neutral loss monitoring of 30 amu from m/z 180 to 240 is presented in **Figure 4-9**. The prescan of the ExpMix (**Figure 4-9A**) shows the detection of a variety of ions, including those from the ExpMix, over the m/z range from 180 to 240. The neutral loss monitoring of 30 amu (**Figure 4-9B**) depicts all of the ions in the prescan that fragmented, via CID, to produce a neutral loss of 30 amu. The ions present in the mass spectrum were all identified. The ion at m/z 196 is the $[M-H]^-$ ion of the 2A-4,6-DNT. The ions identified at m/z 212, 213, and 214 are the $[M-H]^-$, $M^-$ and $^{13}C\ M^-$ ions of TNB. The ion identified at m/z 218 is the $M^-$ ion of DNN. The ion at m/z 226 is the $[M-H]^-$ ion of TNT. The ion at m/z 227 is both the $M^-$ ion of TNT and the $[M-H]^-$ ion of picramide. The ion at m/z 228 is predominately the $M^-$ of picramide, but may also be the $^{13}C\ M^-$ ion of TNT. The ion at m/z 229 is the $^{13}C\ M^-$ ion of picramide. The ions at m/z 236 and 237 are not readily recognized as ions indicative of any of the nitroaromatic compounds in the mixture, but daughter ion spectra show that these ions do undergo a neutral loss of 30 amu. This experiment was able to identify all of the nitroaromatic compounds present in the ExpMix over this particular m/z range.

To demonstrate the selectivity of this method for the fragment and molecular ion of the nitroaromatic compounds, a second experiment was conducted. In this experiment (**Figure 4-10**) the prescan m/z range was increased to include the adduct ions of the nitroaromatic compounds. The prescan mass spectrum (**Figure 4-10A**) is displayed at a m/z range from 180 to 300. Over this range, the adduct ions of some of the nitroaromatic

compounds are detected at m/z 270, 284, and 285. These ions do not undergo a neutral loss of 30 amu during CID fragmentation. The neutral loss monitoring of 30 amu (**Figure 4-10B**) depicts all of the ions in the prescan which were selected for interrogation and identified as fragmenting with a neutral loss of 30 amu. The ions identified include those identified in **Figure 4-9** at m/z 213, 226, 227, 228, and 229. The ion at m/z 196, which is the $[M-H]^-$ ion of 2A-4,6DNT, was not identified because its intensity was too low to be included in the 18 most intense ions. The new ions identified are at m/z 242, 243, and 263. The ions at m/z 242 and 243 are the $[M-H]^-$ and $^{13}C$ $[M-H]^-$ ions of TNC. The ion at m/z 263 is the $M^-$ ion of TNN. The adduct ions at m/z 270, 283, 284, and 285 were not identified as nitroaromatic compound ions because their fragmentation does not result in a neutral loss of 30 amu.

## Conclusion

The data in this chapter, demonstrate that P&NL monitoring on the QITMS is a viable technique for screening analytical samples on a chromatographic time scale. This technique can yield valuable information, analogous to parent and neutral loss scans on tandem-in-space instruments, and compound-class screening of analytical samples.

Using both the spiked and unspiked pig plasma samples, the technique of neutral loss monitoring was demonstrated to be capable of detecting acylcarnitines in biological matrices at physiological concentrations. In the spiked sample, the neutral loss monitoring of 59 amu detected both the $[M+H]^+$ and $[M+Na]^+$ ions of the spiked acylcarnitines. It also detected an ion at m/z 340 that had a neutral loss of 59 amu, but was not identified as an acylcarnitine ion based upon its product spectrum. Parent ion monitoring of m/z 85 detected only a few acylcarnitines in the spiked pig plasma samples

due to LMCO limitations and the low intensity of the $[M+H]^+$ ions for the low MW acylcarnitines, which resulted in them not being selected for interrogation. The neutral loss monitoring of 59 amu was successful in detecting acylcarnitines in an unspiked pig plasma sample. The identified acylcarnitines included those that were in the synthetic mixtures as well as those not in the synthetic mixture.

A few conclusions can be drawn concerning the application of P&NL monitoring for the detection of acylcarnitines in complex mixtures. First, the neutral loss monitoring of 59 amu is the most inclusive means to screen for acylcarnitines because it will allow for the detection of all acylcarnitines, independent of MW or ion type ($[M+H]^+$ or $[M+Na]^+$). Next, it is important to minimize the potential for false negatives in the screening experiment due to a non-selection of the acylcarnitine ion for interrogation if it is not one of the most intense 18 ions in the prescan. To accomplish this goal, one can modify the selection criteria for the m/z to be interrogated. This could be accomplished by interrogating a set of the second most intense 18 ions. Or, if there is a specific and limited list of acylcarnitine ions which are of concern to the investigator, a "to-do" list can be created and only those ions will be interrogated by the analytical scan of the P&NL monitoring technique. Finally, because of the potential for false positives, in the screening experiment, methods are required for the confirmation of the suspected acylcarnitine ion. This can be accomplished either by a complimentary P&NL monitoring experiment, such as the neutral loss monitoring of 161 amu or the parent ion monitoring of either m/z 85 or 144, or by a daughter ion experiment. Ultimately, the technique of P&NL monitoring on the QITMS can be a valuable screening method for acylcarnitines.

For the screening of explosives, the neutral loss monitoring of 30 amu is the best method to identify the negative molecular and fragment ions of the nitroaromatic compounds. However, this method does not identify the adduct ions formed from the negative-ESI of the explosive compounds. Because of the diverse chemical structures and the various fragmentation patterns for each of the nitroaromatic compounds, there is no single daughter ion that can be successfully used for the screening of the entire compound class using parent ion monitoring. This may be problematic because if the neutral loss monitoring of 30 amu is being used to screen for nitroaromatic compounds, there is no complimentary method to use, on the fly, that will improve the confidence in the identification of the nitroaromatic compounds. However, because the neutral loss of 30 amu is most always the loss of NO in any CID experiment, there is a high confidence that the identification of the nitroaromatic compounds using the neutral loss monitoring of 30 amu will be accurate.

**A**

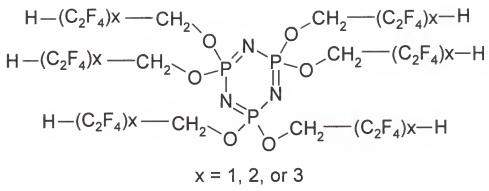


**B**

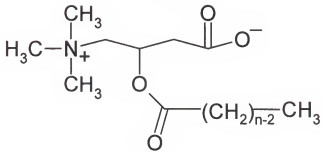


FIGURE 4-1: Structures of Ultramark 1621 and Acylcarnitine Compounds

A. Structures of Ultramark 1621 molecules from MW 921 to 2221, which increase by 100 amu with each additional $C_2F_4$. B. Structures for the acylcarnitine class of compounds, where n = the number of carbons in the ester chain. In solution, these compounds form a zwitterion.

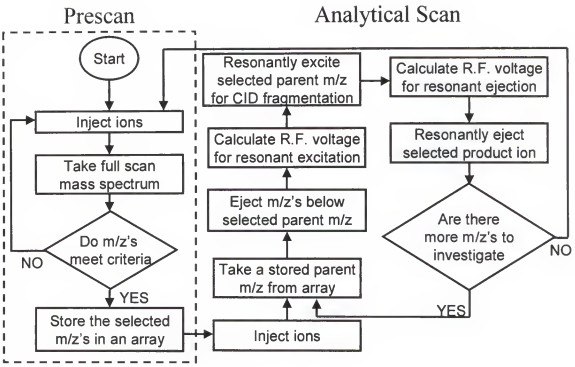


FIGURE 4-2: Flow Chart for Parent and Neutral Loss Monitoring on a Quadrupole Ion Trap

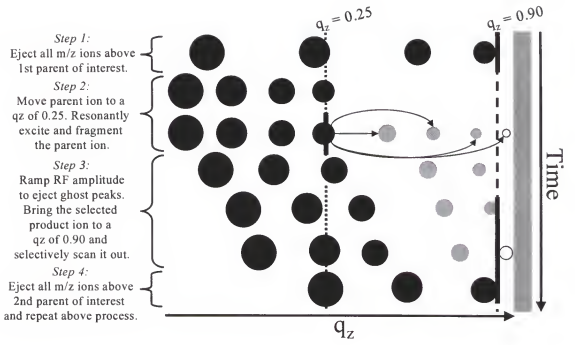


FIGURE 4-3: Illustration of Parent and Neutral Loss Monitoring

Illustration of parent and neutral loss monitoring in $q_z$ space along the $a_z$= 0 line. The shaded area on the right represents the edge of the stability diagram. The black circles represent parent ions, the gray circles represent product ions, and the open circles represent ions that are not axially stable in the ion trap.

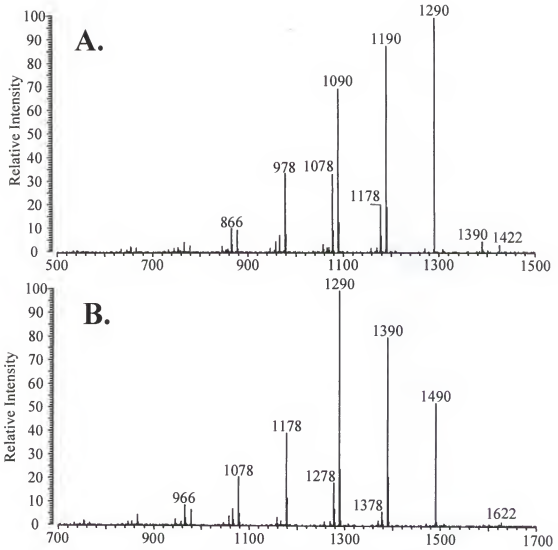


FIGURE 4-4: Daughter Ion Mass Spectra of Ultramark $[M+H]^+$ Ions

A. Product ion mass spectrum of $[M+H]^+$ at m/z 1422 B. Product ion mass spectrum of $[M+H]^+$ at m/z 1622. Both spectra were obtained at a resonant excitation $q_z$ of 0.25 and collision energy of 60%.

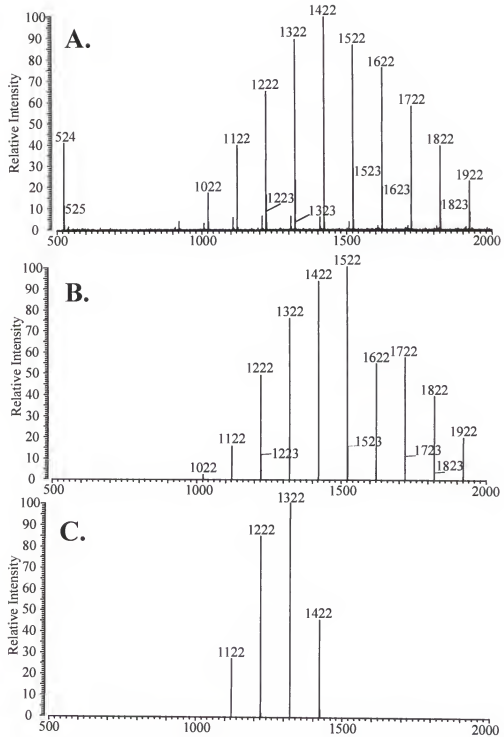


FIGURE 4-5: P&NL Monitoring of LCQ Tuning Solution to Screen for Ultramark $[M+H]^+$ Ions

A. Prescan of LCQ tuning solution. B. Neutral loss monitoring of 132 amu. C. Parent ion monitoring of m/z 1090. Both B and C were at a $q_{ex}$ at 0.25 and collision energy of 60%.

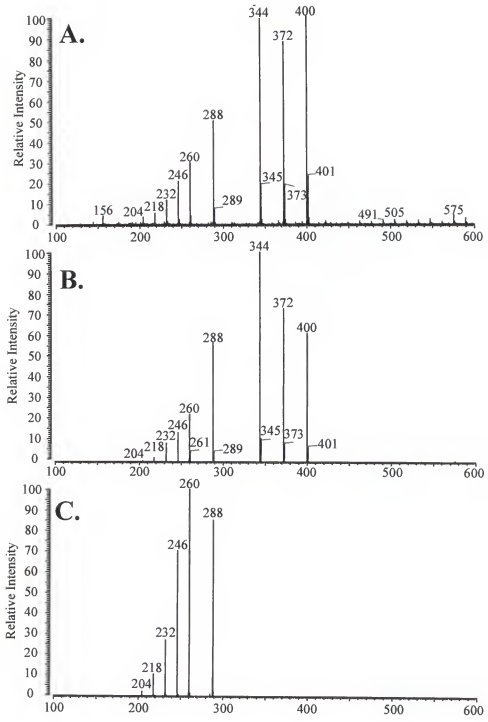


FIGURE 4-6: Parent and Neutral loss Monitoring of CMIX to Screen for Acylcarnitine $[M+H]^+$ Ions

A. Prescan of CMIX solution. B. Neutral loss monitoring of 59 amu. C. Parent ion monitoring of m/z 85. Both B and C were at a $q_{ex}$ at 0.25 and collision energy of 60%.

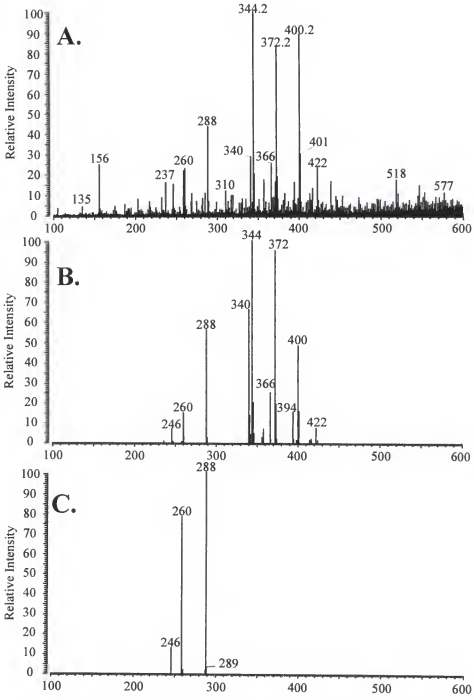


Figure 4-7: Parent and Neutral Loss Monitoring of Spiked Plasma to Screen for Acylcarnitine $[M+H]^+$ Ions

A. Prescan of spiked plasma with 15 µM CMIX. B. Neutral loss monitoring of 59 amu. C. Parent ion monitoring of m/z 85. Both B and C were at a $q_{ex}$ at 0.25 and collision energy of 60%.

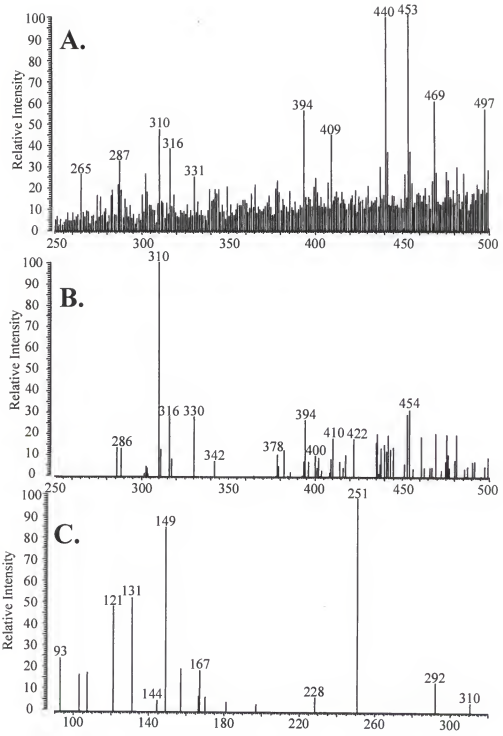


Figure 4-8: Neutral Loss Monitoring of Pig Plasma to Screen for Acylcarnitine $[M+H]^+$ Ions

A. Prescan of an unspiked pig plasma sample. B. Neutral loss monitoring of 59 amu. C. Product ion spectrum of m/z 310 from m/z 90 - 320.

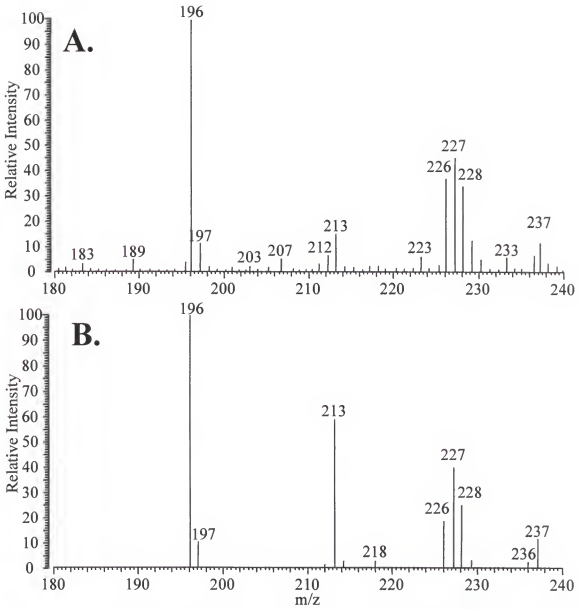


FIGURE 4-9: Neutral Loss Monitoring of 30 amu to Screen for Nitroaromatic Compound Ions in ExpMix

A. Prescan of ExpMix solution from m/z 180 - 240. B. Neutral loss monitoring of 30 amu acquired with a resonant excitation $q_z$ at 0.25 and collision energy of 30%.

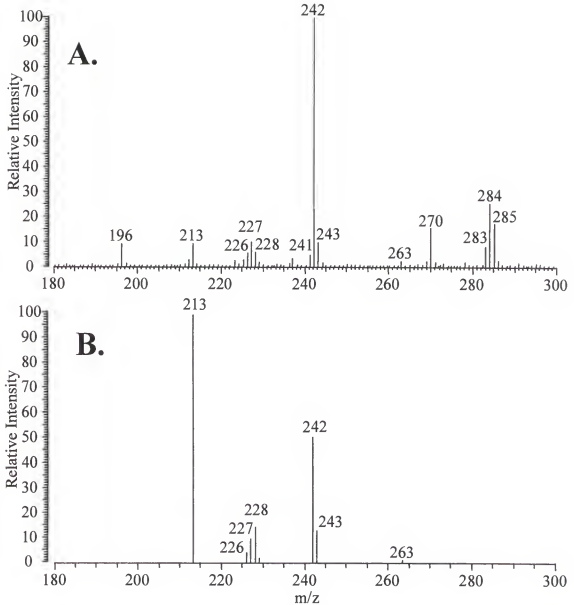


FIGURE 4-10: Neutral Loss Monitoring of 30 amu to Screen for Nitroaromatic Compound Ions in ExpMix

A. Prescan of ExpMix solution from m/z 180 - 300. B. Neutral loss monitoring of 30 amu. acquired with a resonant excitation $q_z$ at 0.25 and collision energy of 30%.

# CHAPTER 5
# INVESTIGATIONS IN THE DEVELOPMENT OF LIQUID CHROMATOGRAPHY/ ELECTROPSRAY IONIZATION – MASS SPECTROMETRY METHODS WITH ADDITIVES FOR THE ANALYSIS OF NITRO EXPLOSIVES

In this chapter, the development of an analytical method for the trace analysis of explosives for both environmental and forensic applications is discussed. A method incorporating liquid chromatography (LC) / electrospray ionization (ESI) – mass spectrometry (MS) and tandem mass spectrometry (MS/MS) has the potential of being an extremely sensitive and selective method for the identification of explosives in a variety of matrices. The desire for this method is that it will be capable of accurately identifying and quantifying explosives at concentrations approaching 500 parts-per-trillion (ppt) in both aqueous and organic solutions without extensive sample preparation. This method is intended to be rugged, reproducible, and not time-intensive. Potential forensic applications of this method include the analysis of military explosives to assess composition and purity, post-explosion residues, and extracts from potential points of contact with an explosive. Potential environmental applications include the analysis of both soil samples and water samples to identify areas and sources of environmental contamination from the manufacturing and disposal of explosives.

## Introduction

The previous chapters in this dissertation have shown that the negative-ESI-MS of explosives produces characteristic ions, which may be employed for the analysis of nitroaromatic compounds, nitramines, and a nitrate ester. However, the formation of

adduct ions and the variation of relative intensities among the characteristic ions produced for each explosive, depending on the conditions of the sample and/or instrumentation, is of concern. To obtain reproducible negative-ESI mass spectra for each explosive, it is important that the solvent, sample, and the instrument are free of any impurities. Any impurities in the solvent, sample, or system, will alter the appearance of the mass spectra. The most detrimental impurities to the reproducibility of the mass spectra for the explosives are those which may be readily deprotonated in solution or produce intense ions in the negative-ESI mode. The presence of impurities has been observed to have the greatest impact of the ESI-MS of nitramines and nitrate esters. Ions that have been observed to affect the mass spectrum include trifluoroacetate, propionate, nitrate, nitrite, chloride, acetate, and formate.

In this chapter, the effects of the impurities, or additives, on the appearance of the negative ESI mass spectra of five explosives, 1,3,5,7-tetranitro-1,3,5,7-tetrazacyclooctane (HMX), 1,3,5-trinitro-1,3,5,-triazacyclohexane (RDX), tetryl, 2,4,6-trinitrotoluene (TNT), and pentaerythritol tetranitrate (PETN), were investigated. Previous research has shown that additives can be used to improve the sensitivity of LC/ESI-MS for explosives [Miller et al., 1996; Miller et al., 1997; McClellan et al., 1999A] and the ionization efficiency of negative-ESI-MS for small molecules [Cole and Zhu, 1999]. Of interest are the effects the additives will have of the appearance of the mass spectra, which adduct ions will be preferentially formed, and the relative intensities of the ions. Also of interest is the impact these additives will have on obtaining MS/MS spectra for the electrosprayed ions due to differences in ion fragility, fragmentation pattern, and collision-induced dissociation (CID) efficiency.

We have previously shown that LC/ESI-MS, without additives, is a viable method for the analysis of explosives [Yinon et al., 1998; McClellan et al., 1999A]. However, that method does not have a large linear dynamic range because as the concentration of the analyte varies, the ions produced by ESI-MS change and the appearance of the mass spectrum changes. One of the biggest complications for this method is the production of dimer ions for the eluting analyte molecule. For the explosives, there is a limited concentration range where dimer ions are not produced. In this chapter, the development of this LC/ESI-MS method and the most recent results will be discussed. The addition of additives is explored to improve the sensitivity and linear dynamic range of the method.

The development of an LC/ESI-MS/MS method has been difficult for the analysis of explosives because of the number of characteristic ions which are produced by negative-ESI for each explosive and the fragility of the $[M-H]^-$ ions and other adduct ions for the nitramines and nitrate esters. The large number of characteristic ions causes difficulties because there is not one ion to choose for an MS/MS experiment; also, this ion's relative intensity may change under varying conditions (e.g. an unknown trace impurity in the sample or solvent). Both of these problems would have an effect on the linearity of the MS/MS method, separate from any the problems of linearity for the LC/MS methods. Under the "cleanest" of conditions, the major ions produced by the negative-ESI of HMX, RDX, and PETN exhibit ion fragility, and thus are difficult to isolate at narrow isolation widths and from which are difficult to obtain a rich MS/MS daughter ion spectrum. The use of additives is explored in the following pages to develop a more robust LC/ESI-MS/MS method.

## Experimental

### Instrumentation

All experiments were performed on the Finnigan LCQ (San Jose, CA), a commercial, bench-top ESI-QITMS instrument. For investigations of adduct ion formation and MS/MS, samples were infused into the mass spectrometer at a flow rate of 5 μL/min using the LCQ syringe pump. Other investigations used an LC pump to introduce the analytical samples. All investigations utilized negative-ESI and the HMX.LCQTune method for instrument control (Chapter 2). For data acquisition in negative ion mode, the AGC target values for full scan and $MS^n$ scans were lowered by a factor of three, compared to the values for positive ions, as there is an increased ion signal gain for [Schwartz et al., 1998], to values of $2 \times 10^7$ for full scan and $2 \times 10^6$ for $MS^n$.

A Hewlett Packard 1090 HPLC pump coupled to an Allure C18 column (100 mm in length x 2.1 mm i.d., 5μm particle size) from Restek Corporation (Bellefonte, PA) was used for all LC/MS experiments. The mobile phase was 50% HPLC grade water ($H_2O$) : 35% HPLC grade isopropanol (IPA) : 15 % HPLC grade methanol (MeOH). All separations were accomplished under isocratic conditions, with a flow rate of 160 μL/ min for the initial set of LC/MS experiments and 150 μL/min for the second set of experiments using propionic acid for both the LC/MS and LC/MS/MS experiments. Samples were injected from a 10 μL sample loop. For studies pertaining to the effects of additives on LC/MS, the additive solution was coupled to the eluting solution from the LC column by a peek "T-shaped" union. The additive solution was infused at a flow rate of 5 mL/ min using the LCQ syringe pump. The pressure of the system was 148 +/- 3 bar

when the LC eluent was introduced directly into the LCQ, and 169 +/- 4 bar infusing in the additive solution.

Samples

For studies in this chapter, the five most often used and manufactured military explosives [Yinon, 1999] were investigated. These explosives are 1,3,5,7-tetranitro-1,3,5,7-tetrazacyclooctane (HMX), 1,3,5-trinitro-1,3,5,-triazacyclohexane (RDX), tetryl, 2,4,6-trinitrotoluene (TNT), and pentaerythritol tetranitrate (PETN). All explosives were provided by Dr. Jehuda Yinon of the Weizmann Institute of Science, and obtained from the Analytical Laboratory of the Israeli Police Headquarters. All samples were acquired in a crystalline form.

The samples were initially dissolved in acetone to a concentration of approximately 1000 to 2000 ppm (1-2 μg/mL). For experiments using infusion analysis, the samples were then diluted to a concentration of approximately 15 to 30 ppm (**Table 5-1**) in a 50% HPLC-grade isopropanol (IPA): 50% HPLC-grade water ($H_2O$) solution (v/v), with 0.1% ammonium hydroxide ($NH_4OH$). For LC/MS and LC/MS/MS experiments, the samples were mixed together to a concentration of approximately 10 to 20 ppm each in acetone from the original solution. The samples were then diluted in HPLC water to concentrations of approximately 2 part-per-million (**Table 5-2**). These solutions were used as the stock solutions for all LC/MS samples, which were constituted via serial dilutions.

TABLE 5-1: Concentration of Explosives Analyzed by ESI-MS

| Explosive | Concentration (ppm) |
|---|---|
| HMX | 24 |
| RDX | 30 |
| Tetryl | 15 |
| TNT | 17 |
| PETN | 21 |

Note: Each explosive was diluted in a 50% IPA: 50% $H_2O$ solution (v/v), with 0.1% $NH_4OH$ and either 4 mM $NH_4Cl$, 3 mM $NaNO_2$, 0.01% (6.7 mM) propionic acid, 1 mM $NH_4NO3$, and 0.001 % (0.0009 mM) TFA.

TABLE 5-2: Concentration of Explosives in LC/MS Stock Solutions

| Explosive | 2 ppm Stock Conc. (ppm) |
|---|---|
| HMX | 2.4 |
| RDX | 3.0 |
| Tetryl | 1.5 |
| TNT | 1.7 |
| PETN | 2.1 |

Note: Concentration of each explosive in the 2 ppm stock solution used in explosive experiments. The 2 ppm stock solution was used to make standards for the LC/MS experiments with no additive, $NaNO_2$, and propionic acid. The solvent for the stock mixture was HPLC water.

Additives

For additive studies, the effects of chloride, nitrite, propionate, nitrate, and trifluoroacetate were investigated. For the introduction of these ions, the following compounds were added: ammonium chloride ($NH_4Cl$), Puratronic Grade (Alfa Aesar), MW 53.49; sodium nitrite ($NaNO_2$), ACS certified (Fisher Scientific), MW 69.00; propionic acid (PA), ACS certified (Aldrich), MW 74.08; and trifluoroacetic acid (TFA), 99% Pure (Acros), MW 114.02. For infusion studies, these additives were directly added

to the solvent system before the explosive was diluted to the analytical concentration. The concentration of the additives was optimized for the maximum adduct ion abundance, while keeping the chemical noise due to cluster ions formed by the additives to a minimum in the negative-ESI mass spectra. The optimized concentrations were 4 mM $NH_4Cl$, 3 mM $NaNO_2$, 0.01% (6.7 mM) propionic acid, 1 mM $NH_4NO_3$, and 0.001% (0.0009 mM) TFA. For LC/MS studies with $NO_2^-$ and propionate, a solution containing the additive was infused into the system after the chromatographic columnusing a peek "T-shaped" union. The solution concentrations were 10 mM for $NaNO_2$ and 0.2% (0.13 mM) propionic acid.

## Results and Discussion

### Effects of Additives on ESI-MS and Ion Intensity

#### ESI-MS

The initial investigations pertained to adduct ion formation for the nitramines, HMX and RDX. These two compounds have been found to be the most susceptible to adduct ion formation in the presence of impurities. Experiments were conducted to assess the effects of adding $NH_4Cl$, $NaNO_2$, propionic acid, $NH_4NO_3$, and TFA to solutions containing HMX and RDX.

The reference points for these investigations are the negative-ESI mass spectra obtained with the nitramines dissolved in the initial, standard solvent system of 50% IPA: 50% $H_2O$, with 0.1% $NH_4OH$ (**Figure 5-1**). The negative-ESI mass spectrum of HMX, acquired in profile mode, (**Figure 5-1A**) is dominated by the $[M+NO_3-H]^-$ ion at m/z 357, the $[M-H]^-$ ion at m/z 295, and the $[M+103]^-$ ion at m/z 399. Other ions visible in the mass spectrum are the $[M-NO_2-H]^-$ ion at m/z 341, the $[M+Cl]^-$ ion at m/z 331, and

fragment ions at m/z 147 and 221. The base peak intensity for the negative-ESI mass spectrum of HMX is 1.44 x $10^5$. The negative-ESI mass spectrum of RDX, acquired in profile mode, (**Figure 5-1B**) is dominated by the same types of ions, the $[M+NO_3\text{-}H]^-$ ion at m/z 283, the $[M\text{-}H]^-$ ion at m/z 221, and $[M+103]^-$ ion at m/z 325. The $[M\text{-}H]^-$ ion is noticeably less intense in the negative-ESI mass spectrum of RDX compared to that of HMX. Other ions visible in the mass spectrum are the $[M\text{-}NO_2\text{-}H]^-$ ion at m/z 267, the $[M+NO_2]^-$ ion at m/z 268, and the $[M+PA\text{-}H]^-$ ion at m/z 295. The base peak intensity for the negative-ESI mass spectrum of RDX is 1.23 x $10^5$.

The first additive to be discussed is $NH_4Cl$. Chloride was suspected to preferentially form adduct ions with HMX and RDX from past experience with negative-ESI. The source of the chloride impurity in previous experiments has been assumed to be the HPLC water used as a solvent. The addition of chloride formed adduct ions with both of the nitramines. The negative-ESI mass spectrum for RDX with the chloride additive is displayed in **Figure 5-2A**. For the sake of brevity, when there is no difference in the behavior of RDX and HMX is identical only one mass spectrum for each additive will be included in this chapter. In the negative-ESI-MS of both HMX and RDX with the chloride additive, the $[M+Cl]^-$ ions are the only analyte ions produced, with base peak intensities of 1.58 x $10^5$ for HMX and 0.94 x $10^5$ for RDX. Though both HMX and RDX preferentially form the $[M+Cl]^-$ ion, there is not an improvement in base peak intensity for the addition of this additive. The use of chloride as an additive is also problematic because there are many non-sample related ions (e.g. the cluster of ions around m/z 163 and 198, which result from an unknown impurity) that result in a high background. Chloride would not be a good choice as an additive for a LC/MS assay.

The next additive investigated was $NH_4NO_3$. The negative-ESI mass spectrum for HMX with the nitrate additive is displayed in **Figure 5-2B**. In the negative-ESI-MS of both HMX and RDX with the nitrate additive, the $[M+NO_3]^-$ ion is the only analyte adduct ion produced, with base peak intensities of $5.63 \times 10^5$ for HMX and $2.45 \times 10^5$ for RDX. The direct addition of nitrate into the system produced an ion different than the previously observed $[M+NO_3\text{-}H]^-$ ion (**Figure 5-1**). The next additive investigated was $NaNO_2$. The negative-ESI mass spectrum of RDX with the nitrite additive is displayed in **Figure 5-3A**. In the negative-ESI-MS of both HMX and RDX with the nitrite additive, the $[M+NO_2]^-$ ion is the only analyte adduct ion produced with base peak intensities of $6.99 \times 10^5$ for HMX and $3.91 \times 10^5$ for RDX. Again, the direct addition of nitrite into the system produced an ion different than the previously observed $[M+NO_2\text{-}H]^-$ ion. For both RDX and HMX, the addition of nitrite forms a more intense adduct ion compared to both chloride and nitrate. Both of these additives would be good choices as an additive for a LC/MS assay. The only potential problem with these additives is that, at higher concentrations, they begin to form dimers, trimers, and other cluster ions, which increases the chemical noise of the system, as is becoming apparent in **Figure 5-3A**.

The next two additives presented are propionic and trifluoroacetic acids. Both of these acids are readily deprotonated in solution and have strong electron withdrawing groups. Therefore, they form intense negative ions via negative-ESI and have a propensity to form intense adduct ions with analyte molecules, as cations do in positive-ESI. Both of these additives preferentially formed adduct ions with HMX and RDX. Negative-ESI of HMX and RDX, in the presence of propionic acid (PA), produces the $[M+PA\text{-}H]^-$ adduct ion; the negative-ESI of HMX and RDX, in the presence of

trifluoroacetic acid, produces the $[M+TFA-H]^-$ adduct ion. The negative-ESI mass spectrum for HMX with the propionic acid additive is presented in **Figure 5-3B**. Both of these additives preferentially form adduct ions of a greater intensity than the base peak in the reference mass spectra (**Figure 5-1**). The intensity of the $[M+PA-H]^-$ ion is 13.3 x $10^5$ for HMX and 4.12 x $10^5$ for RDX, while the intensity of $[M+TFA-H]^-$ ion is 8.19 x $10^5$ for HMX and 7.68 x $10^5$ for RDX. At concentrations necessary to assure good analyte adduct ion formation, the monomer ion and dimer ion, either the $[2PA-H]^-$ or $[2TFA-H]^-$ ion, are of approximately equal intensity. In the case of propionic acid, having a $[2PA-H]^-$ at m/z 147, this does not cause a problem for the LC/MS assay as all analyte ions have a higher m/z and the analytical m/z range can begin above m/z 147. However, in the case of TFA, the m/z of the $[2TFA-H]^-$ ion is 227. This causes a problem with the LC/MS analysis of TNT, which has a base peak ion at m/z 226, because the intensity of the TFA dimer ion is constant and much greater than the [M-H]- ion of TNT. Therefore, the eluting TNT molecule can not be readily detected in the presence of TFA.

A comparison of the ion intensities and base peak m/z for each of the samples discussed is presented in **Table 5-4**. For HMX, the additives that produce the highest intensity negative-ESI base peak ions, in order of greatest intensity, are propionic acid, TFA, and nitrite. For RDX, the additives that produce the highest intensity negative-ESI base peak ions, in order of greatest intensity, are TFA, propionic acid, and nitrite. The effects of these three additives on the ion intensity of negative-ESI-MS for tetryl, TNT, and PETN were investigated. The trend for the formation of adduct ions for the negative-

ESI of PETN was similar to that of RDX, as the addition of TFA formed the adduct ion of greatest intensity, followed by propionic acid and nitrite.

TABLE 5-4: Comparison of Intensities for Base Peak Ions for the negative-ESI of HMX and RDX

| | HMX | | RDX | |
|---|---|---|---|---|
| Additive | Intensity (x $10^5$) | Ion (m/z) | Intensity (x $10^5$) | Ion (m/z) |
| No Additive | 1.44 | 357 | 1.23 | 283 |
| $NH_4Cl$ | 1.58 | 331 | 0.94 | 257 |
| $NH_4NO_3$ | 5.63 | 358 | 2.45 | 284 |
| $NaNO_2$ | 6.99 | 342 | 3.91 | 268 |
| Propionic Acid | 13.3 | 369 | 4.12 | 295 |
| Trifluoroacetic Acid | 8.19 | 409 | 7.68 | 335 |

Note: The base peak intensity is increased with the addition of nitrate, nitrite, propionic acid, and TFA compared to the base peak of the reference spectra, with no additives. For HMX, propionic acid produces the most intense adduct ion; for RDX it is TFA.

It was observed that the addition of additives to the samples of tetryl and TNT did not result in the formation of adduct ions, as it did for the nitramines and the nitrate ester, but it still had some effect upon the ESI spectra of the nitroaromatic compounds. The reference negative-ESI mass spectrum, with no additives, for tetryl is presented in **Figure 5-4A**. The addition of nitrite does not drastically alter the appearance of the negative-ESI mass spectrum of tetryl (**Figure 5-4B**). For both spectra, the base peak is the $[M+Acetone-H]^-$ ion, at m/z 344. The only difference is the reduction of the $[M-H]^-$ of the hydrolysis product, n-methylpicramide, at m/z 241. The addition of propionic acid, however, greatly reduces the intensity of the $[M+Acetone-H]^-$ ion and increases the intensity of the $[M-NO]^-$ ion of tetryl (**Figure 5-5A**). The addition of TFA generates the production of a small $[M+TFA]^-$ adduct ion, but does not drastically decrease the

intensity of the $[M+Acetone-H]^-$ ion. For TNT, only the addition of propionic acid alters the appearance of the mass spectrum from the reference negative-ESI mass spectrum (**Figure 5-6A**). The negative-ESI mass spectrum of TNT in the presence of propionic acid (**Figure 5-6B**) shows a decrease in the ion intensity of the $[M+Acetone-H]^-$ ion and an increase in the intensity of the $[M-H]^-$ ion.

Tandem Mass Spectrometry

The additives that improved the ion ionization efficiency for the nitramines and nitrate ester were propionic acid, TFA, nitrite, and nitrate. These additives were investigated for their effects on the daughter ion mass spectra of all five explosives. For each explosive and each additive, a daughter ion mass spectrum was acquired of the base peak in the negative ESI spectrum and the CID efficiency was determined. The results, including the parent ion m/z, daughter ions, and CID efficiency, are presented in **Table 5-5**.

The daughter ion mass spectra for the $[M+NO_2]^-$ and $[M+PA-H]^-$ adduct ions of HMX are presented in **Figure 5-7**. The daughter ion mass spectra are quite similar. Both parent ions fragment to lose the adduct neutral, forming the $[M-H]^-$ ion of HMX; the major daughter ion for each is at m/z 147, which corresponds to the loss from the $[M-H]^-$ daughter ion of 2 $N(NO_2)CH_2$. The other daughter ions are identical and structurally informative. The daughter ions for the $[M+NO_3]^-$ adduct ion (**Figure 5-8A**) and the $[M+TFA-H]^-$ adduct ion (**Figure 5-8B**) of HMX, in contrast, are not structurally informative. Both adduct ions fragment to lose the entire analyte molecule, with the adduct retaining the charge.

Table 5-5: Data for MS/MS Spectra for Negative-ESI of Each Explosive with Additives

| | Parent Ion | m/z | Daughter Ions (m/z) | CID Efficiency (%) |
|---|---|---|---|---|
| **HMX (296 amu)** | | | | |
| $NaNO_2$ | $[M+NO_2]^-$ | 344 | 147, 174, 192, 221, 295, 247 | 25.4 |
| $NH_4NO_3$ | $[M+NO_3]^-$ | 358 | 62 | 11.0 |
| Propionic Acid | $[M+PA-H]^-$ | 369 | 147, 174, 192, 221, 247, | 18.2 |
| Trifluoroacetic Acid | [M+TFA-H]- | 409 | 113 | 28.8 |
| **RDX (222 amu)** | | | | |
| $NaNO_2$ | $[M+NO_2]^-$ | 268 | 93, 221, 176, 147 | 4.4 |
| $NH_4NO_3$ | $[M+NO_3]^-$ | 284 | 62 | 8.0 |
| Propionic Acid | $[M+PA-H]^-$ | 295 | 221, 93, 120, 147 | 4.6 |
| Trifluoroacetic Acid | [M+TFA-H]- | 335 | 113 | 29.8 |
| **Tetryl (287 amu)** | | | | |
| $NaNO_2$ | $[M+Ac-H]^-$ | 344 | 250, 268, 241, 207, 286, 297 | 10.7 |
| Propionic Acid | $[M-NO]^-$ | 257 | 181, 210, 211, 226 | 11.2 |
| Trifluoroacetic Acid | $[M+Ac-H]^-$ | 344 | 250, 268, 241, 207, 286, 297 | 9.9 |
| Trifluoroacetic Acid | $[M+TFA-H]^-$ | 400 | 113, 257 | 19.4 |
| **TNT (227 amu)** | | | | |
| $NaNO_2$ | $[M-H]^-$ | 226 | 196, 183, 197, 166, 155 | 7.0 |
| $NaNO_2$ | $[M+Ac-H]^-$ | 284 | 226, 237 | 15.3 |
| Propionic Acid | $[M-H]^-$ | 226 | 196, 183, 197, 166, 155 | 7.8 |
| Trifluoroacetic Acid | $[M-H]^-$ | 226 | 196, 183, 197, 166, 155 | 7.8 |
| **PETN (316 amu)** | | | | |
| $NaNO_2$ | $[M+NO_2]^-$ | 362 | 293, 315, 253 | 2.2 |
| Propionic Acid | $[M+PA-H]^-$ | 389 | 253 | 4.1 |
| Trifluoroacetic Acid | $[M+TFA-H]^-$ | 429 | 113 | 23.0 |

Note: Daughter ion mass spectra for each of the five explosives in the presence of nitrite, propionic acid, and TFA. The CID efficiency is the percent ratio of the total ion current of the daughter ions to the selected ion current of the parent ion at zero collision energy. Abbreviations are used for acetone (Ac), propionic acid (PA), and trifluoroacetic acid (TFA).

Daughter ion mass spectra such as this are not very helpful in the successful identification of an unknown analyte, since they provide only the molecular weight of the analyte from the neutral loss. The fragmentation of the adduct ions for RDX and PETN behave in the same manner as those for HMX; CID of the nitrite and propionate adduct ions yields structural information pertinent to the analyte molecule, whereas CID of the nitrate and TFA adduct ions does not.

LC/MS and LC/MS/MS

From the data obtained on the effects of additives on ion intensity and daughter ion mass spectra, it was determined that both propionic acid and nitrite would be viable additives for LC/ESI-MS and LC/ESI-MS/MS methods for the analysis of explosives. Both additives preferentially produce adduct ions with the nitramines and nitrate ester and do not suppress the ionization of the nitroaromatic compounds. Furthermore, CID of the $[M+PA-H]^-$ and $[M+NO_2]^-$ adduct ions of HMX, RDX, and PETN produce daughter ion mass spectra that are rich in structural information, unlike CID of the $[M+TFA-H]^-$ and $[M+NO_2]^-$ adduct ions.

Without Additives

The initial LC/MS assay was developed without any additives. The LC/MS chromatogram (plotting the intensity of the base peak in each spectrum) for the separation of the five explosives, at a concentration of 10 ppb, with no additives, is presented in **Figure 5-9**. The elution order of the explosives is HMX at 1.7 min., RDX at 2.3 min., tetryl at 3.3 min., TNT at 4.44 min. and PETN, at 6.4 min. The peaks at 0.9 and 1.4 are not associated with the explosive samples and are considered to be void peaks.

The mass spectra for the peaks eluting at 1.7 min. (HMX), 2.3 min. (RDX), and 6.4 min. (PETN) are indicative of the problems encountered with no control of the ionization process for the negative-ESI of the explosives. The mass spectrum of the peak at 1.7 min. is presented in **Figure 5-9B**, which confirms the identity of the peak as HMX. The mass spectrum shows a base peak at m/z 341, which corresponds to the $[M+NO_2-H]^-$ ion. Other identifiable ions in the mass spectrum include the $[2M+Cl]^-$ ion at m/z 627, the $[2M+NO_3-H]^-$ ion at m/z 653, the $[M+Cl]^-$ ion at m/z 331, and the $[M+NO_3]^-$ ion at m/z 358. The mass spectrum at 2.3 min. is presented in **Figure 5-10A**, confirming the peak is RDX. At 10 ppm, RDX forms a relatively high abundance of dimer ions during the ESI process. The peaks present in the mass spectrum include, the base peak, $[2M+Cl]^-$, at m/z 479, the $[2M+NO_3]^-$ ion at m/z 506, the $[M+NO_2-H]^-$ ion at m/z 267, [the $[M+NO_3]^-$ ion at m/z 284, the $[M+TFA-H]^-$ ion at m/z 335, and the $[2M+103]^-$ ion at m/z 547. The mass spectrum of the peak for PETN, at 6.4 min., is presented in **Figure 5-10B**. The two most intense ions in the mass spectrum are at m/z 361, the $[M+NO_2-H]$- ion, and at m/z 378, the $[M+NO_3]^-$ ion. Other ions in the mass spectrum are at m/z 475, corresponding to an unidentified [M+159]- ion, at m/z 666, the $[2M+Cl]^-$ ion, and at m/z 351, the $[M+Cl]^-$ ion.

The development of LC/MS and LC/MS/MS assays with no control over the ionization process has proven difficult because the relative abundances of the ions in the mass spectra vary dramatically depending on analyte concentration and on undetected impurities in the LC/MS system [McClellan et al., 1999A]. Also, as evident by the mass spectra in **Figures 5-9 and 5-10**, the production of a wide array of ions, some of which can not readily be identified, but, which nonetheless, are associated with the eluting

explosive, pose problems for quantitation. The question arises, which ions should be used for quantitation? If one of the chosen ions for quantitation is not always present in the mass spectrum, then quantitation of the explosives will be in error. If an unknown impurity is present in the sample to be analyzed or is introduced during sample preparation or separation, the mass spectra may be drastically changed. The mass spectra is also influenced by the concentration of the sample, as varying concentrations lead to differences in the relative abundance of adduct ions and dimer ions. These complications all lead to non-linear calibration curves. Therefore, alternate methods were explored using additives to control the ionization process.

With Additives

The first set of investigations pertaining to the development of an LC/MS method employing additives to control the negative-ESI process was conducted to compare the use of nitrite and propionic acid as the additive. These two additives were chosen because of their superior performance in the initial infusion studies. Both of these additives were found to preferentially form characteristic adduct ions with HMX, RDX, and PETN to and did not negatively affect the ionization processes for tetryl and TNT. These two additives were also chosen because CID of the adduct ions for HMX, RDX, and PETN produced structurally informative daughter ion mass spectra, unlike the CID of the nitrate and TFA adduct ions. This will be important for the development of the LC/MS/MS assay, since it would be preferable to use the same additive for both assays.

The elution order of the five explosives and the elution time are the same with or without additives, as the additives are infused into the system after the chromatographic separation, and therefore do not effect the elution order or elution time. The first peak, eluting at 1.7 min., is the HMX peak. The mass spectrum for HMX for the nitrite assay

(**Figure 5-11A**) shows that the base peak is the $[M+NO_3]^-$ ion at m/z 342; and the only other identified HMX ion is the $[2M+NO_2]^-$ ion at m/z 638. The mass spectrum for HMX for the propionic acid (PA) assay (**Figure 5-11B**) shows that the base peak ion is the $[M+PA-H]^-$ ion at m/z 369. Other identified ions in the mass spectrum are $[2M+Cl]^-$ at m/z 627, the $[2M+PA-H]^-$ ion at m/z 665, and the $[M+NO_2-H]^-$ ion at m/z 341. The mass spectra for HMX with both are far simpler than without additives. There is slightly more dimerization in the nitrite assay than the propionic acid assay for HMX.

The second peak, eluting at 2.3 min., is the RDX peak. The mass spectrum for RDX for the nitrite assay (**Figure 5-12A**) shows that, as was observed with HMX, the base peak is the $[M+NO_3]^-$ ion at m/z 268; and the only other intense ion is the $[2M+NO_2]^-$ ion at m/z 490. The mass spectrum for RDX for the PA assay (**Figure 5-12B**) shows that the base peak ion is the $[M+PA-H]^-$ ion at m/z 295. The other identified RDX ion in the mass spectrum is the $[2M+PA-H]^-$ ion at m/z 517. Once again, the mass spectra with both additives for the nitramine produces a simpler mass spectrum, which has a more intense base peak than in the LC/MS assay with no additives. As for HMX, the assay with the nitrite additive appears to produce a greater amount of dimerization that the assay with the propionic acid.

The third peak, eluting at 3.3 min., is tetryl. The mass spectrum for tetryl for the nitrite assay (**Figure 5-13A**) shows that the base peak ion is the $[M+NO]^-$ ion at m/z 257, as it also is for the propionic acid assay mass spectrum of tetryl (**Figure 5-13B**). There is a significant difference in the intensity of the other ions present in the mass spectrum, including the ions at m/z 288, 318, and 346. However, these differences were proven not to be reproducible, which may be problematic for quantitation of tetryl. The peak at 4.5

min. is TNT. For both assays, the base peak, and indeed the only peak, in the mass spectrum, is the $[M-H]^-$ ion of TNT and there is minimal dimerization.

The fifth and last peak in the chromatogram is the PETN peak, at 6.4 min. The mass spectrum for PETN for the nitrite assay (**Figure 5-14A**) shows that the base peak ion, the $[M+NO_3]^-$ ion at m/z 362, is the only ion present in the mass spectrum. The mass spectrum for PETN for the propionic acid (PA) assay (**Figure 5-14B**) shows that the base peak ion is the $[M+PA-H]^-$ ion at m/z 388. Other identified, less intense ions in the mass spectrum are $[M-H]^-$ ion at m/z 315 and the $[M+NO_2-H]^-$ ion at m/z 361. Dimerization does not occur for either of the two assays for PETN at 10 ppm.

Both nitrite and propionic acid proved to be viable additives for the LC/MS analysis of the five explosives. However, the limits of detection and linear dynamic range are different for each of the explosives. A calibration curve is presented for each of the five explosives in the presence of nitrite (**Figure 5-15**) and propionic acid (**Figure 5-16**). For the nitrite method, the calibration curve was obtained using the sum of the $[M+NO_2]^-$ and $[2M+NO2]^-$ ions for HMX, RDX, and PETN, the $[M-NO]^-$ ion for tetryl, and the $[M-H]^-$ ion for TNT. For the propionic acid method, the calibration curve was obtained using the sum of $[M+PA-H]^-$ and $[2M+PA-H]^-$ ions for HMX, RDX, PETN, the $[M-NO]^-$ ion for tetryl, and the $[M-H]^-$ ion for TNT.

For both assays, the limits of detection (LOD) and linear dynamic range were the same for each of the explosives, except tetryl, which had an improved linear range for the propionic acid assay. For each explosive, the limit of detection was approximately 1 ppb. The linear dynamic range, however, varied from explosive to explosive did not have the same similarities. The dynamic range for HMX was 1 to 25 ppb for both assays. For

RDX, the linear range was from 2 ppb to 150 ppb for both assays. For tetryl, the linear dynamic range was 1 ppb to 15 ppb for the nitrite assay and 1 to 75 ppb for the propionic acid assay. For TNT, the linear dynamic range was 2 to 85 ppb for both assays. Finally, for PETN, the linear range was found to be 2 to 100 ppb for each assay.

From the results of the LC/MS assays with nitrite and propionic acid, it was determined that both of these additives would be applicable to a LC/MS/MS method. Initially, propionic acid was chosen as the additive of choice for the MS/MS method. However, the method has proven difficult to implement for the analysis of all explosives, especially RDX, TNT, and PETN. More work must be done to make the LC/MS/MS method viable for the analysis of explosives.

## Conclusion

In this chapter, the effects of additives on the negative-ESI mass spectra of explosives have been presented. The addition of additives has the greatest impact on the ionization of HMX, RDX, and PETN. Of the additives explored, nitrite, propionic acid and TFA produce the most intense adduct ions. Through MS/MS investigations, it was determined that the adduct ions produced in the presence of nitrite, $[M+NO_2]^-$, and propionic acid, $[M+PA-H]^-$, fragment via CID to produce structurally relevant daughter ions. Conversely, the adduct ions formed in the presence of nitrate, $[M+NO_3]^-$, and TFA, $[M+TFA-H]^-$, fragment to produce the $NO_3^-$ and $[TFA-H]^-$ ions, which yield no relevant structural information about the analyte molecules. For an analytical MS/MS method, the use of propionic acid and nitrite would be better for the identification of HMX, RDX, and PETN.

The knowledge gained from these studies was applied to the development of novel LC/MS and LC/MS/MS methods for the analysis of explosives. While the methods show promise, more work must be done to improve the limits of detection and linear range. While the limits of detection for the assays using both propionic acid and nitrite are approximately 1 ppb for all explosives, the linear dynamic range for the individual explosive varies. It is hoped that the continued development of these methods can obtain lower limits of detection, perhaps by exploiting the greater sensitivity of MS/MS.

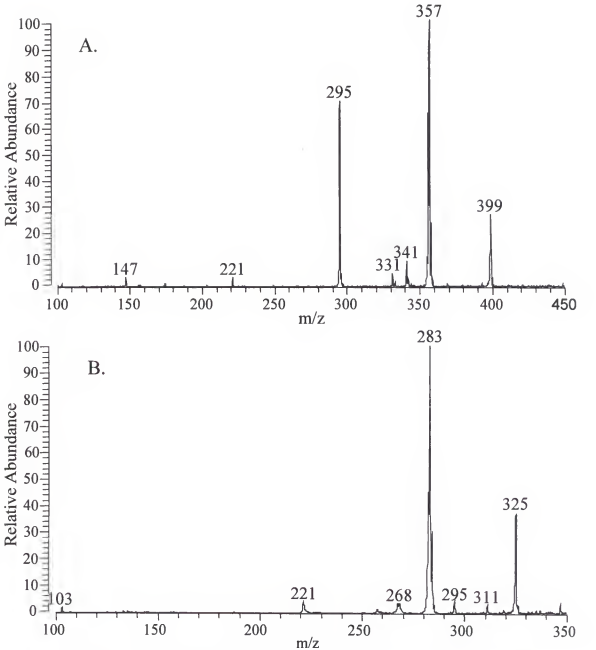


FIGURE 5-1: Negative-ESI Mass Spectra for Nitramines with No Additive

A. Negative-ESI mass spectrum of HMX with no additive present in solution. B. negative-ESI mass spectrum of RDX with no additive present in solution. The molecular weight of HMX is 296 Da.; the molecular weight of RDX is 222 Da.

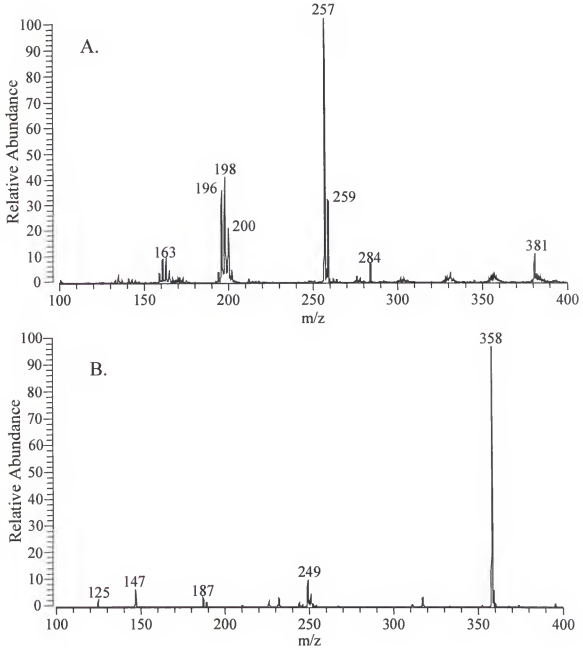


FIGURE 5-2: Negative-ESI Mass Spectra of Nitramines with Chloride and Nitrate Additive

A. Negative-ESI mass spectrum of RDX in the presence of chloride to form the $[M+Cl]^-$ ions at m/z 257 and 259. Chloride adduct ions of impurities are present around m/z 163 and 198. B. Negative-ESI mass spectrum of HMX in the presence of nitrate to produce the $[M+NO_3]^-$ adduct ion at m/z 358.

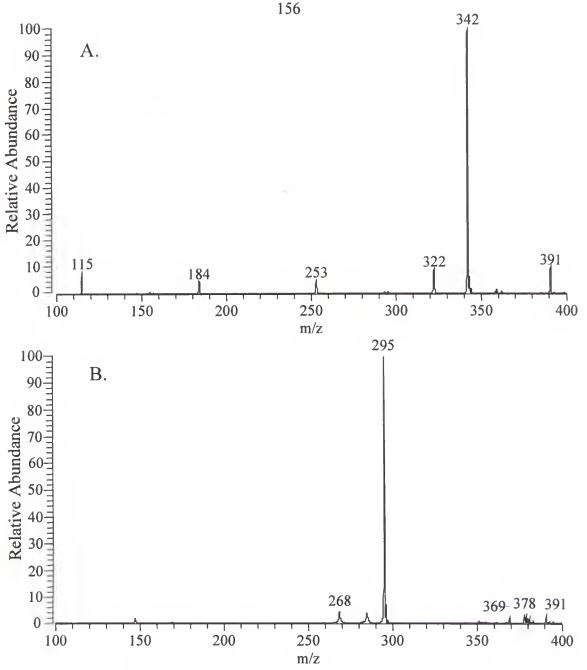


FIGURE 5-3: Negative-ESI Mass Spectra of Nitramines with Nitrite and Propionic Acid Additive

A. Negative-ESI mass spectrum of HMX in the presence of nitrite to form the $[M+NO_2]^-$ ion at m/z 342. B. Negative-ESI mass spectrum of RDX in the presence of propionic acid to produce the $[M+PA-H]^-$ adduct ion at m/z 295.

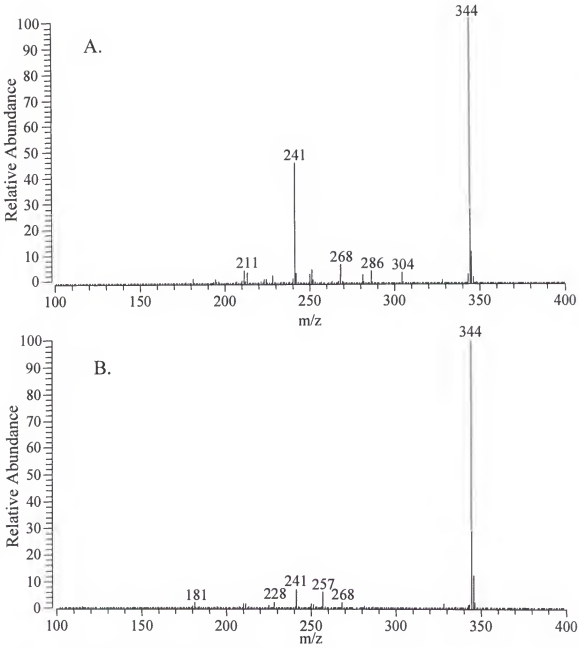


FIGURE 5-4: Negative-ESI Mass Spectra of Tetryl with No Additive and Nitrite Additive

A. Negative-ESI mass spectrum of tetryl with no additive. The molecular weight of tetryl is 287 Da. B.: Negative-ESI mass spectrum of tetryl in the presence of nitrite.

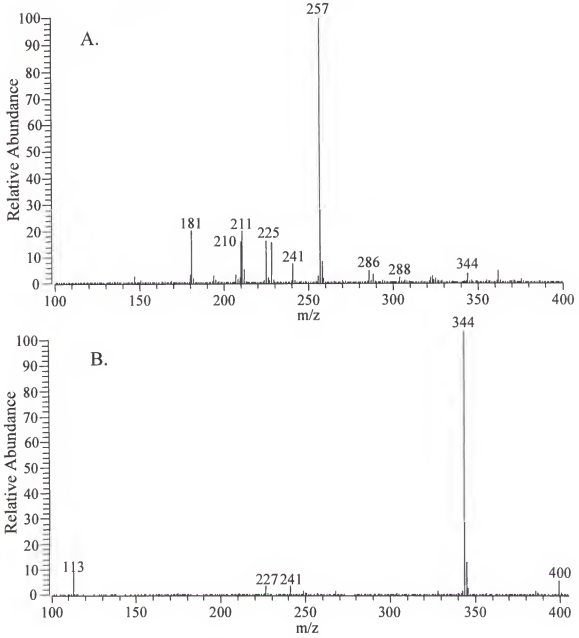


FIGURE 5-5: Negative-ESI Mass Spectra of Tetryl with Propionic Acid and Trifluoroacetic Acid

A. Negative-ESI mass spectrum of tetryl in the presence of propionic acid. B. Negative-ESI mass spectrum of tetryl in the presence of TFA.

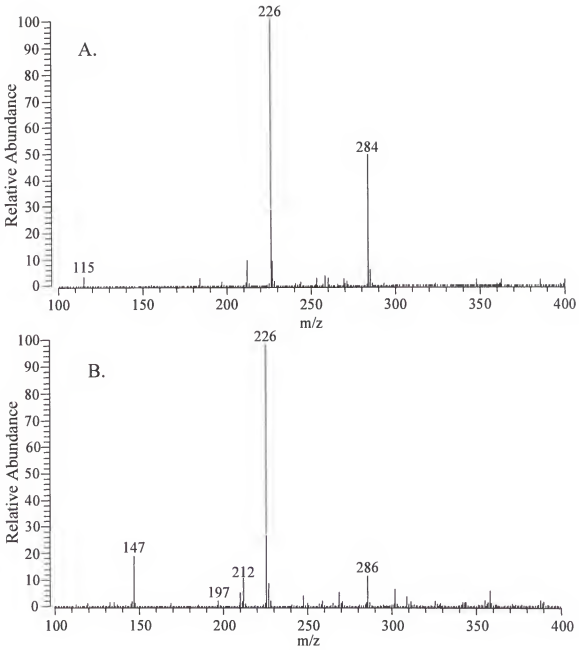


FIGURE 5-6: Negative-ESI Mass Spectra of TNT with No Additive and Propionic Acid

A. Negative-ESI mass spectrum of TNT with no additive. The molecular weight of TNT is 226 Da. B. Negative-ESI mass spectrum of TNT in the presence propionic acid.

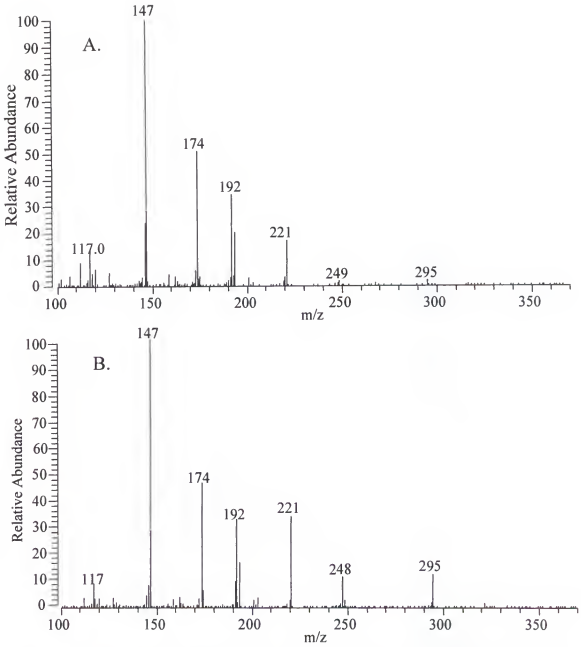


FIGURE 5-7: Daughter Ion Mass Spectra of the $[M+NO_2]^-$ ion and $[M+PA-H]^-$ ion of HMX

A. Daughter ion mass spectrum of the $[M+NO_2]^-$ ion (m/z 342) of HMX. B. Daughter ion mass spectrum of the $[M+PA-H]^-$ ion (m/z 369) of HMX. The two daughter ion mass spectra are very similar.

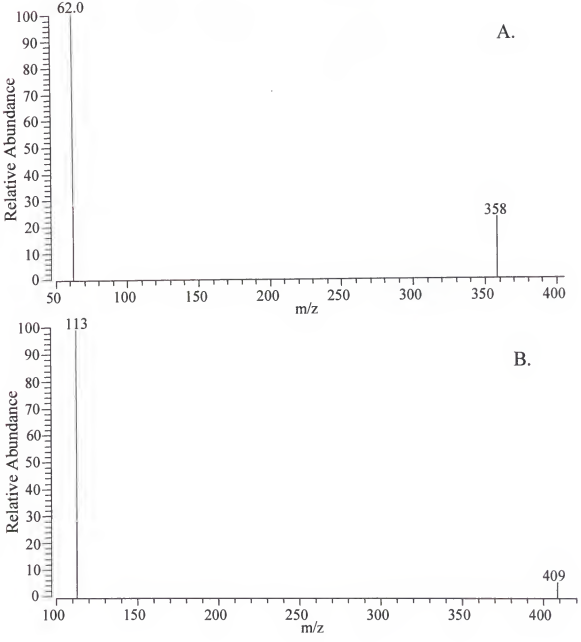


FIGURE 5-8: Daughter Ion Mass Spectra of the $[M+NO_3]^-$ Ion and $[M+TFA]^-$ Ion of HMX

A. Daughter ion mass spectra of the $[M+NO_3]^-$ ion (m/z 358) of HMX. B. Daughter ion mass spectra of the $[M+TFA-H]^-$ ion (m/z 409) of HMX.

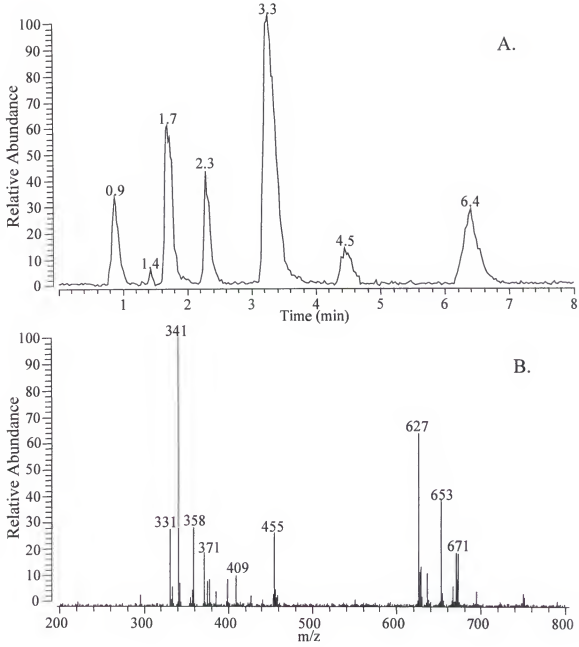


FIGURE 5-9: LC/MS Chromatogram of Explosive Mixture and Mass Spectrum of HMX Peak

A. LC/MS chromatogram of explosive mixture with no additive. The identity of the peaks: HMX elutes at 1.7 min., RDX elutes at 2.3 min., Tetryl elutes at 3.3 min., TNT elutes at 4.5 min., and PETN elutes at 6.4 min. B. Mass spectrum of HMX peak at 1.7 min.

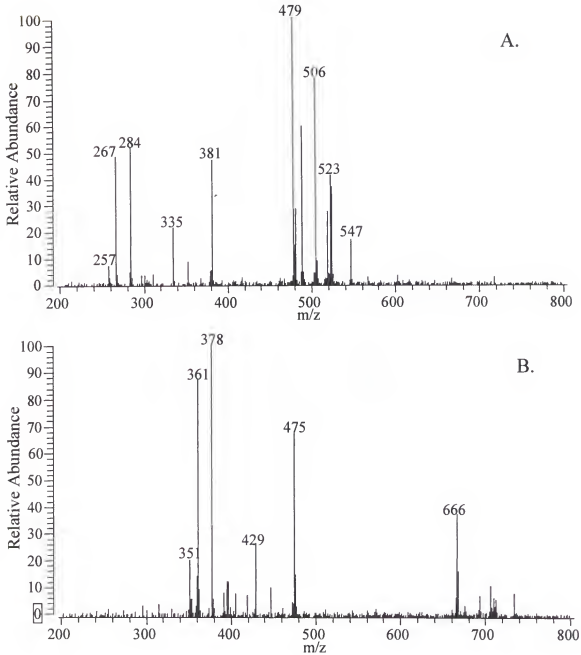


FIGURE 5-10: Mass Spectra of RDX and PETN LC/MS Peaks

A. Mass spectrum of RDX LC/MS peak at 2.3 min. B. Mass spectrum of PETN LC/MS peak at 6.4 min.

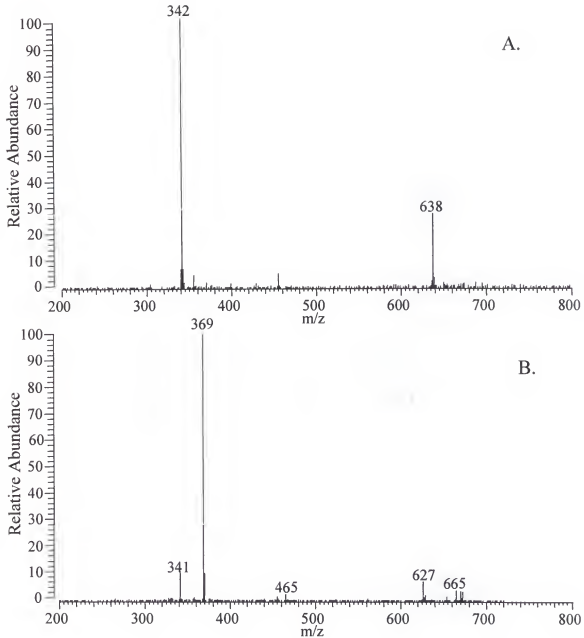


FIGURE 5-11: Mass Spectra of HMX Peak for the LC/MS Methods with Nitrite and Propionic Acid

A. Mass spectrum of HMX peak at 1.7 min. for the nitrite LC/MS method. B. Mass spectrum of HMX peak at 1.7 min. for the propionic acid method.

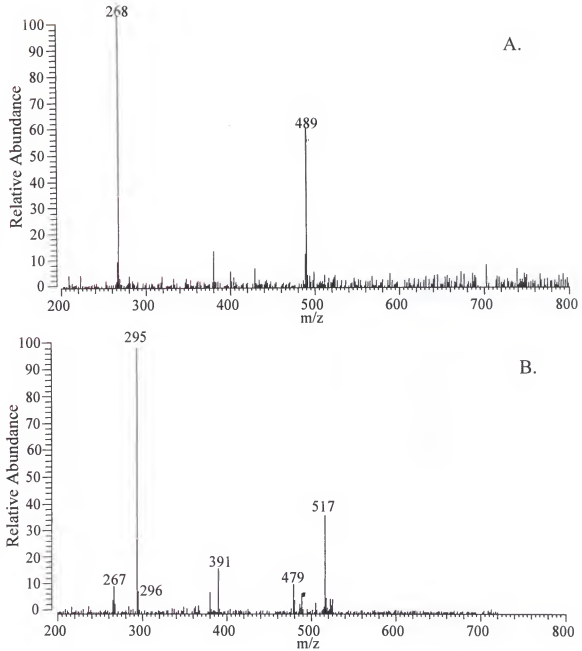


FIGURE 5-12: Mass Spectra of RDX Peak for the LC/MS Methods with Nitrite and Propionic Acid

A. Mass spectrum of RDX peak at 2.3 min. for the nitrite LC/MS method. B. Mass spectrum of HMX peak at 2.3 min. for the propionic acid method.

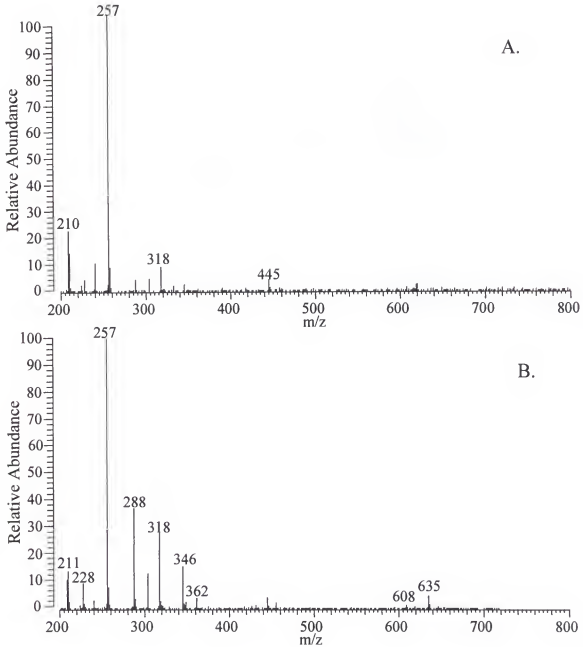


FIGURE 5-13: Mass Spectra of Tetryl Peak for the LC/MS Methods with Nitrite and Propionic Acid

A. Mass spectrum of tetryl peak at 3.3 min. for the nitrite LC/MS method. B. Mass spectrum of tetryl peak at 3.3 min. for the propionic acid method.

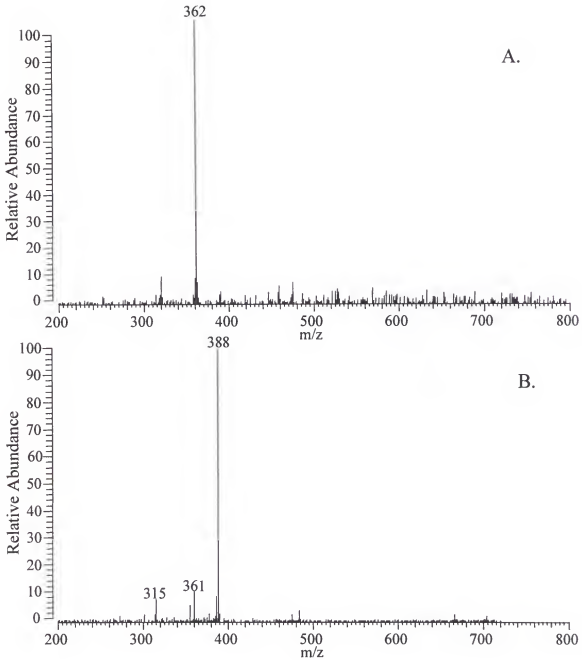


FIGURE 5-14: Mass Spectra of PETN Peak for the LC/MS Methods with Nitrite and Propionic Acid

A. Mass spectrum of the PETN peak at 6.4 min. for the nitrite LC/MS method. B. Mass spectrum of the PETN peak at 6.4 min. for the propionic acid method.

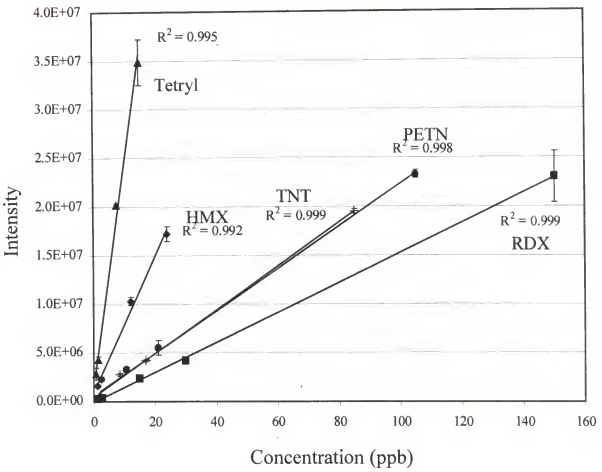


FIGURE 5-15: Calibration Curves for Nitrite LC/MS Method

Calibration curves for each explosive, using the nitrite LC/MS method, is presented over the linear dynamic range for each explosives. Each data point is the average of 3 replicate injections with error bars (one standard deviation). The correlation coefficient for each calibration curve is given.

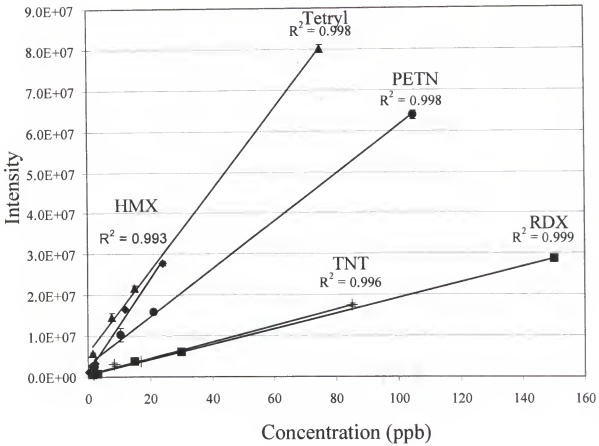


FIGURE 5-16: Calibration Curves for Propionic Acid LC/MS Method

Calibration curves for each explosive, using the propionic acid LC/MS method, is presented over the linear dynamic range for each explosives. Each data point is the average of 3 replicate injections with error bars (one standard deviation). The correlation coefficient for each calibration curve is given.

# CHAPTER 6
# CONCLUSIONS AND FUTURE WORK

In this dissertation, it has been shown that electrospray ionization, when coupled with liquid chromatography, quadrupole ion trap mass spectrometry, and tandem mass spectrometry, is a highly selective and sensitive analytical method for the analysis of explosives. The development of this analytical method required investigations into the negative-ESI process for the nitro explosives, the fragile ion characteristics of some of the ions generated by the negative-ESI of nitramines and nitrate esters, and the use of additives to control the ionization process of nitramines and nitrate esters. These investigations have led to the development of a sensitive LC/ESI-MS method for routine forensic and environmental analysis of explosives. Also, methods for parent and neutral loss monitoring on the LCQ for nitroaromatic explosives as well as for other compounds such as acylcarnitines.

## Conclusions

Negative-ESI has been shown to produce characteristic ions for explosives in each of the three classes, nitroaromatic compounds, nitramines, and nitrate esters; the ions produced, however, are not solely the typical $[M-H]^-$ ions. Thus a detailed study of the production of analyte ions from the explosives was undertaken. Two of the nitroaromatic compounds, amino-dinitrotoluene (A-DNT) and trinitrocresol (TNC), preferntially produce the $[M-H]^-$ molecular ion. Negative-ESI of other nitroaromatic compounds, TNT, picramide, trinitrobenzene (TNB), and trinitronaphthalene (TNN),

negative-ESI produces both $M^-$ and $[M-H]^-$ ions, as well as various fragment and adduct ions. Negative-ESI of TNB produces only a very low intensity $[M-H]^-$ ion. For these nitroaromatic compounds, there is a clear competition between the production of the $M^-$ ion and the $[M-H]^-$ ion via negative-ESI. The formation of the $[M-H]^-$ ion may be the result not of deprotonation in solution, but of an alternate method of ionization, such as a two-step mechanism in which an adduct ion is first produced, followed by the loss of the neutral adduct molecule, leaving the charge on the nitroaromatic compound. For example, the CID of the $[M+Acetone-H]^-$ adduct ion shows that it readily loses acetone to form the $[M-H]^-$ ion. The production of the $M^-$ ion is attributed to the electrochemical processes (redox) that play a role in the production of ions in ESI [Van Berkel, 1997]. In previous work [Yinon et al., 1997], it was shown that negative-ESI of explosives produces predominantly $M^-$, $[M+NO]^-$ and $[M+NO_2]^-$ adduct ions, and $[M-NO]^-$ and $[M-OH]^-$ fragment ions for nitroaromatic compounds. The use of a solvent system containing 50% IPA, 50% $H_2O$, and 0.1% $NH_4OH$, has been shown to minimize the production of fragment and adduct ions for TNT and the other nitroaromatic compounds. However, if there is not a facile deprotonation site of the molecule, both the $M^-$ and $[M-H]^-$ ions are commonly produced for the nitroaromatic compounds using this solvent.

The negative-ESI-MS analysis of tetryl is complicated by the hydrolysis of the compound to produce N-methylpicramide. Therefore, the mass spectrum includes ions from both of the two compounds. While the hydrolysis reaction has been documented to occur in solution [Yinon and Zitrin, 1993], it is also suspected to occur at the ESI needle. Neither the production of the $M^-$ or the $[M-H]^-$ ion of tetryl is especially favored via

negative-ESI. Therefore, the most intense ions of tetryl are generally either adduct or fragment ions.

The negative-ESI mass spectra of RDX, HMX, and PETN show that these analytes behave very similarly to each other during the ionization process. These compounds readily form adduct ions with a wide variety of impurities that may be in the system, including propionate, formate, chloride, nitrite, and nitrate. When acquired in profile mode, some of the peaks in the full scan negative-ESI mass spectra of HMX, RDX, and PETN appear to be broader than those in the spectra of the nitroaromatic compounds, reflecting their fragile nature.

Daughter ion mass spectra were acquired for all of the ions detected in the negative-ESI mass spectra of all the explosives. For the nitroaromatic compounds, an isolation width of 1.0 amu was sufficient to isolate each of the ions, including the adduct ions. However, for the nitramines and nitrate esters, an isolation width of 1.0 amu was too narrow to isolate any of the ions for interrogation by MS/MS, and resulted in no isolated intensity. To obtain adequate isolation intensity of the nitramine and nitrate ester ions, the width of isolation had to be widened to a width of at least 3.0 amu and for some ions as wide as 7.0 amu, depending on the ion, as a result of their fragile nature. The CID fragmentation of the nitroaromatic compounds produced rich mass spectra that provided a number of characteristic daughter ions to enable their identification; compared with data from EI-MS and CI-MS/MS experiments in the literature. For the compounds that produced both $[M-H]^-$ and $M^-$ molecular ions, the daughter ion mass spectra of the ions were remarkably different. Generally, all nitroaromatic compounds undergo some of the same neutral losses, the most characteristic of which is the loss of 30 amu, corresponding

to the loss of NO. For HMX, RDX, and PETN, the daughter ion mass spectra were generally richer for the adduct ions than for the $[M-H]^-$ ions.

The difficulty in obtaining informative daughter ion spectra with adequate intensity for the nitramines and nitrate esters are due to their fragile ion nature. It was also noted that these ions, which were difficult to isolate, exhibited broad peak shapes (in profile mode) and mass shifts (in centroid mode). Broad peak shape and mass shifts are not limited to explosive ions, as other ions have been shown to exhibit broad peak shapes, due to peak-fronting and mass shifts under normal, non-space charge conditions. The abnormal peak shape for these ions have been determined to occur because they are "fragile" and may fragment during the application of the resonance ejection amplitude during mass analysis. The effects of fragile ions were studied using ions that include protonated, deprotonated, and adduct ions of explosives, acylcarnitines, and macrolide antibiotics.

It has been shown that the fragility of ions has an effect on both mass resolution and on the intensity of the ion isolated for MS/MS. The effects of a fragile ion on mass resolution are most evident at the slower scan speeds, as the difference in peak widths between fragile ions and non-fragile ions become more significant and more readily detected. In slow scan, the peak widths of fragile ions, at 10% peak height, are greater than 0.31 amu and may approach values as great as 1.09 amu. Conversely, the $W_{10\%}$ for non-fragile ions is consistently 0.30 amu or less. It has also been shown that different ions formed from the same compound, including protonated, deprotonated, or adduct ions, may result in peaks with different peak widths. Examples include the macrolide compounds, where the $[M+H]^+$ ions are fragile and, thus, have a larger peak width than

the $[M+Na]^+$ ions, and the acylcarnitine compounds, where the $[M+H]^+$ ions have smaller peak widths than the fragile $[M+Na]^+$ ions.

The ability to obtain an adequate isolation intensity for a selected parent ion at unit resolution during MS/MS is dependent on the ion's fragility. Fragile ions are more greatly affected by the application of the isolation waveform during the selection of the parent ion for MS/MS experiments. As a result, if the isolation of a fragile ion is attempted at unit resolution, the intensity of the ion will diminish substantially (often completely). For the isolation of fragile ions, the isolation waveform notch width must be increased and/or the time period of isolation must be decreased to obtain adequate isolation intensity. Fragile ions also require lower collision energies to achieve efficient CID. Taking into account these data, we have developed a criterion, based on the minimum isolation width and the slow scan $W_{10\%}$ of each ion, for assessing the degree of ion fragility. As either or both of the minimum isolation width and the slow scan $W_{10\%}$ increase, so does an ion's fragility. These investigations have proved useful in understanding the behavior of ions from the ESI of nitramines and nitrate esters in the QITMS, and have led to the design of improved MS/MS experiments for the analysis of explosives.

The effects of additives on the negative-ESI mass spectra of explosives have been investigated. The use of additives has the greatest impact on the ionization of HMX, RDX, and PETN. Of the additives explored, nitrite, propionic acid and TFA produce the most intense adduct ions. Through MS/MS investigations, it was determined that the adduct ions produced in the presence of nitrite, $[M+NO_2]^-$, and propionic acid, $[M+PA-H]^-$, fragment via CID to produce structurally relevant daughter ions. Conversely, the

adduct ions formed in the presence of nitrate, $[M+NO_3]^-$, and TFA, $[M+TFA-H]^-$, fragment to produce solely the $NO_3^-$ and $[TFA-H]^-$ ions, which yield no relevant structural information about the analyte molecules. For an analytical MS/MS method, the use of propionic acid and nitrite would be better for the identification of HMX, RDX, and PETN. The knowledge gained from these studies was applied to the initial development of novel LC/MS and LC/MS/MS methods for the analysis of explosives. Results show that assays with nitrite and propionic acid are viable for both LC/MS and LC/MS/MS methods.

A novel and practical technique for performing both parent and neutral loss (P&NL) monitoring experiments on a quadrupole ion trap mass spectrometer has been presented. This technique is capable of performing scans analogous to the parent and neutral loss scans routinely applied on tandem-in-space instruments and allows for the screening of a sample to detect analytes of a specific compound class on a chromatographic time-scale. Using both the spiked and unspiked pig plasma samples, the technique of neutral loss monitoring was demonstrated to be capable of detecting acylcarnitines in biological matrices at physiological concentrations. A few conclusions can be drawn concerning the application of P&NL monitoring for the detection of acylcarnitines in complex mixtures. First, the neutral loss monitoring of 59 amu is the most inclusive means to screen for acylcarnitines because it will allow for the detection of all acylcarnitines, independent of molecular weight or ion type ($[M+H]^+$ or $[M+Na]^+$). Next, it is important to minimize the potential for false negatives in the screening experiment due to a non-selection of the acylcarnitine ion for interrogation if it is not one of the most intense 18 ions in the prescan. To accomplish this goal, one can modify the

selection criteria for the m/z to be interrogated, for instance by also interrogating a set of the second most intense 18 ions. Or, if there is a specific and limited list of acylcarnitine ions which are of concern to the investigator, a "to-do" list can be created and only those ions will be interrogated by the analytical scan of the P&NL monitoring technique. Finally, because of the potential for false positives, in the screening experiment, methods are required for the confirmation of the suspected acylcarnitine ion. This can be accomplished either by a complimentary P&NL monitoring experiment, such as the neutral loss monitoring of 161 amu or the parent ion monitoring of either m/z 85 or 144, or by a daughter ion experiment. Ultimately, the technique of P&NL monitoring on the QITMS can be a valuable screening method for acylcarnitines.

For the screening of explosives, the neutral loss monitoring of 30 amu is the best method to identify the molecular and fragment ions of the nitroaromatic compounds. However, this method does not identify the adduct ions formed from the negative-ESI of the explosive compounds. Because of the diverse chemical structures and the various fragmentation patterns for each of the nitroaromatic compounds, there is no single daughter ion that can be successfully used for the screening of the entire compound class using parent ion monitoring. Furthermore, if the neutral loss monitoring of 30 amu is being used to screen for nitroaromatic compounds, there is no complimentary MS/MS method to use that will improve the confidence in the screening for nitroaromatic compounds. However, since the neutral loss of 30 amu for anything other than NO is quite uncommon, screening for nitroaromatic compounds using the neutral loss monitoring of 30 amu should rarely produce false positives.

## Future Work

Preliminary results have shown that LC/ESI-MS is a viable method for the analysis of nitro explosives, but more investigations are required to develop a method that is routine for the analysis of samples for trace levels of explosives in both environmental and forensic samples. First, the negative-ESI of explosives still requires added investigations to more thoroughly understand the electrospray process. New investigations are currently being undertaken in our group to investigate the electrochemical reactions occurring during the negative-ESI of TNT and HMX. It is the hope that through these studies, more insight will be gained into the origins of adduct ion formation with explosives and into how the ESI process can be better controlled. These experiments may also suggest other methods besides adduct ion formation that will preferentially produce one major ion for each explosive.

To gain insight into the role of redox chemistry in adduct ion formation during ESI, it is proposed that a high-efficiency electrochemical cell inserted in-line to drive the redox reactions of the explosives to completion before the ESI needle. The reduction products of the nitroaromatics, nitrate esters, and nitramines can then be analyzed by both UV detection, APCI-MS, and ESI-MS. It is hoped that these electrochemical investigations will help explain the adduct ions formed during electrospray. To improve the selectivity of these experiments, an LC column may be inserted either before or after the electrochemical cell. From these experiments, it may be possible to determine which adduct ions in the ESI mass spectrum are formed as the result of redox reactions at the ESI needle (e.g. the $[M+NO_2\text{-}H]^-$ ion) and which were formed via other mechanisms (e.g. the $[M+TFA\text{-}H]^-$ ion).

Ultimately, as the LC/MS method is improved, it will be necessary to analyze real-world samples to validate the method and prove its analytical utility. One series of samples may be soil obtained from the proximity of an explosive manufacturing site. By extracting the organic compounds from these soil samples with an organic solvent such as acetone, they may be analyzed by LC/MS and LC/MS/MS for the presence of explosives. It may be necessary to increase the number of standard explosives analyzed by LC/MS to obtain a better picture of the contamination in the soil.

Finally, methods should be developed using atmospheric pressure chemical ionization (APCI) - MS for the analysis of explosives samples. Preliminary results have shown that APCI-MS is more sensitive than ESI-MS for the analysis of nitroaromatic compounds. In APCI, the analyte molecules are ionized after they are in the gas phase, and thus they do not have to be either protonated or deprotonated in solution for optimum ionization, as is generally necessary in ESI-MS.

## LIST OF REFERENCES


Asano, K.G.; Glish, G.L.; McLuckey, S.A. *Proceedings of the 36th ASMS Conference on Mass Spectrometry and Allied Topics*. San Francisco, CA. **1988**, 636.

Asbury, G.R.; Klasmeier, J.; Hill, Jr., H.H. *Talanta*. **2000**, 50.

Aleksandrov, M.L.; Gall, L.N.; Krasnov, V.N.; Nikolaev, V.I.; Pavelenko, V.A.; Shkurov, V.A. *Dokl. Akad. Nauk SSSR*. **1984**, *277*, 379.

Bailey, C.G.; Yan, C. *Anal. Chem*. **1998**, *70*, 3275.

Banks, J.F. *Electrophoresis*. **1997**, *18*, 2255.

Berberich, D.W.; Yost, R.A.; Fetterolf, D.D. *J. Forensic Sciences*. **1988**, *33*, 946.

Bhadra, D.G. *Environ. Sci. Technol*. **1999**, *33*, 446.

Bieber, L.L. *Ann. Rev. Biochem*. **1988**, *57*, 261.

Bier, M.E.; Schwartz, J.C. In *Electrospray Ionization Mass Spectrometry*. Cole, R.B., Ed.; John Wiley & Sons, Inc.: New York, NY. **1997**, 254.

Bier, M.E.; Schwartz, J.C.; Zhou, J.; Taylor, D.M.; Syka, J.E.P.; James, M.; Fies, W. J.; Stafford, G.C. *Proceedings of the 43rd ASMS Conference on Mass Spectrometry and Allied Topics*. Atlanta, GA. **1995**, 1117.

Bortolini, O.; Spalluto, G.; Traldi, P. *Org. Mass Spectrom*. **1994**, *29*, 269.

Borum, P.R. In *Clinical Aspects of Human Carnitine Deficiency*. Borum, P.R., Ed.; Pergamon Press: New York, **1985**, 157.

Brittain, R.D.; Speltz, D.; Bolton, B. *Proceedings of the 41st ASMS Conference on Mass Spectrometry and Allied Topics*. San Francisco, CA. **1993**, 459.

Bruins, A.P. *J. Chromatogr. A*. **1998**, *794*, 345.

Busch, K.L.; Glish, G.L.; McLuckey, S.A. *Mass Spectrometry / Mass Spectrometry: Techniques and Aplications of Tandem Mass Spectrometry*. VCH Publishers, Inc.: New York, **1988**.

Cassada, D.A.; Monson, S.J.; Snow, D.D.; Spalding, R.F. *J. Chromatogr. A*. **1999**, *844*, 87.

Cassetta, B.; Garofolo, F. *Org. Mass Spectrom*. **1994**, *29*, 517.

Chace, D.H.; Hillman, S.L.; Van Hove, J.L.K.; Naylor, E.W. *Clinical Chem*. **1997**, *43*, 2106.

Chen, L.; Wang, T.-C.L.; Ricca, T.L.; Marshall, A.G. *Anal. Chem*. **1987**, *59*, 449.

Cleven, C.D.; Cox, K.A.; Cooks, R.G.; Bier, M.E. *Rapid Commun Mass Spectrom*. **1994**, *8*, 451.

Cole R.B., Ed. *Electrospray Ionization Mass Spectrometry*. John Wiley & Sons, Inc.: New York, NY. **1997**.

Cole, R.B.; Zhu, J. *Rapid Commun. Mass Spectrom*. **1999**, *13*, 607.

Colon L.A.; Guo Y.; Fermier A. *Anal. Chem*. **1997**, *69*, 461A.

*Montreal Convention on the Marking of Plastic Explosives for the Purpose of Detection*. Montreal, **1991**.

Cooks, R.G.; Benyon, J.H.; Caprioli, R.M.; Lester, G.R. *Metastable Ions*. Elsevier: New York, **1973**, 28-30, 37-88.

Cooper, P.W.; Kurowski, S.R. *Introduction to the Technology of Explosives*. Wiley-VCH, Inc.: New York, NY. **1996**.

Cox, K.A.; Cleven, C.D.; Cooks, R.G. *Int. J. Mass Spectrom. Ion Process*. **1995**, *144*, 47.

Dawson, P.H. *Quadrupole Mass Spectrometry and Its Applications*. Elsevier Scientific: New York, NY. **1976**.

Degnore, J.P. *Fundamental Studies of Quadrupole Ion Traps: Investigation of Mass Shifts and Improved Ion Ejection*. Ph.D. Dissertation, University of Florida. **1997**.

Dole, M.; Mack, L.L.; Hines, R.L.; Mobley, R.C.; Ferguson, L.D.; Alice, M.B. *J. Chem. Phys*. **1968**, *49*, 2240.

Douse, J.M.F. *J. Chromatogr*. **1981**, *208*, 83.

Emmett, M.R.; Caprioli R.M. *J. Am. Soc. Mass Spectrom.* **1994**, *5*, 605.

Feller, A.G.; Rudman, D. *J. Nutr.* **1988**, *118*, 541.

Fenn, J.B.; Mann, M.; Chin, K.M.; Shek, F.W.; Whitehouse, C.M. *Science*. **1989**, *246*, 64.

Gaskell, S.J. *J. Mass Spec.* **1997**, *32*, 677.

Gill, L.A.; Wells, J.M.; Patterson, G.E.; Amy, J.W.; Cooks, R.G. *Anal. Chem.* **1998**, *70*, 4448.

Gomez, A.; Tang, K. *Phys. Fluids*. **1994**, *6*, 2317.

Gross, M.L. In *Methods in Enzymology: Mass Spectrometry*. McCloskey, J.A., Ed.: Academic Press, Inc.: San Diego, CA. **1990**, *193*, 131.

Hadd, A.G. *Anal. Chem.* **1997**, *69*, 3407.

Heinig, K.; Henion, J. *J. Chromatogr. B.* **1999**, *735*, 171.

Ikonomou, M.G., Blades, A.T.; Kebarle, P. *Anal. Chem.* **1991**, *63*, 1989.

Iribarne, J.V.; Thomson, B.A. *J. Chem. Phys.* **1976**, *64*, 2287.

Jenkins, T.F.; Leggett, D.C.; Grant, C.L.; Bauer, C.L. *Anal. Chem.* **1985**, *58*, 170.

Johnson, J.V.; Pedder, R.E.; Yost, R.A. *Int. J. Mass Spectrom. Ion Process*. **1991**, *106*, 197.

Johnson, J.V.; Pedder, R.E.; Yost, R.A.; Story, M.S. *U.S. Patent 5,075,991*. **1992**.

Johnson, J.V.; Pedder, R.E.; Yost, R.A.; Story, M.S. *U.S. Patent 5,171,991*. **1992**.

Johnson J.V.; Yost R.A. *Anal. Chem.* **1985**, *57*, 758A.

Johnson, J.V.; Yost, R.A.; Kelley, P.E.; Bradford, D.C. *Anal. Chem.* **1990**, *62*, 2162.

Kaiser, R.E.; Cooks, R.G.; Stafford, G.C.; Syka, J.E.P.; Hemberger, P.H. *Int. J. Mass Spectrom. Ion Process*. **1991**, *106*, 79.

Karger B.L.; Hancock W.S., Eds. *Methods in Enzymology*. **1996**, 270.

Kebarle, P.; Ho, Y. In *Electrospray Ionization Mass Spectrometry*. Cole, R.B., Ed.; John Wiley & Sons, Inc.: New York, NY. **1997**, 3.

Kebarle, P.; Tang L. *Anal. Chem.* **1993**, *65*, 972A.

Kolla, P. *J. Chromatogr. A*. **1994**, *674*, 309.

Lang, M.J.; Burns, S.E. *J. Chromatogr. A*. **1999**, *849*, 381.

Londry, F.A.; Morrison, R.J.S.; March, R.E. *Proceedings of the 45th ASMS Conference on Mass Spectrometry and Allied Topics*. Atlanta, GA. **1995**, 1124.

Lopez, L.L.; Drexler, D.M.; Mylchreest, I.; Schwartz, J.C. *Proceedings of the 47th ASMS Conference on Mass Spectrometry and Allied Topics*. Dallas, TX. **1999**, 1867.

Louris, J.N.; Schwartz, J.C.; Stafford, G.C.; Syka, J.E.P.; Taylor, D.M. *Proceedings of the 40th ASMS Conference on Mass Spectrometry and Allied Topics*. Washington, D.C. **1992**, 1003.

Louris, J.N.; Cooks, R.G.; Syka, J.E.P.; Kelly, P.E.; Stafford, Jr., G.C.; Todd, J.F.J. *Anal. Chem.* **1987**, *59*, 1677.

Mack, L.L.; Kralik, P.; Rheude, A.; Dole, M. *J. Chem. Phys*. **1970**, *52*, 4977.

Major, F.G.; Dehmelt, H.G. *Phys. Rev*. **1968**, *170*, 91.

March RE. *Rapid Commun. Mass Spectrom*. **1998**, *12*, 1543.

March, R.E.; Hughes, H.E. *Quadrupole Storage Mass Spectrometry*. John Wiley & Sons: New York, NY. **1989**.

March, R.E.; Todd, J.F.J., Eds. *Practical Aspects of Ion Trap Mass Spectrometry, v. I Fundamental Ion Trap Mass Spectrometry*. CRC Press: New York, NY. **1995**.

Marshall, A.G.; Hendrickson, C.L.; Jackson, G.S. *Mass Spectrom. Rev*. **1998**, *17*, 1.

Marshall, A.G.; Wang, T.-C.L.; Ricca, T.L. *J. Am. Chem. Soc*. **1985**, *107*, 7893.

Mathieu, E. J. Math. Pure Appl. **1868**, 13, 137.

McClellan, J.E.; Holden, M.A.; Yinon, J.; Yost, R.A. Proceedings of the 47th ASMS Conference on Mass Spectrometry and Allied Topics. Dallas, TX. **1999**, 2444.

McClellan, J.E.; Mulholland, J.J.; Murphy III, J.P.; Yost, R.A. Proceedings of the 47th ASMS Conference on Mass Spectrometry and Allied Topics. Dallas, TX. **1999**, 2848.

McClellan, J.E.; Quarmby, S.T.; Borum, P.R.; Yinon, J.; Yost, R.A. Pittcon Abstracts. New Orleans, LA. **1998**, 1033.

Miller, M.L.; Leibowitz, J.; Martz, R. Proceedings of the 44th ASMS Conference on Mass Spectrometry and Allied Topics. Portland, OR. **1996**, 1389.

Miller, M.L.; Mothershead, R.; Leibowitz, J.; Mount, K.; Martz, R. Proceedings of the 44th ASMS Conference on Mass Spectrometry and Allied Topics. Palm Springs, CA. **1997**, 52.

Millington, D.S.; Norwood, D.L.; Kodo, N.; Roe, C.R.; Inoue, F. Anal. Biochem. **1989**, 180, 331.

Muffatt F. Chromatographia. **1998**, 48, 481.

Mulholland, J. J.; Yost, R. A. Proceedings of the 47th ASMS Conference on Mass Spectrometry and Allied Topics. Dallas, TX. **1999**, 2881.

Murphy, J.P.; McClellan, J.E.; Yost, R.A. Proceedings of the 47th ASMS Conference on Mass Spectrometry and Allied Topics. Dallas, TX. **1999**, 2850.

Murphy III, J.P.; Yost, R.A. Rapid Commun. Mass Spectrom. **2000**, 14, 270.

Naylor, E.W.; Chace, D.H. J. Child Neurology. **1999**, 14, S4.

Oehrle, S.A. J. Chromatography A. **1996**, 745, 233.

Paul, W. Rev. Mod. Phys. **1990**, 62, 531.

Paul, W.; Steinwedel, H. U.S. Patent. **1960**, 2939952.

Quarmby, S.T. Fundamental Studies of Ion Injection and Trapping of Electrosprayed Ions On a Quadrupole Ion Trap Mass Spectrometers. Ph.D. Dissertation, University of Florida. **1997**.

Quarmby, S.T.; Yost, R.A. U.S. Patent Applied for, No. 08//837,030. April 11, **1997**.

Quarmby, S.T.; Yost, R.A. Int. J Mass Spectrom. **1999**, 190/191, 81.

Quirke, J.M.E.; Van Berkel G.J.; Adams C.L. Anal. Chem. **1994**, 66, 1302.

Renner, T.; Baumgarten, D.; Unger, K.K. Chromatographia. **1997**, 45, 199.

Schwartz, J. C.; Bier, M. E.; Taylor, D. M.; Zhou, J.; Syka, J.E.P.; James, M.; Stafford, G. C. Proceedings of the 43rd ASMS Conference on Mass Spectrometry and Allied Topics. Atlanta, GA. **1995**, 1114.

Schwartz, J.C.; Lopez, L.; Tiller, P. Proceedings of the 47th ASMS Conference on Mass Spectrometry and Allied Topics. Dallas, TX. **1999**, 2791.

Schwartz, J.C.; Quarmby, S.T.; Schoen, A.E. Proceedings of the 46th ASMS Conference on Mass Spectrometry and Allied Topics. Orlando, FL. **1998**, 484.

Sewell, A.C.; Bohles, H. J. Eur J Pediatr. **1995**, 154, 871.

Smith R.D. J. Mass Spec. **1997**, 32, 425.

Smith, R.D.; Loo, J.A.; Ogorzalek, R.R.; Busman, M.; Udseth, H. Mass Spec. Rev. **1991**, 10, 359.

Stafford, G.C.; Kelley, P.E.; Syka, J.E.P.; Reynolds, W.E.; Todd, J.F.J. Int. J. Mass Spectrom. Ion Process. **1984**, 60, 85.

Stafford, G.C.; Kelley, P.E.; Stephens, D.R. U. S. Patent. **1985**, 4540884.

Stafford, G.C.; Taylor, D.M.; Bradshaw, S.C.; Syka J.E.P.; Uhrich, M. Proceedings of the 35th ASMS Conference on Mass Spectrometry and Allied Topics. Denver, CO. **1987**, 775.

Straub, R.F.; Voyksner, R.D. J. Am. Soc. Mass Spectrom. **1993**, 4, 578.

SW-846 Method 8330. Nitromaromatics and nitramines by high performance liquid chromatography. Washington, D.C.: U.S. EPA, Office of Solid Waste and Emergency Response, **1994**.

Syka, J.E.P. 9th Asilomar Conference on Mass Spectrometry. **1992**.

Syka, J.E.P. In Practical Aspects of Ion Trap Mass Spectrometry V. I Fundamentals of Ion Trap Mass Spectrometry. March, R. E., Todd, J. F. J., Eds.; CRC Press: New York, NY. **1995**, 169.

Todd, J.F.J. Mass Spec. Rev. **1991**, 10, 3.

Traldi, P.; Catinella, S.; Bortolini, O. Org. Mass Spectrom. **1992**, 27, 927.

Traldi, P.; Favretto, D. Rapid Commun. Mass Spectrom., **1992**, 8, 543.

Traldi, P.; Favretto, D.; Catinella, S.; Bortolini, O. Org. Mass Spectrom. **1993**, 36, 745.

Urbanski, T. Chemistry and Technology of Explosives. Pergmon: New York, NY. **1964**.

Van Berkel, G.J.; Zhou, F. Anal. Chem. **1995**, 67, 2916.

Van Berkel, G.J. In Electrospray Ionization Mass Spectrometry. Cole, R.B., Ed.; John Wiley & Sons, Inc.: New York, NY. **1997,** 65.

Van Berkel, G.J. Anal. Chem. **1998**, 70, 1544.

Walsh, M.E.; Ranney T. J. Chrom. Science. **1998**, 36.

Weieboldt, R.; Campbell, D.A.; Henion, J. J. Chromatogr. B. **1998**, 708, 121.

Wells, J.M.; Plass, W.R.; Patterson, G.E.; Ouyang, Z.; Badman, E.R.; Cooks, R.G. Anal. Chem. **1999**, 71, 3405.

Welsh, T.; Block, H. Fresenius J Anal. Chem. **1997**, 357, 904.

Wheat, T.E.; Lilley, K.A.; Banks, J.F. J. Chromatogr. A. **1997,** 781, 99.

Wuerker, R.F.; Shelton, H.; Langmuir, R.V. J. Appl. Phys. **1959**, 30, 342.

Yamashita, M.; Fenn, J. B. J. Phys. Chem. **1984**, 88, 4451.

Yinon, J. J. Chromatogr. A. **1996**, 742, 205.

Yinon, J. Forensic and Environmental Detection of Explosives. John Wiley & Sons: New York, NY. **1999**.

Yinon, J.; McClellan, J.E.; Yost R.A. Rapid Commun. Mass Spectrom. **1997,** 11, 1961.

Yinon, J.; McClellan, J.E.; Yost, R.A. Pittcon Abstracts. Orlando, FL. **1999**, 358.

Yinon, J.; Zitrin, S. Modern Methods and Applications in Analysis of Explosives. John Wiley & Sons: New York, NY. **1993**.

Yost, R.A.; Boyd, R.K. In Methods in Enzymology: Mass Spectrometry. McCloskey, J.A., Ed.: Academic Press, Inc.: San Diego, CA. **1990**, 193, 154.

Yost, R.A.; Fetterolf, D.D. Mass Spec. Rev. **1983**, 2, 1.

Yost, R.A.; McClennen, W.; Snyder, A.P. Proceedings of the 35$^{th}$ ASMS Conference on Mass Spectrometry and Allied Topics. Denver, CO, **1987**, 789.

Zhou, J.; Schwartz, J.C. Proceedings of the 43rd ASMS Conference on Mass Spectrometry and Allied Topics. Atlanta, GA. **1995**, 1116.

## BIOGRAPHICAL SKETCH

I, Joseph (Dewey, Buddha) Edward McClellan, was born in Durham, NC at Mr. Duke's Hospital on the campus of Duke University to a set of extremely loving and wonderful parents, Marilyn A. and Joseph R. McClellan. I was uniquely named after both of my grandfathers, Edward Joseph O'Day and Joseph Edward McClellan. Though I have lived in many different places along the East Coast, including the Maryland / District of Columbia area, Massachusetts, and Rhode Island, I spent most of my life, including my learning years, in Erie, PA. Presently, my parents, sister and a majority of my school-age friends still live in and around Erie. Erie is and always will be my home. I have one sister, Kathleen (Katie) Michelle, who is pretty O.K. as a person (now); and, contrary to popular belief, I do love her very much (almost as much as I love to antagonize her). Currently, Katie attends Duke University, where she stresses way too much and hopes to attend law school.

At about the age of 11, I learned how to play the game of golf, which has dramatically shaped my life and outlook. Though I never became a great golfer, I often define myself as, among other things, a golfer. I have had the opportunity to play competitive golf since the age of 13 and have had the wonderful pleasure of playing on both the high school and collegiate levels. My sister, who began playing very early in life, became a much better golfer than I (for a girl) and is a two-time Erie District Women's Golf Association champion. Through the game of golf, I have learned a lot about life, people, and myself. I have met an extremely wide range and diverse group of

people and, as a result, have made a wide variety of friends, including life-long friends, beer-drinking friends, golf team friends, and caddie friends (who are a totally different breed of people). From the successful, important, and respected members of the club, whom I regularly caddied for, played with, and listened to, I learned what it takes to succeed in life, both personally and professionally. Through these experiences, I have also come to appreciate why it is always important to strive towards and aspire for the best. I will always treasure my experiences on the golf course with my father, sister, and friends, and look forward to playing for many years to come.

After graduating from McDowell High School, in Erie, PA, I attended The College of the Holy Cross, in Worcester, MA. From August 1991, when I first stepped on to the gorgeous campus nestled on Mt. St. James, until the day I graduated in May of 1995 with a B.A. in Chemistry, I had the time of my life. Holy Cross is a special place because of its tradition in educational excellence, but the thing that makes the Cross truly special are the people that populate "the school on the hill". There are many people from Holy Cross whom I will never forget and many I hope to have as eternal friends, such as my senior year roommates, Vincent Morrow, Matty Gale, Derek Gittus, Bill "Snapps" McElligott, and Chuck Fox, who will always be "My Roommates", and Kim Peterson. At Holy Cross, I had the pleasure of doing undergraduate research for two years with Professor Jane M. Van Doren. I had a lot of fun with Jane and my cohorts at Holy Cross, Bill Foley (HC '95), Adrienne Bernard (HC '95), and Jim Murphy (HC '96). Through my research at Holy Cross, I learned how to "do good science" and about instrumentation, such as the Flowing Afterglow Langmuir Probe (lovingly known as the FALP) coupled

to a quadrupole mass analyzer, which became invaluable experiences when I entered graduate school.

I arrived at the University of Florida in August of 1995 and was accepted into the analytical chemistry research group of Professor Richard A. Yost in the spring of 1996. While at UF, I had the pleasure of teaching for nine semesters as a teaching assistant in general chemistry and analytical chemistry. As an analytical chemistry teaching assistant, I had the pleasure of teaching for Professor James D. Winefordner, which was truly an enlightening experience. In 1998, I was awarded the Department of Chemistry Teaching Award for my instruction in instrumental lab. As a member of the Yost Group, I had the opportunity to do research in quadrupole ion trap mass spectrometry and study small molecules, including acylcarnitines, explosives, and natural products. During my tenure in the Yost Group, I had the opportunity to attend and present at three American Society for Mass Spectrometry Conferences, in Palm Springs, CA, Orlando, FL, and Dallas TX, two Pittcon Conferences, in New Orleans, LA and Orlando, FL, one International Association of Forensic Scientists Conference in Los Angeles, CA, and one Gordon Research Conference in New London, CT. Each of these conferences allowed ne the opportunity to grow as a scientist. In recognition of my research, I was awarded the University of Florida Threadgill Dissertation Fellowship and the Roger G. and Jo Bates Fellowship in Analytical Chemistry.

Upon graduation from the University of Florida, with a Doctor of Philosophy in Chemistry, I will begin a postdoctoral fellowship at the Boston University School of Medicine Mass Spectrometry Resource under the direction of Professor Catherine

Costello. At BUSM, I will be involved in basic research and collaborative studies of biopolymers, specifically proteoglycans, by analytical mass spectrometry.

I certify that I have read this study and that in my opinion it conforms to acceptable standards of scholarly presentation and is fully adequate, in scope and quality, as a dissertation for the degree Doctor of Philosophy.

Richard A. Yost, Chairman
Professor of Chemistry

I certify that I have read this study and that in my opinion it conforms to acceptable standards of scholarly presentation and is fully adequate, in scope and quality, as a dissertation for the degree Doctor of Philosophy.

Benjamin A. Horenstein
Associate Professor of Chemistry

I certify that I have read this study and that in my opinion it conforms to acceptable standards of scholarly presentation and is fully adequate, in scope and quality, as a dissertation for the degree of Doctor of Philosophy.

David A. Powell
Scientist of Chemistry

I certify that I have read this study and that in my opinion it conforms to acceptable standards of scholarly presentation and is fully adequate, in scope and quality, as a dissertation for the degree Doctor of Philosophy.

Weihong Tan
Assistant Professor of Chemistry

I certify that I have read this study and that in my opinion it conforms to acceptable standards of scholarly presentation and is fully adequate, in scope and quality, as a dissertation for the degree of Doctor of Philosophy.

Peggy L. Borum
Professor of Food Science and Human Nutrition

This dissertation was submitted to the Graduate Faculty of the Department of Chemistry in the College of Liberal Arts and Sciences and to the Graduate School and was accepted as partial fulfillment of the requirements for the degree of Doctor of Philosophy.

August, 2000

Dean, Graduate School